Lappeenranta
University of Technology

Tatiana Minav

ELECTRIC-DRIVE-BASED CONTROL AND ELECTRIC ENERGY REGENERATION IN A HYDRAULIC SYSTEM

Thesis for the degree of Doctor of Science (Technology) to be presented with due permission for public examination and criticism in the Auditorium 1382 at Lappeenranta University of Technology, Lappeenranta, Finland, on the 12th of August, 2011, at noon.

Acta Universitatis
Lappeenrantaensis 436

Supervisor Professor Juha Pyrhönen
Department of Electrical Engineering
Institute of Energy Technology
Faculty of Technology
Lappeenranta University of Technology
Finland

Reviewers Professor E. Lomonova
Department of Electrical Engineering
Eindhoven University of Technology
The Netherlands

Professor T. Andersen
Institute of Energy Technology
Aalborg University
Denmark

Opponents Professor E. Lomonova
Department of Electrical Engineering
Eindhoven University of Technology
The Netherlands

Professor T. Andersen
Institute of Energy Technology
Aalborg University
Denmark

ISBN 978-952-265-103-7
ISBN 978-952-265-104-4 (PDF)
ISSN 1456-4491
Lappeenrannan teknillinen yliopisto
Digipaino 2011

Abstract

Tatiana Minav

Electric-drive-based control and electric energy regeneration in a hydraulic system

Over the recent years, development in mobile working machines has concentrated on reducing emissions owing to the tightening rules and needs to improve energy utilization and reduce power losses. This study focuses on energy utilization and regeneration in an electro-hydraulic forklift, which is a lifting equipment application.

The study starts from the modelling and simulation of a hydraulic forklift. The energy regeneration from the potential energy of the load was studied. Also a flow-based electric motor speed control was suggested in this thesis instead of the throttle control method or the variable displacement pump control.

Topics related to further development in the future are discussed. Finally, a summary and conclusions are presented.

Lappeenranta, June 23, 2011

150 p.

Acta Universitatis Lappeenrantaensis 436

Diss. Lappeenranta University of Technology

ISBN 978-952-265-103-7, ISBN 978-952-265-104-4 (PDF)

ISSN 1456-4491

Keywords: electro-hydraulic drive, energy efficiency, hydraulics, mobile machines, regeneration, pump, servomotor.

UDC 621.22:681.5:621.65/.69:620.97

Acknowledgements

This study has mainly been carried out at the Department of Electrical Engineering of Lappeenranta University of Technology (LUT) during the years 2008–2011. People from the Control Systems Department of Saint-Petersburg State Electrotechnical University LETI, Russia, also contributed to the research work.

I express my deep gratitude to my supervisors, Professor Juha Pyrhönen and Dr. L. Laurila at Lappeenranta University of Technology for their valuable guidance. I am also grateful to Professor Heikki Handroos and Dr. Huapeng Wu for technical discussions, which helped me a great deal. I acknowledge the help of Professor Viktor Vtorov from Saint-Petersburg Electrotechnical University LETI for his support. I also express my thanks to Antti Virtanen from the Department of Electrical Energy Engineering, Tampere University of Technology for the help with the realization of measurements with the super capacitor.

I thank Ms. Julia Vauterin for her sincere support in the educational process, Tiina Väisänen and Dr. Hanna Niemelä for language editing and all the team of the Department of Electrical Engineering of Lappeenranta University of Technology (LUT) for their contribution to this work, especially Dr. Markku Niemelä, Dr. Olli Pyrhönen, Paula Immonen, Martti Lindh and Piipa Virkki.

The honoured pre-examiners of the thesis, Professor E. Lomonova and Professor T. Andersen also deserve my greatest appreciation. The feedback I received from them significantly helped me to finalize the work.

I address my special thanks to Jani Heikkinen, Dr. Valentin Dzhankhotov and Denis Filatov for their valuable comments, corrections and continuous support. I also thank my family for continuous support.

The research was enabled by the financial support of the Finnish Funding Agency for Technology and Innovation (Tekes) and the Forum for Intelligent Machines (FIMA) at the Department of Electrical Engineering of Lappeenranta University of Technology, Lappeenranta, and Tampere University of Technology, Finland.

Finally, this work is dedicated to my mother Alla. Your love is my breath.

Tatiana Minav,

June 2011,

Lappeenranta, Finland.

Dedicated

to the memory of my mother Alla

Contents

1 Introduction

Mobile working machines play an important role in modern industry. These machines are widely used for instance in the mining, process and goods manufacturing industry, forest harvesting and harbour terminal work. Figure 1.1 illustrates typical examples of mobile working machines. This study concentrates on evaluating the opportunities of improving the energy efficiency of the lifting and lowering system. The Rocla forklift shown in Figure 1.1b works as a test bench in the experimental part of the work.

(a) (b) (c)

photo: Cargotec photo: Rocla photo: Sandvik

Figure 1.1: Examples of mobile working machines: a) straddle carrier, b) forklift truck and c) mine underground truck.

Mobile working machines can be classified as light mobile machines that operate by battery power and heavy machines that work using a diesel engine. Both of these types include mechanical structures, which are driven by hydraulics.

Typical mobile working machines have the following characteristics:

1. Open and closed hydraulic systems are widely used in mobile working machines. An open system is characterized by a common oil tank in atmospheric pressure.

2. Hydraulic cylinders and rotary actuators are commonly used as actuators for linear movement. They are typically controlled by hydraulic valves that control the pressurised fluid flow. Non-symmetrical double-acting cylinders form a typical difficulty in operating the hydraulic systems.

3. A hydraulic pump supplies hydraulic power to actuators.

4. Directional valves are the main components for controlling hydraulic actuators.

5. There are losses in pumps, valves and cylinders as a result of leakages and friction.

6. Mobile working machines are often equipped with hand-operated joysticks where the position control feedback is established by the machine driver (open-loop control).

Mobile working machines are often diesel operated, but there is a trend towards diesel-electric hybrid drives and even fully electric work machines. A hydraulic system is a power transmission system which uses oil to carry the power and energy. The energy can be transmitted either directly for instance to load potential energy or with the help of suitable intermediate devices.

One of the strongest features of hydraulics is its straightforward capability of working as a force transformer. It is easy to multiply the force by a high factor based on the cross-sectional areas of the pistons. With this simple amplification principle, even a human being can easily lift masses of thousands of kilograms. Power inputs and outputs of the hydraulic systems are mechanical: a rotating, torque transmitting shaft, a reciprocating plunger, and the like. The main advantage of the hydraulic systems is the simplicity of the hydraulic power production, transmission, storage and control. With that, the hydraulic forces are easily limited and balanced. Another important advantage is that hydraulics is mechanically relatively safe and compact.

The drawbacks of hydraulic systems are losses such as friction, leakages and the need for special actions to protect hydraulic elements against rust, corrosion and dirt. Hydraulic oil may also pose problems, especially environmental ones. Hydraulic systems are exposed to an unfriendly climate and a dirty atmosphere, as in the case of mobile hydraulics. Although hydraulic power systems have notable drawbacks, they are used in a wide range of industrial and other applications because so far there is no replacement for the compact force amplification of hydraulics. Often there is a desire to produce similar forces with magnetic systems. So far, however, this has been impossible. Magnetic forces are produced by the Maxwell stress generated by the magnetic field strength H (Pyrhönen et al., 2008).

$$\sigma_F = \frac{1}{2}\mu_0 H^2 \tag{1.1}$$

The stress occurs in the direction of lines of force. In the case of a linear movement plunger, the stress term can be divided into its normal and axial components:

$$\sigma_{Fn} = \frac{1}{2}\mu_0\left(H_n^2 - H_{ax}^2\right) \tag{1.2}$$

$$\sigma_{Fax} = \mu_0 H_n H_{tan}. \tag{1.3}$$

Considering magnetic force production, the axial component σ_{Fax} is of the greatest interest in this case. In a hydraulic cylinder, the force F is produced by the system pressure p_s affecting the piston end surface S_p:

$$F = p_s S_p. \tag{1.4}$$

Typical operating pressures in hydraulic systems go up to 30 MPa. Hence, for instance a S_p = 100 cm^2 piston produces a force of 300 kN.

In Equation 1.3, $\mu_0 H_n = B_n$, which is the normal flux density in the system. If iron is used, the maximum practical value of B_n equals 2 T. In the case of a magnetic-force-producing cylinder, the force is generated by the cylinder surface, not the piston end, as in a hydraulic system. To make the task easier, let us assume that the force-producing length is 1 m and the perimeter of the cylinder is 0.3 m. In this case, the magnetic force producing surface is S_{cyl} = 0.3 m^2. To produce 300 kN, we would need an axial stress of 1000 kPa. If the air gap flux density is 2 T and the field strength is 500 kA/m, we obtain the value desired. The problem, however, is that the corresponding stresses used in traditional rotating electrical machines are limited between approximately 10 and100 kPa, which means that we would need 10–100 times as much stress to compete with a normal hydraulic system even though $S_p << S_{cyl}$. The only possibility to achieve such forces with a magnetic system might be utilization of superconducting windings in the magnetic force cylinder. In practice, it seems reasonable to utilize hydraulic systems also in the future.

The opportunities of utilizing electric systems in hydraulic work machines have been neither fully understood nor exploited. Storing electric energy has been so difficult that the opportunities of the technology have remained unexploited. However, the properties of modern accumulators and super capacitors, such as energy density, power density and lifetime, are on the edge to making a fast change in the penetration of electric drives into work machines possible (Mecrow, 2008). Electric drives controlling hydraulic systems give superior accuracy and speed for the machine force or torque control (Helduser, 1999). The torque of a modern vector-controlled alternating current (AC) motor drive can be changed from zero to the rated torque in a millisecond or a few milliseconds depending on the operating status of the electric drive (Noguchi, 2007; Luukko, 2007). Such a speed in torque or force control enables accurate position control and energy recovery in work machines even in the most demanding applications (Bekner, 2008). The direct torque control (DTC) technique has been recognized as a viable and robust solution to achieve these requirements. Recent advancements in DTC systems include the use of stator flux vector control in the field weakening region

(Vaclavek, 2008), torque ripple minimization techniques (Gilez, 2008), space vector modulation (Chen, 2010) and the neuro-fuzzy technique (Xu, 2010).

During the latest decades, mankind has been concentrating on talks to reduce CO_2 emissions. In addition, now there are government mandated Tier IV reduction regulations for harmful exhaust gases for diesel powered equipment (Wagner, 2010; EPA, 2011). It has, however, become more and more important to consider energy economy and energy consumption in all fields of human activities, also in heavy work machines (Rydberg, 2007). Now hybrid technologies are the main trend of industry and research facilities (Paulides, 2008); in-wheel motors and electromagnetic active suspensions systems become part of this trend (Gysen, 2010; Lomonova, 2010). According to Kunze (2010), a hydraulic hybrid can be considered the greatest innovation potential for the sector. According to W. Backé, there are many innovations which make fluid power successful. In hydraulics starting already from 1990s, load sensing (LS) valves were introduced in industry to improve energy efficiency. Load sensing control is based on variable displacement pumps and it is normally used in open circuits. The load-caused pressure is measured and the pump flow is adjusted to maintain a constant pressure drop across the valve orifice. This results in a constant flow, and hence, constant piston speeds despite the load changes. LS valves with variable-displacement pumps or so-called pure pump control have significantly reduced the energy consumption in hydraulic systems (Liang, 2002; Ruggeri, 2008). Pump-controlled actuators (PCA) or displacement-controlled actuators offered new advantages for designer of mobile machines according to M. Ivantysynova (2008). Digital hydraulics is one promising available technology, which can solve common problems within the hydraulic world: digital valves (Siivonen, 2009; Linjama, 2005; Yao, 2002) and digital pumps (Linjama, 2009b). According to research conducted in Tampere University of Technology, the most promising approaches from the energy saving point of view are systems based on digital cylinders, digital pump-motor-transformers combined with digital valve systems (Linjama, 2009c and 2009a).

Energy consumption can also be reduced in mobile working machines by converting potential energy or dynamic energy into other types of energy, such as hydraulic, rotating dynamic energy or electric energy. There are examples of the commercial application of kinetic energy regeneration systems (KERS). (KERS, 2010; Anh, 2008) In the field of mobile machines, there are three well-known types of energy regeneration systems (ER) based on a hydraulic accumulator (Ding, 2007; Yang, 2007; Hui, 2010), a battery or a combination with a super capacitor (Inoue, 2008; Iannuzzi, 2008; Wang, 2009), or a flywheel system (Boyes, 2000). The idea of using potential energy for regeneration is not new. It has already been implemented for instance in lifts (Yang, 2007), excavators (Yoon, 2009), cranes (Liang, 2001; Lin, 2010b) and forklifts (Andersen, 2005; Rydberg, 2005).

Figure 1.2 illustrates the schematic of an excavator described by Yoon (2009).

From Figure 1.2, it can be seen that the boom cylinder is driven by an electric motor/generator combined with a bi-directional hydraulic pump and a hydraulic control circuit. A three port/three position valve, controlled by an electric signal, with a proportional pressure relief valve is installed to adjust the distribution of flow in lines. In addition, an orifice cartridge valve is used to perform the holding function. The author describes two possible cases: "slow" and "fast" downward movement. In the generating function in the "slow down" mode, the reverse rotation of the pump as a hydraulic motor rotates the generator, which converts the mechanical energy into electric power, which again is stored in the battery. As a result, most of the potential energy is converted into electric power and saved into the battery in this mode. In the "fast" mode, the piston is retracted so that the flow from the cylinder is partly directed to the tank to allow fast flow (Yoon, 2009).

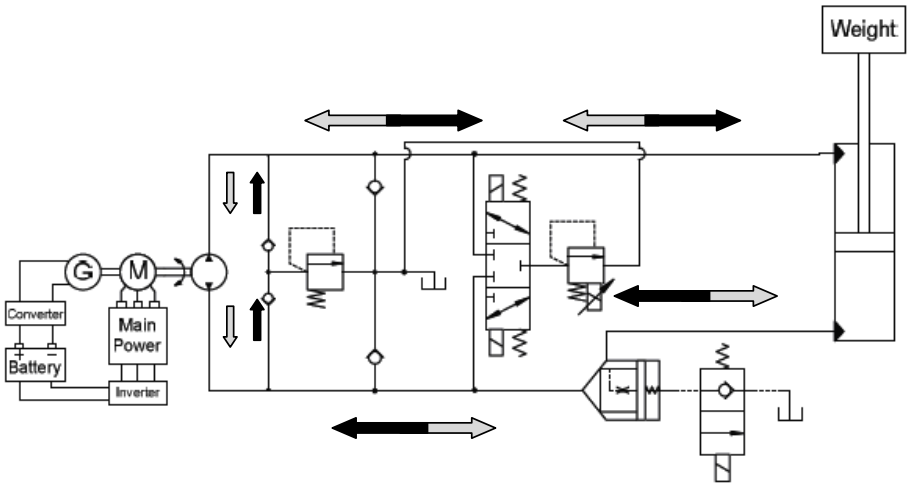

Figure 1.2: Hybrid circuit main components for an excavator (Yoon, 2009). Grey lines illustrate the movement of flow during lifting motion and black lines during lowering motion.

A test setup of a forklift described by Andersen is represented in Figure 1.3. The author proposed to minimize throttling losses by switching to on/off valves in the system. A concept for a velocity-controlled pump is proposed. A conventional gear pump is used. According to the author, the efficiency of the main lift function in the forklift trucks can be increased by a considerable amount.

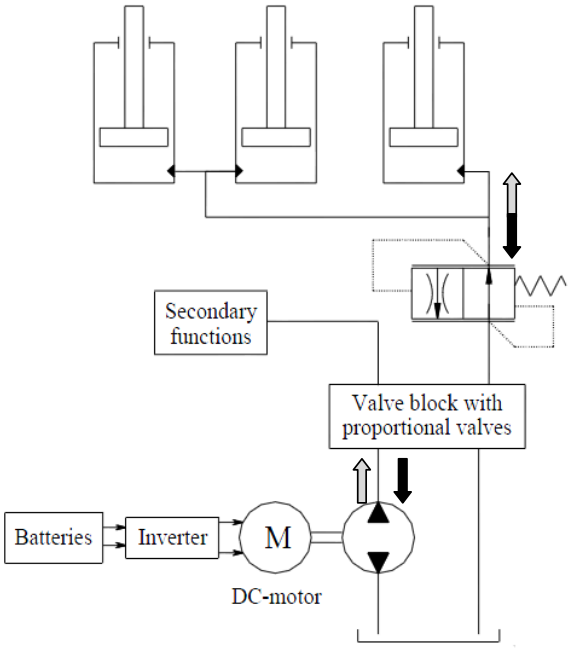

Figure 1.3: Hydraulic diagram of a forklift (Andersen, 2005). The valve block with proportional valves and the upper on-off valve let the oil runs freely when lifting. During lowering, the upper on-off valve and the valve block direct oil to the pump, which rotates as a motor. Regeneration of energy takes place. Grey lines illustrate the movement of flow during lifting motion and black lines during lowering motion.

Figure 1.4 shows an example of a displacement-controlled drive with a differential cylinder. The authors told that the system uses a servo pump with a low pressure adjustment system, which is sufficient for many applications. “The coupling of actuators on the low pressure side and the mechanical coupling of servo pumps by a common distributing gear allows here the use of potential load and brake energy for another drive implemented in the machine” (Rahmfeld, 2001). In Figure 1.4, a charge pump (4) together with a hydraulic accumulator (5) is used for this task. The main advantage of this concept is that in the case of more than one actuator in a machine, the low pressure lines can be coupled.

Two pilot-operated check valves (3) ensure that the low pressure side of the cylinder (2) is always connected to the hydraulic accumulator (5), which depends on the operating quadrant. A servo pump (1) works as the final control element of the linear drive. If the loads are positive and the movements of the cylinder are forward, the servopump works in the pumping mode and sucks oil additionally from the accumulator. When the cylinder moves backwards under the same load condition, the servo pump works in motoring mode under an aiding load, and the accumulator is filled from the low

pressure side. The adjustment system of the servo pump is also supplied by the charge pump (4), which is, as mentioned above, also used for the balancing of volumetric losses of the servo pump. Of course, this actuator needs two high pressure relief valves and one low pressure one (Rahmfeld, 2001).

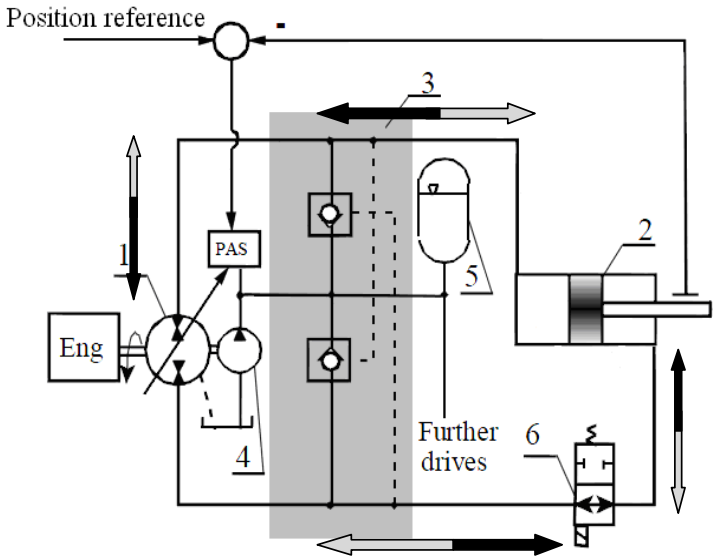

Figure 1.4: Displacement-controlled drive with differential cylinder (Rahmfeld, 2001). Grey lines illustrate movements of flow during lifting motion and black lines during lowering motion.

There are many examples of applications where energy regeneration is possible. Therefore, the idea to improve energy utilization also in mobile machines such as forklifts becomes obvious, and it has been studied in this thesis. In the study, the original non-regenerative AC electric drive (Figure 1.5 a and b) and the hydraulic pump of the forklift were replaced by the hydraulic and electric systems shown in Figure 1.5 c. The test setup was built for theoretical and experimental re-evaluation of the concept proposed for instance in (Andersen, 2005). Comparison of Figures 1.5 b and 1.5 c provides a simplification of the hydraulic structure, which is achieved by replacing the "complicated" valve by a "simple" poppet valve. Appendix A contains detailed information of the experimental test setup.

The objectives of this study are to evaluate the influence of different factors on the energy recovery in an electro-hydraulic forklift, to analyse the reasons for poor energy utilization in conventional forklift systems and to find strategies to improve their energy efficiency. This objective covers many areas of engineering sciences. Figure 1.6 shows the position of this study related to some engineering science fields. Areas that are included in this study are control systems, hydraulics, electrical machines and drives. The study is located on the border between hydraulics and electrical engineering.

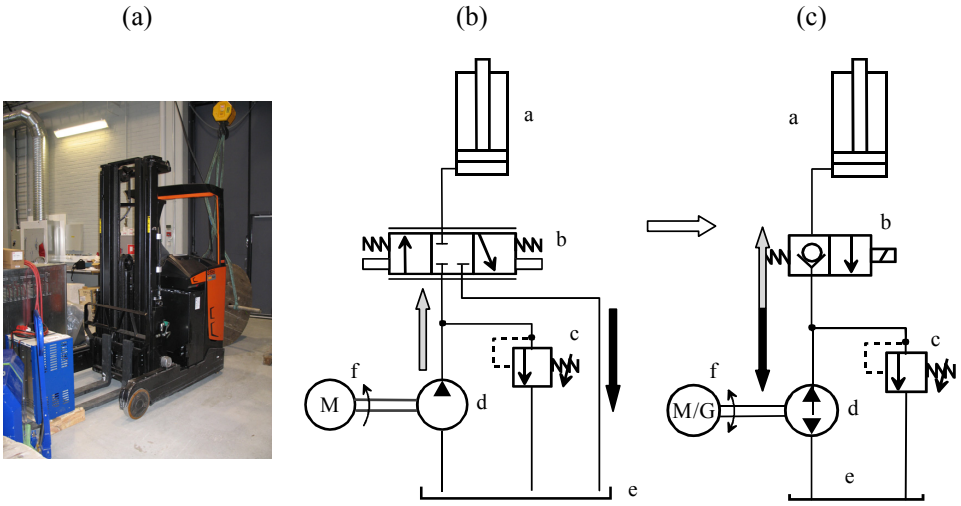

Figure 1.5: (a) Photo of the conventional Rocla HS16F electro-hydraulic forklift working as the test bench in the study. (b) Conventional electro-hydraulic circuit of the main lift function without energy regeneration from potential energy: a) single-acting cylinder, b) proportional valve, c) pressure relief valve, d) external gear pump, e) oil tank, f) induction motor. (c) Electric and hydraulic circuits of the main lift function with energy regeneration from potential energy: a) single-acting cylinder, b) two-way normally closed poppet valve, c) pressure relief valve, d) pump/motor, e) oil tank, and f) variable-speed permanent magnet synchronous machine drive system. The grey lines indicate oil flow during lifting and the black lines during lowering.

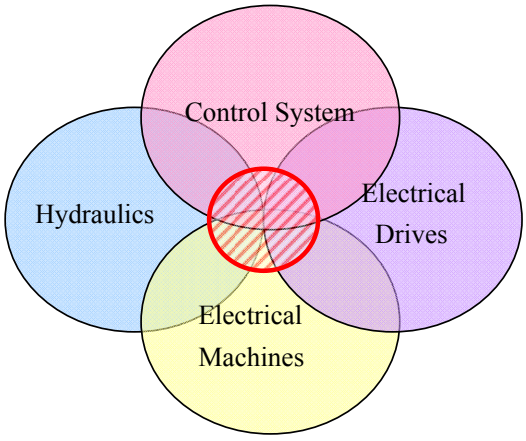

Figure 1.6: Position of this study related to some fields of engineering.

1.1 Scope of the work

The aim of this doctoral thesis is to show that it is possible to significantly improve the energy efficiency and position control of hydraulic systems in general and especially in forklifts by recovering the potential energy and by controlling the movements of the fork smoothly utilizing the capabilities of modern electric servo drive. Such a recovery system is based on the electro-hydraulic position control approach in the forklift by operating the hydraulic machine both as a motor and as a pump with low losses. The work concentrates in using simple energy efficient hydraulic machine system control based on electric motor speed control instead of valve control methods or more complicated variable displacement pump control. The work also shows that the movement control of the hydraulic system can be efficiently and smoothly achieved by using proper control algorithms for the electric drive. The thesis consists of modelling the system, providing a new control system for such an arrangement and practical measurement results that show the energy efficiency improvements. The results of the study can be used in the development of new hydraulic lifting applications.

1.2 Scientific contributions

The thesis contains a systems engineering study of an electric forklift covering all its main features affecting the energy efficiency. The main scientific contributions of this thesis include the following:

1. A control structure for a hydraulic cylinder proposed by Andersen (2005) is re-evaluated theoretically and experimentally. The hydraulic cylinder is controlled directly through the electro-hydraulic drive. No traditional throttle control methods are used for speed control. This kind of a structure is characterized by high energy efficiency.

2. A detailed efficiency analysis of several electro-hydraulic system components is carried out.

3. An algorithm is provided for the position control of a hydraulic cylinder piston. This algorithm allows controlling the position of the load without feedback sensors for the physical position of the cylinder piston.

4. An analysis of flow ripple and a possible compensation method or methods were carried out. An algorithm of ripple caused by the hydraulic pump compensation is proposed.

5. An energy efficiency comparison of different energy storage arrangements in a forklift is given.

6. As a practical scientific result it was possible to show that an electric drive with an appropriate control algorithm (in this case fuzzy adaptation of PID controller parameters) is capable of smoothly controlling hydraulic lifting systems in a direct servo drive pump control.

The last item is an important result as experts in the field had many doubts about the possibilities of achieving smooth movements with a direct electric servo drive pump control before the experimental verification provided in this study. In these very same experiments, it was also shown that a hydraulic pump, especially a piston pump, can be used without problems even at the lowest rotational speeds.

1.2.1 List of publications

The most relevant publications related to this thesis are

1. Minav, T., Laurila, L., Immonen, P., Haapala, M. and Pyrhönen, J. (2009). "Electric energy recovery system efficiency in a hydraulic forklift." In *IEEE EUROCON* 2009, Russia, St. Petersburg.
2. Minav, T., Laurila, L. and Pyrhönen, J. (2010). **"**Energy Recovery Efficiency Comparison in an Electro-hydraulic Forklift and in a Diesel Hybrid Heavy Forwarder." In *Speedam 2010*, Italy, Pisa.
3. Minav, T., Immonen, P., Pyrhönen, J. and Laurila, L. (2010). "Effect of PMSM Sizing on the Energy Efficiency of an Electro-Hydraulic Forklift." In *ICEM 2010*, Italy, Rome.
4. Minav, T., Laurila, L. and Pyrhönen, J. (2011). "Axial Piston Pump Flow Ripple Compensation by adjusting the pump speed with an electric drive." In *SICFP 2011*, Finland, Tampere.
5. Minav T., Laurila L., Immonen P., Pyrhönen J., Vtorov V. and Niemelä M. (2011). "Electric energy recovery system for a hydraulic forklift – theoretical and experimental evaluation." *IET Electric Power Applications*, Vol.5, issue 4, April 2011.
6. Minav T., Laurila L., Pyrhönen, J. and Vtorov V. (2011). "Direct pump control effects on the energy efficiency in an electro-hydraulic lifting system," *Journal International Review of Automatic Control*, Vol.4, n.2, March 2011.
7. Minav T., Laurila L., and Pyrhönen, J. (2011). "Permanent Magnet Synchronous Machine Sizing: Effect on the Energy Efficiency of an Electro-hydraulic Forklift." *Transactions on Industrial Electronics*, in press.
8. Minav, T., Filatov, D., Laurila, L., Pyrhönen, J. and Vtorov, V. (2011). "Modelling of an electro-hydraulic forklift in Matlab Simulink." *Journal International Review on Modelling and Simulations*, Vol.4, n.2, April 2011.

1.3 Outline of the work

The contents of this dissertation are divided into the following six chapters.

Chapter 2 gives general information about the hydraulics, current structures of the forklift control and evaluation methods for the efficiency in a forklift. Basic components are discussed and possible problems are observed. The energy recovering control structure is studied in details.

Chapter 3 introduces the theory, presents a Matlab/Simulink model of the system and electric power loss analysis of PMSM.

Chapter 4 shows a controller design for an electro-hydraulic forklift.

Chapter 5 presents a series of different measurements. The objective of these measurements is to show that the position control method can be used as theoretically developed in Chapter 4. The applicability of this method is verified with a series of measurements. Also an analysis of the influence of different factors on the energy recovery in an electro-hydraulic forklift is made, and the system energy consumption and energy storage methods are examined.

Chapter 6 concludes the study presented in this thesis. Topics related to further development in the future are discussed.

2 Electro-hydraulic system and components

In this chapter, the evaluation methods for energy utilization in a forklift are introduced, and the basic components and control structure of the forklift are discussed.

2.1 Evaluating energy utilization

Before investigating any energy-saving system, it is necessary to discuss how to evaluate the utilization of energy in an electro-hydraulic forklift. The following definitions will be used:

Efficiency

Efficiency as a function of time $\eta(t)$ is normally defined as a ratio between the output (P_{out}) and input (P_{in}) powers

$$\eta(t) = \frac{P_{\text{out}}(t)}{P_{\text{in}}(t)}. \tag{2.1}$$

Even though the efficiency $\eta(t)$ is a function of time, it is normally measured trying to keep P_{out} and P_{in} as constant as possible to be able to obtain for example the rated efficiency of a motor without time dependence. Measuring the rated efficiency of an electric motor normally takes several hours in order to reach the thermal equilibrium of the machine before defining the efficiency. In the case of a limited linear movement, however, it is very difficult to apply this definition of efficiency as there is no steady state in the work. Even when abandoning the need to reach thermal equilibrium there is only a few seconds of constant speed operation at some "constant" efficiency, and thus, measuring the efficiency becomes very difficult. In the case of a forklift, we are actually not very interested in the instantaneous efficiency of the system but the ratio of the total output and input energy. Therefore, the cycle efficiency is defined.

Cycle efficiency

The cycle efficiency $\eta_{\text{cycle}}(t)$ for a time interval $[t_1, t_2]$ is defined as

$$\eta_{\text{cycle}}(t) = \frac{\int_{t_1}^{t_2} P_{\text{out}}(t)\mathrm{d}t}{\int_{t_1}^{t_2} P_{\text{in}}(t)\mathrm{d}t} = \frac{E_{\text{out}}}{E_{\text{in}}}, \tag{2.2}$$

where E_{out} is the total output energy and E_{in} is the total input energy of the system during the time interval starting at t_1 and ending at t_2.

Energy efficiency is nowadays a very popular term, especially in politics. According to the author, the above-defined cycle efficiency and energy efficiency could be used as synonyms in this thesis. However, energy efficiency should normally be regarded as a comprehensive term taking the whole life cycle of the system into account.

Energy-saving ratio

To be able to compare different forklift system efficiencies, the energy-saving ratio Γ_s is defined as:

$$\Gamma_s = \frac{E_{old} - E_{new}}{E_{old}}, \tag{2.3}$$

where E_{old} is the energy consumption of the forklift without energy recovery and E_{new} is the energy consumption of the forklift with the energy recovery method. Γ_s describes how much energy can be saved when the new energy-saving method is applied.

2.2 Components of a electro-hydraulic system

Figure 2.1 illustrates the lifting system schematic of a conventional hydraulic forklift truck. The forklift, of course, has also a traction system, but it is regarded as a simpler task to achieve electrical braking than to control the load lowering by the regenerating electric system. In the case studied, the forklift is already equipped with a regenerating electric drive, and hence, there is no need to study the traction drive from the energy efficiency point of view anymore. However, it seems strange that the traction drive is realized as a regenerative drive but the more energy consuming lifting system is not. This fact exemplifies the difficulty of accepting the idea of using the electro-hydraulic system as the lift load position and speed control system. The designers do not yet rely on the electric drives technology in the lowering and position control of the loads. Lowering is carried out with a valve that can immediately be closed if the pilot observes any problems. The same can, of course, be efficiently done also with an electric drive, but the technology is more complicated.

Traditionally, a battery-operated forklift truck uses an electric motor drive to rotate a hydraulic pump. The pump converts mechanical power from a prime mover to hydraulic power at the actuator. Valves are used to control the direction of the pump flow. A linear actuator or a cylinder converts the hydraulic power to usable mechanical power to lift the load upwards. During the lowering of the mass, the position control of the load is realized by hydraulic control valves converting the load and tare potential energy into heat.

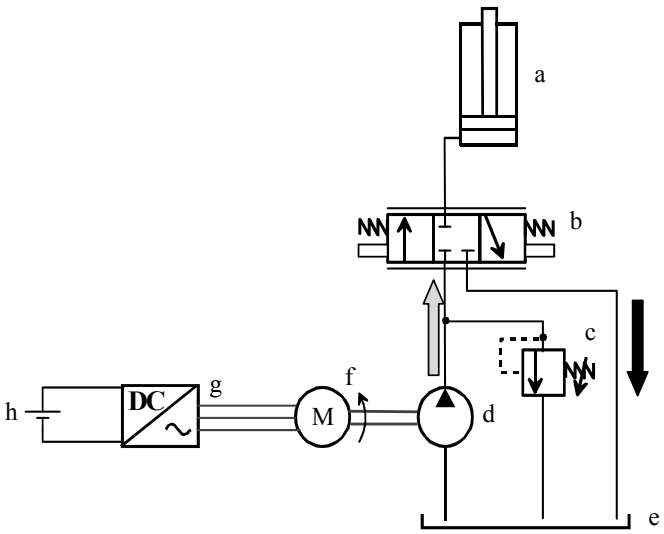

Figure 2.1: Conventional electro-hydraulic circuit of the main lift function of a forklift truck. a) Single-acting cylinder, b) proportional valve, c) pressure relief valve, d) external gear pump, e) open system oil tank, f) electric motor, g) frequency inverter and h) battery. No energy is recovered during lowering, and the potential energy of the load is converted into heat in the control valve. The grey line illustrates movement of flow during lifting motion and the black line during lowering motion.

2.2.1 Conventional hydraulic components

Hydraulic Pumps and Motors

Basically, hydraulic pumps and motors can be classified as positive and non-positive displacement hydraulic machines. The classification of pumps is further illustrated in Figure 2.2. Hydraulic motors closely resemble hydraulic pumps in construction (Airila, 1995). For this reason, a hydraulics motor can be rated according to the same principle as pumps. Pumps operate on the displacement principle. A certain volume of non-compressible low pressure fluid is taken into the pump and, in practice; the same volume (minus leakage) is displaced to another point where the load defines the pressure. Pumps that discharge volumes of liquid separated by periods of no discharge are called the positive-displacement type. There are, however also other types of pumps that discharge liquid in a continuous flow. They are of the non-positive-displacement type, but are normally not used in hydraulic systems.

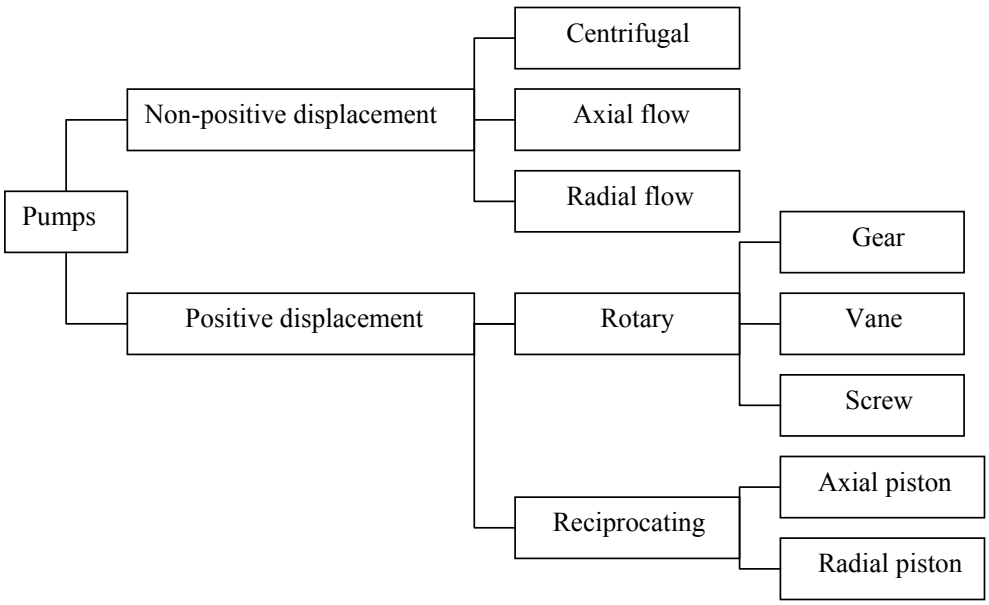

Figure 2.2: Classification of principal types of pumps (Majumdar, 2002).

Positive-Displacement Pumps. In a positive displacement pump, a definite volume of liquid is delivered for each cycle of pump operation, regardless of the resistance, as long as the capacity of the power unit driving the pump is not exceeded or the input flow does not cause cavitations, in which case the output is also limited. If an outlet is completely closed, the unit driving the pump will either stall or break. Therefore, a positive-displacement-type pump requires a pressure-relief valve in the system.

Non-positive-Displacement Pumps. In a non-positive-displacement pump, the volume of liquid delivered for each cycle depends on the resistance provided to the flow. The pump produces a force applied to the liquid that is constant for each particular speed of the pump. Resistance in a discharge line produces a force in the opposite direction. When these forces are equal, the liquid is in a state of equilibrium and does not flow. If the outlet of a non-positive-displacement pump is completely closed, the discharge pressure will rise to the maximum for a pump operating at maximum speed. The pump will just churn the liquid and produce heat, but nothing will break immediately when the flow is blocked and the pump is running. This type is normally not used in hydraulics, but is common in all other types of processes.

In positive displacement pumps, the displacement is the amount of liquid transferred from a pump's inlet to its outlet in one revolution or cycle. There are two types of positive displacement pumps – reciprocating and rotary pumps. Reciprocating pumps are normally piston pumps and rotary pumps are gear pumps. The gear pumps always

have a fixed displacement, but in reciprocating pumps the displacement can be either fixed or variable.

- *Fixed-Displacement Pump*. In the fixed-displacement pump, the output can be changed only by varying the drive speed. The pump can be used in an open-centre system, where the pump output has a flow path back to a reservoir.
- *Variable-Displacement Pump.* The variable-displacement pump is always an axial piston pump, in which the piston stroke lengths can be changed. In such a pump, the flow can be changed either by changing the displacement per rotation or changing the drive speed or controlling them both simultaneously. The pump can be used in a closed-centre system where the pump continues to rotate and keeps the pressure against the load with zero displacement. Only the leakage is compensated by a small positive displacement control setting.

Rotary pumps are commonly used in oil hydraulic systems in low to medium pressure systems. Although there are various rotary pumps, the three prime types are gear, vane and screw pumps. Sliding type vane pumps and screw pumps are not used in mobile machines and will not be described here in more detail.

Gear pumps, however, are important. There are two principal types of gear pumps: external and internal. The construction and operation principles of these pumps are illustrated in Figure 2.3.

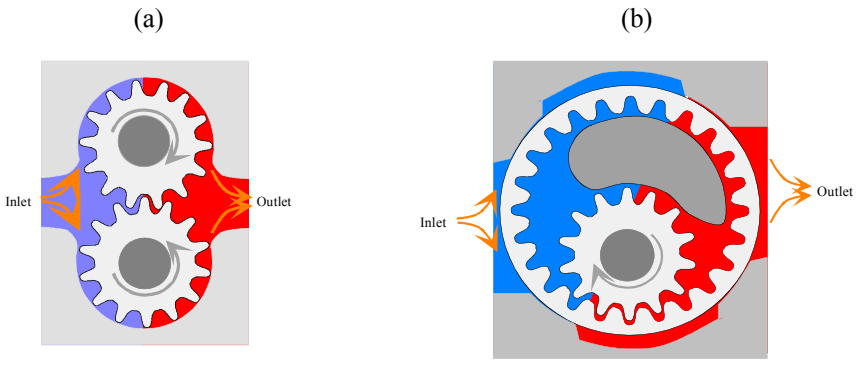

Figure 2.3: a) External gear machine, b) Internal gear machine, schematic drawings (Fig. courtesy of Prof. Pyrhönen).

In an external gear pump, the two identical gears are externally meshed. The inlet port is facing the gear retracting region. Fluid is drawn in a trap between the pairs of teeth in each gear during rotation. This volume of fluid is transported by the two cogwheels into the gear meshing region, and the pump outlet. Fluid leakage between teeth and housing is considerable in gear pumps because the volume changes are small. The advantages of the external gear pumps are their robustness and low price.

An internal gear pump is a multi-purpose device. It can be implemented for wide viscosity and temperature ranges. A gear pump or motor consist of two meshed cogwheels, suitably housed with a shaft to one of the gears. An internal gear pump is well known as a silent machine. It consists of an inner and an outer gear separated by a crescent or a moon-shaped piece which acts as a seal. Both cogwheels rotate in the same direction, but the inner cogwheel is faster than the outer cogwheel. (Majumdar, 2002) The internal gear pump produces a fairly non-pulsating flow and can run dry for short periods. It is, at least in principle, also bi-directional, meaning that the same pump can be used to rotate in both directions. Often it can also be applied both as a motor and a pump. Internal gear pumps are reliable and easy to maintain since they have only two moving parts and only one stuffing box (Pump School, 2007).

Reciprocating pumps consist generally of cylinders with pistons. In a cylindrical housing, the pressure producing cylinders and pistons are normally placed in a circle, and the crankshaft is replaced by a swash plate as the machine operates in a rotary form. Because of the capability of operating against high pressure, piston pumps are used for specialized applications. Schematic diagrams of axial piston hydraulic pumps are shown in Figure 2.4. The pump can be of either a straight axis or bent axis construction. In the straight axis construction, the displacement is often controllable, while in the bent axis type, the displacement remains constant.

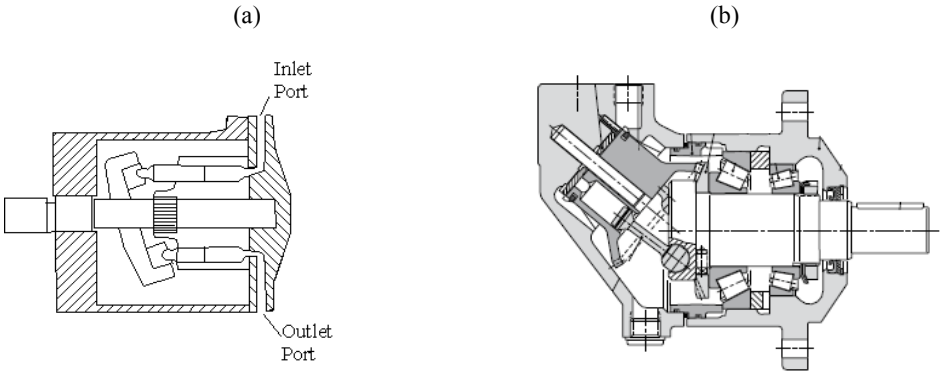

Figure 2.4: a) Axial piston pump (de Silva, 2005). The cylinder block is attached to the shaft with a spline (shown in the figure) forcing the cylinder block and the pistons to rotate. The inclined stroke plate is gliding against a lubricated bearing system on the left. b) Bent-type axial piston motor with fixed displacement (Parker, 2007). The cylinder block and the pistons rotate inside the barrel. The torque exerted on the cylinder block is transmitted by the conical cogwheels attached at the ends of the cylinder block and the driving shaft. The piston rods have spherical bearings against the driving shaft.

In the straight axial piston pump, the chamber barrel is rigidly attached to the drive shaft. The pistons themselves rotate together with the chamber barrel. The end shoes of the pistons are sliding inside a lubricated slanted slot on the stationary stroke plate and

the pistons are forced into a reciprocating motion. As a chamber opening reaches the inlet port of the pump housing, fluid is drawn in. The fluid is then trapped and transported to the outlet port and a displacement is generated as a result of the decreasing volume inside the chamber because of the axial motion of the piston (de Silva, 2005).

By increasing the inclination angle of the stroke plate in the straight axis pump, the piston stroke and the pressure ratio of the pump can also be increased. A lever mechanism is usually available to adjust the piston stroke. A disadvantage of this type of pump is that it is relatively expensive (de Silva, 2005).

According to Merritt (1967), bent-axis machines are quite rugged, efficient and can be used for hydraulic control in industrial systems. The bent-axis machine uses valve plate porting. Fluid is ported by valve plate to one half of the cylinder barrel and forces the pistons in that portion of the barrel away from the valve plate. These pistons rotate the drive shaft as they move to the maximum distance from the valve plate because the piston axis is bent from that the drive shaft. The cylinder barrel is driven through a gear with the shaft that receives torque from the prime mover **(**Merritt, 1967).

Depending on the application, a designer needs to choose what kind of a pump is required for that application. Pressure, efficiency, flow and price must be taken into account. It can be seen that piston pumps have high efficiencies compared with other pumps.

Typical performance curves of different types of pumps are shown in Figure 2.5.

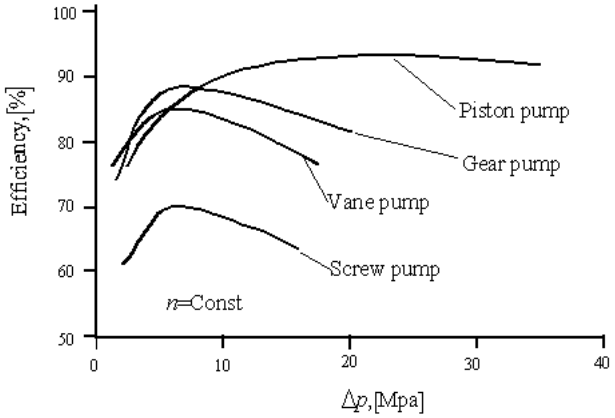

Figure 2.5: Typical efficiencies of different hydraulic pump types (Kauranne, 2006).

A positive displacement pump cannot provide absolutely constant flow. Small pulsations in the flow speed are called the flow ripple. Generally, the ripple causes noise as it makes the hydraulic hoses and pipes vibrate at the ripple frequency. Normally, the

hydraulic system construction filters the ripple so that no ripple in the cylinder piston speed can be observed. Figure 2.6 shows the range of positive displacement pump designs and their relative noise characteristics. The axial piston pump is inevitably the noisiest of the pumps, which of course is a drawback of the pump type.

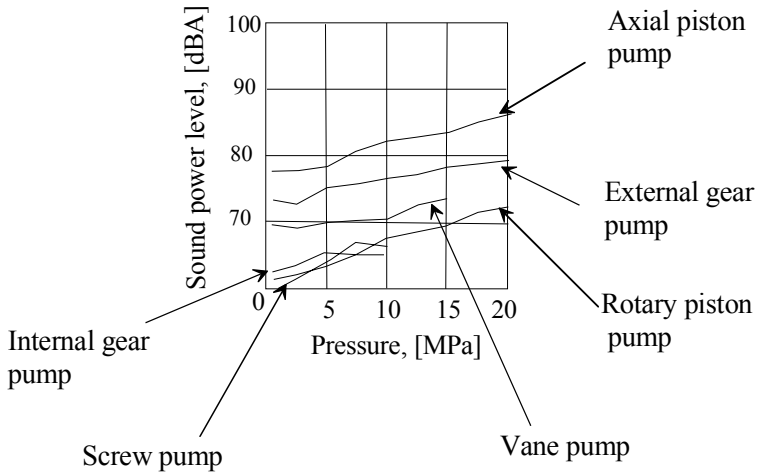

Figure 2.6: Range of positive displacement pump designs and relative noise characteristics (Watton, 2007).

The theory of pressure pulsation is relatively complex. Pressure pulsation depends on the type of hydrostatic machine, working pressure level and in general the pump design. For some applications, the most important requirement is the pressure level and the volume flow.

The pulsating generation of the flow in hydraulic systems works according to the displacement principle. Flow pulsation Δq, or the flow ripple, is the difference between the repetitive maxima and minima of the flow as a function of time. Pulsation occurs at a frequency that is dependent on the filling and emptying of the displacement chambers. The volume flow ripple changes the pressure respectively, if the discharge cross-section is constant. Because of the almost incompressible fluid, the pressure pulsation will produce noise in the system. There are also other possible sources of noise for instance produced by mechanical parts: inaccurate toothing in gears (Manring, 2003), housing and bearing defects. There are also different forms of pulsation: kinematic, kinetic, compression and leakage pulsation. The basic frequency of the flow pulsation is the product of the number of gear teeth (for an external gear pump) or the amount of pistons (for an axial piston pump) and the rotating speed of the pump shaft. The pressure pulsation, similarly to the flow pulsation, is the difference between the maximum and minimum values of the pressure level.

There is also a per unit variable that can be used to describe the level of the pressure pulsation:

$$\delta_{\mathrm{p}} = \Delta p_{\mathrm{st}}/p_{\mathrm{st}}\,, \tag{2.4}$$

where δ_{p} is the pressure pulsation grade, Δp_{st} is the pressure pulsation and p_{st} is the static pressure level. The pressure pulsation, however, is not directly related to the pump but the system also has an effect, which makes the matter complicated.

Kinematic pulsation or so called air-borne noise (ABN) is a result of the volume flow pulsation produced by the geometrical characteristics of the pump. The simplest way to reduce kinematic pulsation is increasing the number of displacement chambers.

Kinetic pulsation naturally exists only in valve-controlled displacement devices. Mechanical elements of valves generate an oscillation effect, and as a result, pulsation. This kind of noise is called structure-borne noise (SBN).

Compression pulsation is pulsation caused by compression when fluid enclosed in the displacement chamber switches between high- and low-pressure chambers. It is also called fluid-borne noise (FBN). In hydraulic piston machines, compression pulsation can be more important compared with kinematic pulsation.

Leakage pulsation is generated by leakage flow in the pump from the high- to the low-pressure side. kage pulsation begins to influence the total pressure pulsation when the system pressure is increased. Also fluid viscosity, temperature and fluid compression affect leakage pulsation. It is equally difficult to estimate leakage and compression pulsation. Because of the difficult mechanism of producing pulsation, we will speak about flow pulsation. Theoretically, all positive displacement pumps are designed to displace volumes of flow. If the discharge volume is plotted against the angular position of vanes, the flow produces a sinusoidal curve. This is the case with most vane and piston units. In the case of gear pumps, sinusoidal dependence may also be assumed. Some authors call this flow periodic, but not sinusoidal. For our theoretical assumption, we will use the sinusoidal theory of pulsation. The volume flow by a single piston q_{n} can be calculated as

$$\alpha = \Omega t, \tag{2.5}$$

$$q_{\mathrm{n}} = \frac{\Omega \cdot V_{\mathrm{th}}}{\pi \cdot n} \cdot \sin\left(\alpha + (i-1)\cdot \frac{2\pi}{n}\right), \tag{2.6}$$

$$Q(t) = \sum_{1}^{n} q_n = \sum_{1}^{n} \frac{\Omega(t) \cdot V_{\mathrm{th}}}{\pi \cdot n} \cdot \sin\left(\alpha + (i-1)\cdot \frac{2\pi}{n}\right), \tag{2.7}$$

where α is the angle, Ω is the rotating angular speed of the pump shaft, Q is flow, V_{th} is pump displacement per revolution, t is time, and n is the amount of pistons.

Equation (2.6) gives positive values for the output and negative values describe the pump input. To achieve a positive flow, the sum of positive volumes of all *n* pistons is calculated (Equation 2.7).

Pulsation is typical for all positive displacement pumps (Lilan, 2007). The flow ripple, the pressure ripple and also noise generated by an axial piston pump are relatively large compared with the rest of the positive-displacement pumps, as shown in Figure 2.6. A piston pump with a single piston has a sinusoidal delivery curve as one input and one output pulse during one complete rotation. Figure 2.7 shows the principal delivery pattern of a piston pump with five pistons.

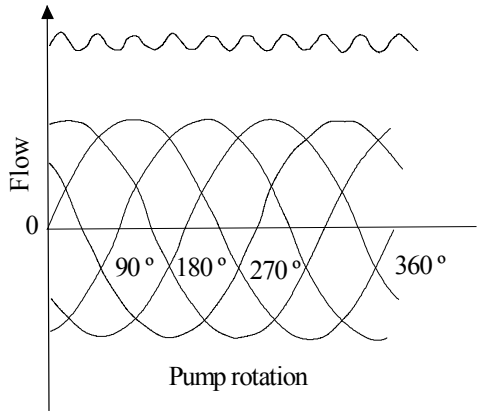

Figure 2.7: Piston pump delivery pattern with five pistons with constant shaft speed (Majumdar, 2002)

With several pistons, the delivery schedule of the pump does not remain as simple as it is for a single piston. For instance, a piston pump that has an even number of pistons produces a volume flow which has an even number of symmetrical half waves in one revolution. If a pump has an odd number of pistons, the output curves are characterized by an increasing amount of half waves and a lower magnitude of pulsation (Manring, 2000).

Figure 2.8 shows that with an increasing number of pistons, the flow ripple decreases. However, this implies an increasing price of the hydraulic machine.

The pulsation of flow, pressure, seems not to be a mechanical problem in a forklift application. Piston pumps, however, produce significantly more noise than the gear pumps as it was shown in Figure 2.6. This kind of an application is not sensitive to high-frequency mechanical oscillations but also in a forklift application silent operation should be a benefit. There are also applications that require quiet and noiseless behaviour, and also accurate flow or pressure characteristics. Because of this, the first methods to reduce FBN were introduced over 30 years ago based on high-frequency

flow fluctuation by using a fast-response servo valve and auxiliary valve. During the following decades, designers concentrated to find a mechanical solution to reduce the pulsation and noise. Harrison and Edge (2000) introduced in their paper a heavily damped check valve (HDVC) that was supposed to "prevent rapid switching action, but retain the self-tuning characteristic necessary for a reduction in flow ripple." Of course, there are other ways to reduce the ripple and the noise. Casoli proposes a new optimized design of an external gear pump (Casoli, 2008), Johansson introduced a change cross angle to reduce noise and vibration in piston pumps (Johansson, 2007). An active control method for FBN was proposed in the dissertation work by L. Wang (2008). Quite a popular and inexpensive method is to use a throttled hydraulic accumulator together with flexible hoses as an RC filters effective at the lowest practical pump speeds. An elegant but expensive way to reduce kinematic pulsation is to increase the number of displacement chambers and use odd numbers, as it was shown above. Due to this fact, there are many other techniques for flow ripples and noise reduction. We can conclude that most of them are based on mechanical systems where multiple pistons and a combination of servo valves and hydraulic accumulators are used as filters. In addition to the noise problem, it was shown by Mehta (2006) that the input shaft torque of the hydraulic pump correlates with the noise. This torque ripple results from discrete piston locations within the pump. It is a reason for the oscillating torques on the shaft (Roccatello, 2009).

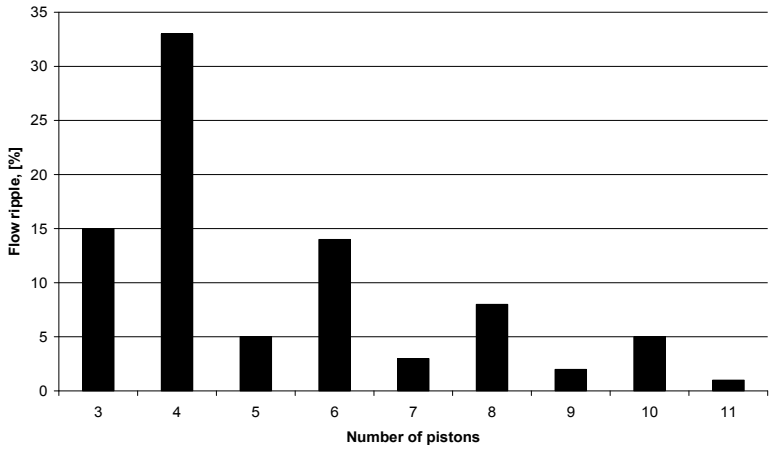

Figure 2.8: Ripple magnitudes for an axial piston pump (Minav, 2011a).

For the current application, it is necessary to find a hydraulic machine suitable for energy recovery. Airila (1995) stated that pumps and motors are similar by construction. Akers (2006), however, claims that it is not universally true. Retailers usually give only negative answers because manufactures, in general, design pumps and motors for specific purposes. For example in a vane pump, the vanes press against the chamber

walls with the help of centrifugal force, but in motors this has to be achieved with springs. Often in pumps the suction inlet is larger than the pressure outlet. Instead, in many motors both connections are of the same size. Also, if a pump can be used to rotate in both directions, it often has high pressure seals on both sides of the chamber of the pump. In contrast, for one directional pumps these high pressure seals are only needed on the high pressure side (Airila, 1995).

The bent axial piston motor seems to be the most universal machine. In pumping, fluid is fed to the low pressure side and then delivered via the pistons to the high pressure side. While pumping, the low pressure side is "the inlet" and the high pressure side is "the outlet". The motor function is the opposite of the pump function. During motor operation, pressurized oil is fed into the inlet. The pistons move up and down within the cylinder block bores. The cylinder block is caused to rotate by pistons and an output torque is produced at the drive shaft. Axial piston units may be operated both as hydraulic motors and pumps. In some cases, pre-pressure is needed to avoid input cavitations while pumping.

The latest development in multi-purpose hydraulic machines is the variable displacement machine called the mooring pump. It can operate with variable displacements both as a motor (negative displacement) and a pump while always rotating in the same direction. This device is especially suitable for hydraulic energy recovery in diesel-electric parallel hybrid drives where the potential energy can be converted to mechanical energy and further delivered to another mechanical load or converted into electricity by the hybrid electrical machine attached to the diesel crankshaft. According to the knowledge of the author, such a machine is only available from Bosch Rexroth (Rexroth, 2010).

One of the latest inventions that can be used in regenerative application in working mobile machines is Artemis hydraulic machine. In this piston machine port plates are replaced with computer-controlled high-speed solenoid valves. The principle is similar as in the pump by Linjama in Figure 2.9. By controlling the sequence of cylinder enabling, the machine can pump fluid to an actuator or let it go back to the tank at an averagely infinitely variable flow-rate. From electrical engineering point of view the Artemis pump applies the same principle as the pulse with modulation (PWM) technology. According to (Artemis, 2010), this digital displacement hydraulic machine has over 90% efficiency, even at partial loads and at high pressures. According to the knowledge of the author, the pump is at the moment not yet commercially available and, therefore, it was not taken in the practical study. It is, however, obvious that the Artemis pump supports the idea of direct pump control.

An alternative way is to use a digital motor-pump, which is described by Linjama in his publication (2009b). This digital pump working principle resembles the Artemis pump principle, and the pump consists of several reciprocating pistons connected to the same mechanical axis, see Figure 2.9. The Artemis pump is a radial pump whereas this Linjama pump is an in-line piston pump. In the Linjama piston pump, each piston has

two active on-off valves. Depending on the state of the valves and the direction of the movement of the piston, the machine can work as a hydraulic motor or a hydraulic pump. An important difference, according to the author, between digital and traditional pump technology is the option to program the process (Linjama, 2009b).

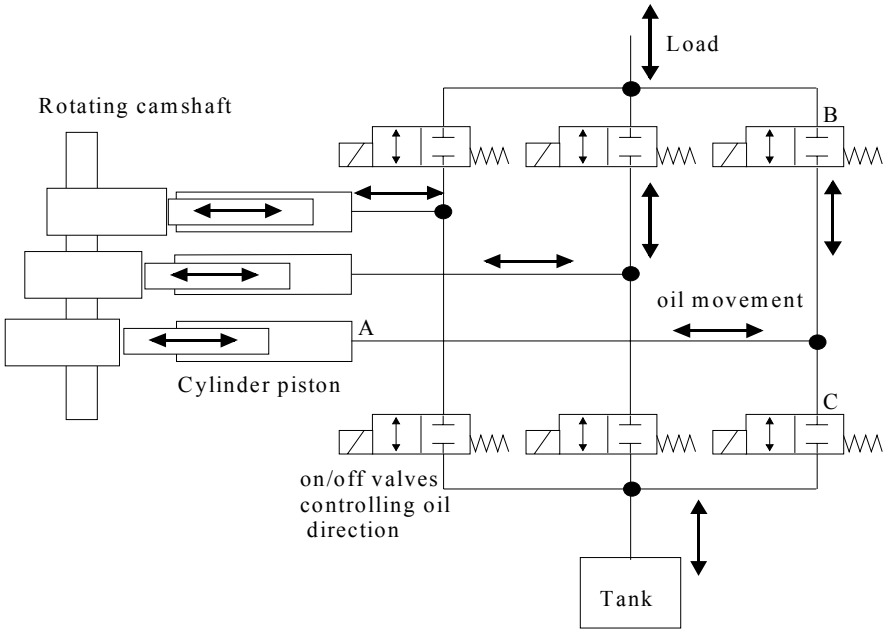

Figure 2.9: Hydraulic circuit diagram of the three-piston digital in-line pump-motor with a camshaft pushing the pistons (modified from Linjama, 2009b). The flow can be "digitally" PWM controlled by opening or closing the on/off valves in a suitable sequence, however, ensuring that the flow is never blocked. For example, the cylinder A has just filled with the oil from tank via the valve C or the load potential energy (via valve B) has pushed the piston to the left. The piston is now ready to push the oil to the line again. Depending on the position of valves B or C it will be delivered to the load or to the tank. Other cylinders and valves work accordingly. The system is capable of PWM fluid flow pulses, which probably makes the system noisy.

Valves

Valves are the most important mechanical links to the fluid interface in hydraulic systems. Basically, there are four main categories of valves in hydraulics. Let us consider them further.

Pressure valves are used to control actuator forces and to determine pre-select pressure levels: *pressure relief valves* limit the maximum permissible system pressure. This valve diverts some flow to the tank if the pressure setting of the relief valve is reached. This valve is needed to control the maximum pressure and to protect the system from

excessive pressure peaks. The relief valve is in the closed condition under normal operation. The spring force, which closes the valve, is adjustable.

Pressure reducing valves limit and maintain a constant downstream pressure that is smaller than the system pressure regardless of pressure fluctuations in the main circuit upstream.

Flow valves are used to control the rate of flow from one part of the hydraulic system to another. They limit the maximum speed of actuators and limit the maximum power available to the sub-circuit by controlling their flow. The poppet valve, gate valve and globe valve are typical on/off flow control valves, meaning that they either let oil flow or prevent oil from flowing.

Directional valves are used as multi-polar switches. They control the flow of oil by changing the paths of the flow to different directions. A schematic diagram of a directional control valve is shown in Figure 2.10. In directional control valves, the flow paths may be connected in two ways: 1) the supply port to an outlet port and simultaneously the other load side to the tank (P to A and B to T), or 2) P to B and A to T. All the flow paths through the valve may also be blocked. This is affected by shifting the internal parts of the valve in the middle. The internal part can be a poppet or a spool. The spool movement can be affected by a spring, by a mechanical system, by pressure, by electrical means (solenoid for instance) or by possible variations in the combinations. (Majumdar, 2001)

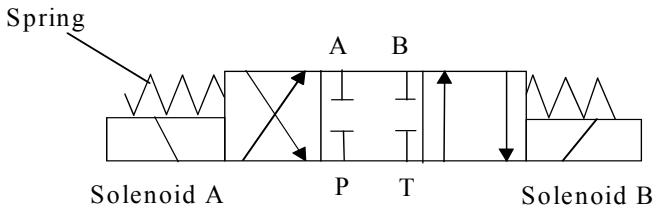

Figure 2.10: Direct-acting solenoid directional ¾ valve.

These valves are usually defined by the number of connections and the different operating positions they have. Most of these valves are used for sequential operation with fixed operating positions, but there are also so called *servo valves* that have an infinite amount of operating positions and are usually adjusted by an electric input signal. A *proportional valve* is also electrically controlled, enabling the volumetric flow rate at the valve output to be controlled proportionately to an electrical input signal. Basically, the proportional control valves are solenoid operated valves with electrical position feedback control. The solenoids mounted with such valves are of a proportional type and can be modulated electrically. The spool movement is measured by an inductive position sensor and the output is fed back to the proportional amplifier, which helps in compensating the input signal.

Check valves are the special type of directional valves that consist of a truncated cone forming a seat, a ball that sits in the cone, closing it from reverse flow, and a preloading spring. The electrical counterpart is a power diode. Check valves permit fluid flow in one direction, blocking the flow in the reverse direction. When there is no fluid flow, the spring provides force for the ball to return it to the seat (Mohieddine, 2003).

An additional example of a directional valve is shown in Figure 2.17b. It is a two-way normally closed poppet valve or counter balance valve. This valve is usually used to prevent the accidental dropping of the load.

Hydraulic actuator

A hydraulic actuator receives pressure energy from the pump and converts it to the mechanical force and motion of the load. An actuator can be linear or rotary. A linear actuator gives force and motion outputs in a straight line, and it is commonly called a hydraulic cylinder. A cylinder is a hydraulic actuator consisting of a piston or plunger that operates in a cylindrical housing by the action of liquid under pressure. The cylinder housing is a tube in which the plunger (piston) operates. The piston rod end of a piston cylinder is used to actuate the load. The end opposite to the rod end is a head end. Graphic symbols of the above-mentioned valves, pumps and cylinders are illustrated in Appendix B.

The four most common types of hydraulic cylinders are shown in Figure 2.11.

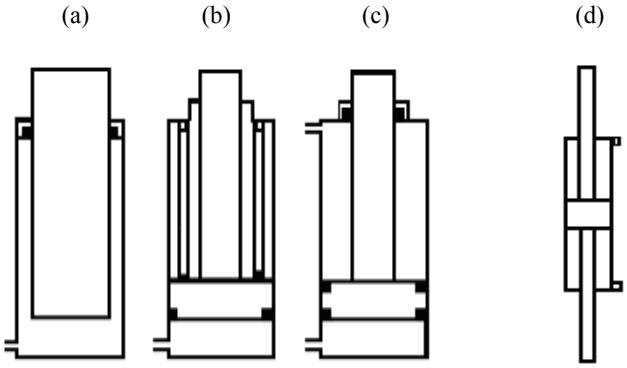

Figure 2.11: Four of the most common types of hydraulic cylinders. a) Single-acting cylinder, b) single-acting cylinder with spring providing movement backwards, c) double-acting non-symmetrical cylinder with both sides hydraulically operated, d) symmetrical double-acting cylinder (Principles of Hydraulics, 1973).

2.2.2 Electrical components

The electric part of the forklift drive can be divided into an energy storage, an electric machine and its control part, that is, a converter. A detailed analysis of the latter two components will be shown in Section 2.3.

Converter

Converters used in low power electro-hydraulic systems are typically two-level converters according to Figure 2.12.

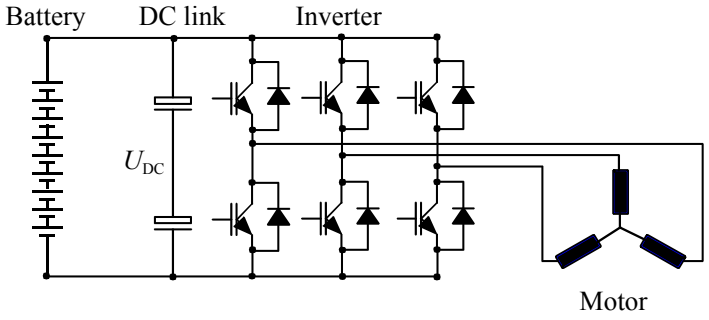

Figure 2.12: Battery supplied two level frequency converter main circuit with DC link capacitors and conductors, an IGBT inverter bridge and a motor three phase winding (Pyrhönen, 2010).

The model of the converter control principle is given in Section 3.2.2.

Motor

Usually, induction machines are used as primer movers in mobile working machines. In our research permanent magnet synchronous servomotors have been used instead because of their high efficiency, high dynamic performance and good control characteristics. These servomotors can also be heavily overloaded. For instance, a CFM90M servo motor by SEW-Eurodrive was used. Its rated and measured parameters are listed in Table C.1 in appendix C. Appendix C contains detailed information of calculating the per unit values. In the motor magnetic circuit calculation and measurements, the stator leakage was found to be $L_{s\sigma} = 0.0962$ pu, and the magnetizing inductance $L_{md} = L_d - L_{s\sigma} = 0.206$ pu. Because of the rotor surface magnets and the resulting very large effective air gap, the magnetizing inductance and thereby also the armature reaction are small and the overloading capability large. It can also be seen that at the rated load, the per unit stator copper loss is approximately 3.6%, and hence, when operating at three times the rated load $i_{s,\,pu} \approx 3$, we obtain 32.4% losses compared with the rated power (Minav, 2011b). The overloading of a servo motor is characterized by the requirements for high and short power peaks. A typical overload capacity varies

between 200% and 300% of the rated torque (Sebastian, 2002). The frequency converter cannot be overloaded similarly to the motor. For a converter, a 150% overload can typically be used for a short time, but not regularly. Such regular overloading is not recommended for IGBT bridges, as heavy thermal cycling easily disintegrates the IGBT structure (Semikron, 2009).

2.3 Efficiency of electro-hydraulic systems

Figure 2.13 shows a conventional hydraulic circuit. Internal leakage in an actuator causes losses and oil overheating and actuator drift, therefore worsening the position control. Internal leakage and sticking in the control valve cause noise and prevent of spool movement. Internal leakage in the pump causes insufficient pressure generation, flow drop, and possible overheating, vibration and noise.

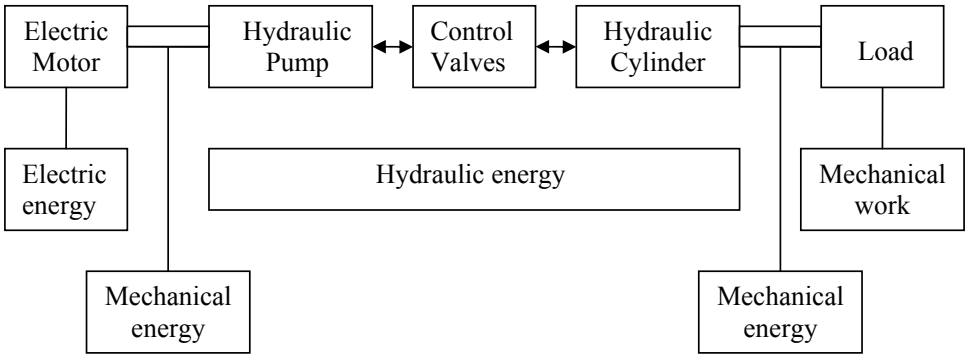

Figure 2.13: Conventional hydraulic circuit (Minav, 2011e).

Let us consider further the main reasons of losses in an electro-hydraulic servo drive. In addition to the above-mentioned hydraulic losses, there are electrical losses in the electric motor drive system. Electrical losses consist of the losses inside the converter and in the electrical machine.

Converter losses

The converter losses take place mostly in the converter DC link, converter internal consumption (powering the gate drivers, processor, cooling fans, etc.) and the inverter bridge switches. The main losses of power electronic switches are static losses, switching losses and driving losses. Static losses include conduction (on-state) and blocking losses. Switching losses include turn-on (E_{ON}) and turn-off (E_{OFF}) losses. (Miller, 2008) Driving losses are IGBT gate driver losses. Gate driving and blocking losses are small and can be neglected. Inverter losses can be regarded as a function of the inverter DC link voltage U_{DC} and the load current i_{load} (Minav, 2011b).

Owing to the high efficiency and control demands, a 400 V servo motor inverter ACSM1 DTC-based converter by ABB was used. Direct torque control (DTC) (Luukko, 2000) technology allows the drive to adjust itself to varying application needs. Hydraulic system position control is possible in the open- or closed-loop control by using an ACSM1. The converter applies FS 100 R12KT4 power modules by Infineon (Infineon, 2010). The rated values for the components are 1200 V and 100 A, and the peak repetitive current is 200 A.

The converter losses take place mostly in the semiconductors and in the auxiliary power systems. The rated RMS current of the converter is 46 A and the maximum current of the converter is 80 A. In many cases studied in the literature, the converter operates at quite a low power compared with its rated values. In such cases, the converter efficiency remains somewhat low. According to ABB, the rated efficiency of the ACSM1 is approximately 98% at nominal power (ABB, 2007).

The switching losses can be calculated using the switching energies given by the component manufacturer. The average switching loss power is defined using the switching energies as

$$P_{\mathrm{sw}} = f_{\mathrm{sw}}(E_{\mathrm{ON}} + E_{\mathrm{OFF}}), \tag{2.8}$$

$$E_{\mathrm{ON}} = E_{\mathrm{IGBT,ON}} + E_{\mathrm{Diode,OFF}} \approx \frac{1}{6} U_{\mathrm{DC}} t_{\mathrm{r}} i, \tag{2.9}$$

$$E_{\mathrm{OFF}} = E_{\mathrm{IGBT,OFF}} + E_{\mathrm{Diode,ON}} \approx \frac{1}{6} U_{\mathrm{DC}} t_{\mathrm{f}} i, \tag{2.10}$$

where a hard-switched inverter is assumed and the inverter current and voltage during the transitions are linear, forming triangular loss power behaviour. The switching waveform rise time t_{r} and fall time t_{f} determine the switching energy together with the DC link voltage U_{DC} (Miller, 2008).

The DTC algorithm with a 3 kHz average switching frequency was used in the definition of the converter efficiency. The efficiencies were simulated by realizing all necessary stable operation points in the simulator and describing the motor with its vector equivalent circuit presentation divided into direct and quadrature axes. All transistor turn-ons and turn-offs, diode turn-on and turn-off losses and conduction losses were calculated separately and summed during one period T using all switchings n_{sw} (Minav, 2011b).

The converter average efficiency is obtained with the output and input energies calculated during a period of stable operation T:

$$\eta_{\text{Conv}} = \frac{E_{\text{in,Conv}} - E_{\text{Conv loss}}}{E_{\text{in,Conv}}} \quad (2.11)$$

Based on the converter component and the motor control information, an efficiency chart for the converter was calculated (Figure 2.14) (Minav, 2011b). Figure 2.14 shows the results for the ACSM104x[4)]x[5)]-046A-4 at different rotational speeds and torques. The internal power losses in this case are in the range of 100 W.

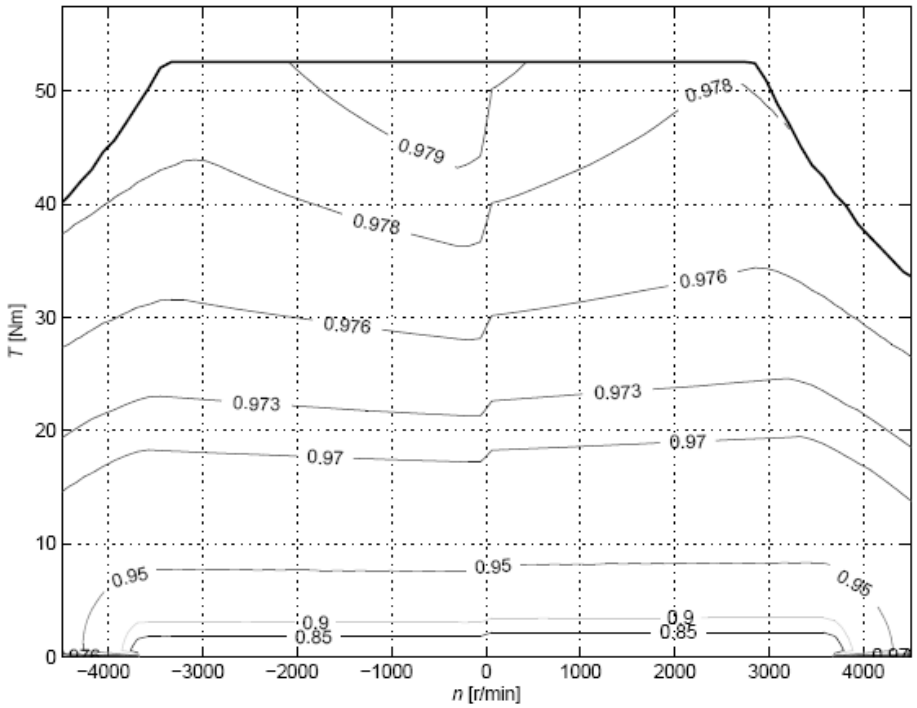

Figure 2.14: Efficiency chart for the 46 A RMS, a 400 V ACSM1 converter driving the servo motor CFM90M with i_d = 0 control used in the tests (Minav, 2010b) (Fig. courtesy of P. Immonen).

Electrical machine losses

Power losses in electrical machines are composed of the following elements: resistive losses in the stator and in the rotor (in the case of an induction machine or a synchronous machine), iron losses, additional losses and mechanical losses. In our case, we have a permanent magnet synchronous machine (PMSM) having no fundamental rotor losses.

The electrical power lost in the PMSM stator winding resistance is called *copper loss*. The copper loss varies with the load in proportion to the current squared and the resistance of the stator, and can be expressed as

$$P_{\mathrm{Cu}} = 3R_{\mathrm{s}} \cdot I_{\mathrm{s}}^{\,2}, \tag{2.12}$$

where R_{s} is the stator resistance and I_{s} the stator current. The efficiency decreases with the increasing temperature as the resistance increases. Stray losses are the losses that remain after primary copper and secondary losses, iron losses and mechanical losses. The largest contributions to the stray losses are harmonic energies generated when the motor operates under load. These energies are dissipated as currents flow in the copper windings, harmonic flux components move in the iron parts and leakages affect the laminate core. Depending on the PWM switching frequency, the overall efficiency of the motor is typically 1–2% lower in a PWM supply than in a sinusoidal supply (Aarniovuori, 2010; Mohan, 2003; Wu, 2006).

Iron losses are of two different types: hysteresis losses and eddy current losses. Depending on the PWM switching frequency, the overall efficiency of the motor is typically 1–2% lower in a PWM supply than in a sinusoidal supply (Aarniovuori, 2010). Iron losses were estimated based on measurement results. The machine has a no load iron loss resistance R_{Fe}, which depends on the rated frequency resistance $R_{\mathrm{Fe,0}}$ and the operating frequency:

$$R_{\mathrm{Fe}} = \frac{R_{\mathrm{Fe,0}}}{\left(\frac{f}{f_{\mathrm{n}}}\right)^{\frac{3}{2}}}. \tag{2.13}$$

Iron losses were estimated based on the calculated no load iron losses $P_{\mathrm{Fe,0}}$ by

$$P_{\mathrm{Fe}} = P_{\mathrm{Fe,0}}\left(\frac{f}{f_{\mathrm{n}}}\right)^{\frac{3}{2}}. \tag{2.14}$$

The machine stator resistance and no load power were measured. The no load friction was evaluated by using traditional machine design methods (Pyrhönen, 2008). The varying *additional losses* were estimated based on the rated additional losses $P_{\mathrm{ad,rl}}$ by

$$P_{\mathrm{ad}} = P_{\mathrm{adrl}} \cdot \left(\frac{I}{I_{\mathrm{n}}}\right)^{2} \cdot \left(\frac{f}{f_{\mathrm{n}}}\right)^{\frac{3}{2}}. \tag{2.15}$$

Mechanical losses include friction in the motor bearings and the fan for air cooling. Bearing losses depend on the shaft speed, bearing type, properties of the lubricants and the load (Pyrhönen, 2008).

Figure 2.15 illustrates the efficiency charts of the CFM90M test motor calculated using the measured machine parameters in a fixed temperature as described in the article by Ruuskanen (2011).

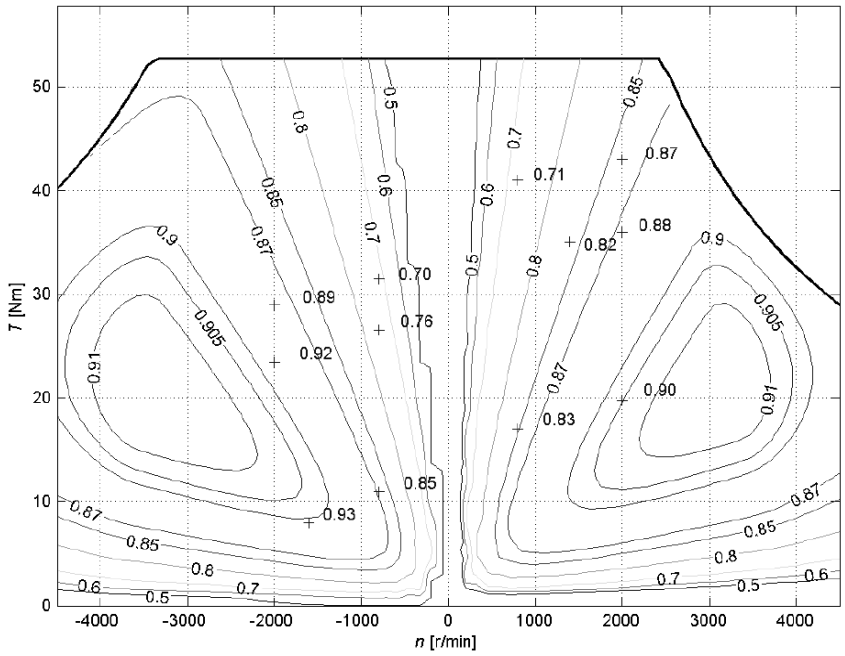

Figure 2.15: Efficiency chart calculated for the CFM90M test motor. Some measured efficiency points in lifting and lowering are indicated with + signs (room temperature) (Minav, 2010b) (Fig. courtesy of P. Immonen).

Pump losses

*Losses in pumps***.** Lack of pressure can be explained by the leakage path in a system. A badly worn pump has difficulties in producing the desired pressure. However, flow loss is frequently caused by leaks also somewhere else in the system (valves, cylinders and motors). Cavitation noise is induced by a restriction in an inlet line, a dirty inlet filter, or too high a drive speed. Air in a system also causes noise. Air will severely damage a pump because it will not have enough lubrication. This can occur from low oil in the reservoir, a loose connection in an inlet, a leaking shaft seal, or no oil in the pump before starting. Also, noise can be caused by worn or damaged parts, which will spread harmful particles through a system, causing more damage if operation continues.

Slippage is oil leaking from a pressure outlet to a low-pressure area or back to an inlet. Some slippage is designed into hydraulic machine for lubrication purposes. Slippage will increase with pressure and as the pump begins to wear. Oil flow through a given orifice size depends on the pressure drop. An internal leakage path is the same as the orifice. Therefore, if pressure increases, more flow will occur through a leakage path and less from an outlet port. Any increase in slippage is a loss of efficiency.

Pipe losses

Losses in pipes take place for instance as a result of pipe friction and leakages. It has been shown that the higher the viscosity of oil is, the greater the loss of energy, and the lower the oil viscosity is, the higher the leakage losses. Oil energy is also lost as a result of the presence of various types of valves, pipe fittings, tees, elbows, and the like. The resistance loss in a pipe can be calculated by using various empirical formulae. The head loss in a straight pipe is determined by the following equation:

$$h_{\mathrm{p}} = \lambda \cdot \frac{v}{2g} \cdot \frac{l_{\mathrm{p}}}{d_{\mathrm{p}}}, \tag{2.16}$$

where h_{p} is the head loss, λ is the friction coefficient, v is the flow velocity of oil, g is acceleration due to gravity, d_{p} is the inside pipe diameter, and l_{p} is the length of the pipe (Majumdar, 2002).

In head losses in pipe fitting, valves are proportional to the square of the fluid velocity:

$$h_{\mathrm{f}} = \frac{K \cdot v^2}{2g}, \tag{2.17}$$

where h_{f} is the head loss in fitting, and K is called the K-factor for valves and fittings. Table 2.1 illustrated values for some valves and fittings (Majumdar, 2002).

Table 2.1: Values of K factor (Majumdar, 2002).

Fittings	Values of K-factor
Check valve- ball type	4
Tee	1.8
Elbow (standard)	0.9
Elbow 45°	0.42

Cylinder losses

Hydraulic cylinders are compact and relatively simple. The key points to watch are the seals and pivots for avoiding *External Leakage and Internal Leakage*. Leakage past the piston seals inside a cylinder can cause sluggish movement or settling under the load. Piston leakage can be caused by worn piston seals or rings or scored cylinder walls. The dirt, grit and air in the oil cause damage and leakage in the cylinder. The total frictional losses vary from 2 to 5% (8% of the theoretical force as the maximum), the value increasing with an increase of pressure (Majumdar, 2002).

Total hydraulic losses

Inefficiencies cause heating of the hydraulic fluid in operation. The heat load of a hydraulic system is equal to the total power loss through the inefficiencies and can be expressed as

$$P_{tot} = P_{pump,loss} + P_{valves} + P_{tub} + P_{cyl}, \tag{2.18}$$

where $P_{pump,loss}$ is the internal loss in the pump, P_{valves} is the valve loss, P_{tub} is the loss in the tubes and P_{cyl} is the loss in the cylinder. The heat losses in the pipe fittings and valves are proportional to the square of fluid velocity (Majumdar, 2002).

2.4 Hydraulic flow control methods and related power losses

During recent years, developments in mobile machines have concentrated on improving efficiency. The technologies have concentrated on developments in the following areas:

1. Load sensing power supply with LS-controlled valves

2. Electro-hydraulic LS (ELS) power supply

3. Secondary control technologies

4. Hydraulic transformers

5. Pump-controlled actuators (PCA)

6. Separate metering valve (SMV) control

7. Energy regeneration technologies

8. Optimized motion control

9. Optimized mechanical structure design

10. Energy-saving in parallel operation (Sun, 2004)

We concentrate on the optimization of flow control during lifting and lowering of the fork. Basically, there are two well-known flow control methods. For improving energy utilization and reducing losses, these control methods need to be studied.

First, we observe the flow control based on valves. Valves are the most important mechanical links to the fluid interface in hydraulic systems. Typical valve control is shown in Figure 2.16 (a). Valves are usually defined by the number of connections and the different operating positions they have. Most of these valves are used for sequential operation with fixed operating positions, but there are also so-called servo valves that have an infinite amount of operating positions and are usually adjusted by an electric input signal (Mohieddine, 2003).

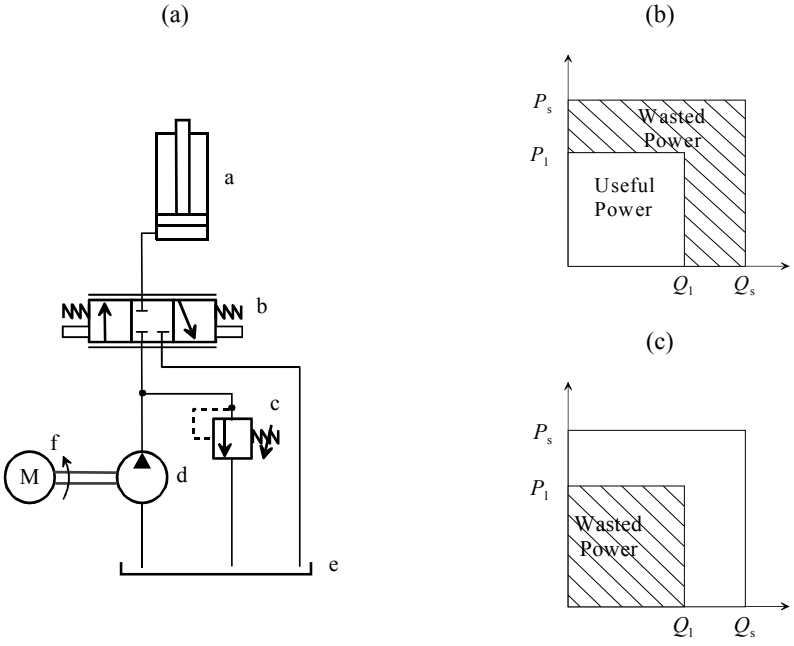

Figure 2.16: (a) Hydraulic circuit. a) Single-acting cylinder, b) proportional valve, c) pressure relief valve, d) fixed displacement pump, e) oil tank, f) electric motor. (b) Lifting consumption. (c) Lowering consumption.

Figure 2.16 (b) illustrates that both pressure and flow dependent losses are present during lifting. In the figure, p_l is load pressure, p_s is system pressure, Q_l is load flow and Q_s is system flow. The pressure losses are very high when a light load is moved at a high velocity. This is because the pressure drops over the control valves are significantly higher. Flow dependent losses occur when the flow demanded by the actuator is less than the constant flow provided by the pump. (Mattila, 2000) Figure 2.16 (c) illustrates the amount of wasted power during lowering. All energy is transferred into heat. According to Liang (2002), the total work losses in valves for one

duty cycle of a hydraulic boom are approximately 66–75% of the total hydraulic work consumption of the boom. Based on this example, we can conclude that valves are not ideal flow control components.

The second way for changing flow is using variable-displacement pumps (Figure 2.17(a)). In a variable-displacement pump, the piston strokes can be changed. The delivery can be changed by moving the displacement control or by changing the drive speed. In a motoring pump, the displacement can be adjusted so that the pump changes its operation to motoring and vice versa. In such an application, the drive can rotate all the time in the same direction and the load velocity up and down is controlled by just tilting the swash plate of the pump. Flow dependent losses are high at low actuator velocities; see Figure 2.17(b). In this case, the pump delivers only the needed amount of flow for the actuator (Mattila, 2000). Figure 2.17(c) illustrates the amount of wasted power during lowering. All energy is transferred into heat.

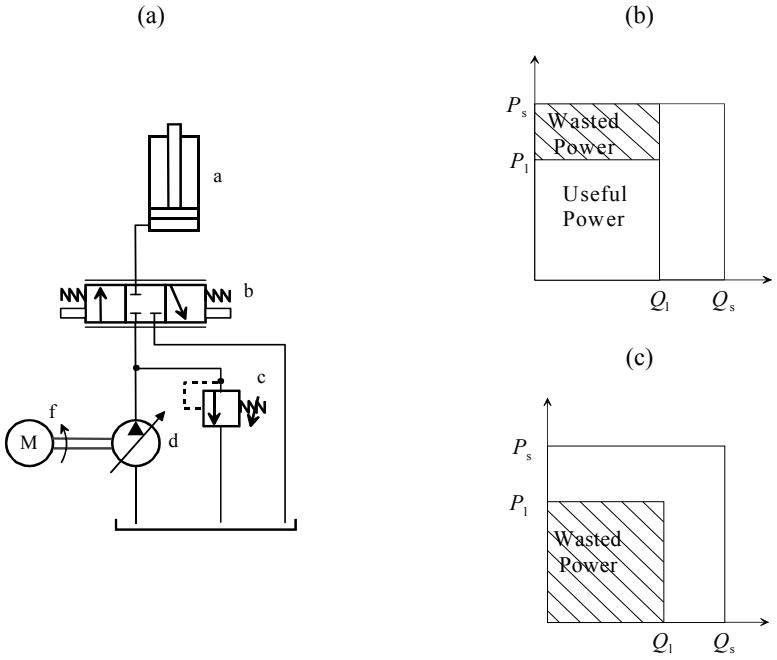

Figure 2.17: (a) Hydraulic circuit: a) single-acting cylinder, b) proportional valve, c) pressure relief valve, d) variable-displacement pump, e) oil tank, f) electric motor. (b) Lifting consumption. (c) Lowering consumption.

Pumps are usually rated according to their volumetric output and pressure. The volumetric output is the amount of liquid that a pump delivers to its outlet per unit of time at a given drive speed. The pressure developed in a system has an effect on the volumetric output of the pump supplying flow to the system. As pressure increases, the

volumetric output decreases. This drop in output is caused by an increase in internal leakage (slippage) from the pump outlet side to its inlet side. Slippage is a measure of the efficiency of a pump and is usually expressed in per cent. There are various types of pump designs available, such as gear, axial piston and vane, and the type chosen depends upon the application. It is a well-known fact that variable-displacement pumps are more expensive compared with fixed-displacement ones.

We study an alternative electric servo motor and a reversible constant displacement pump based system that combines the advantages of the previously mentioned methods. The method of flow control needs to provide different flows depending on the needs and hence produces low losses. Figure 2.18 (a) shows the hydraulic circuit of the main lift function with energy regeneration from potential energy.

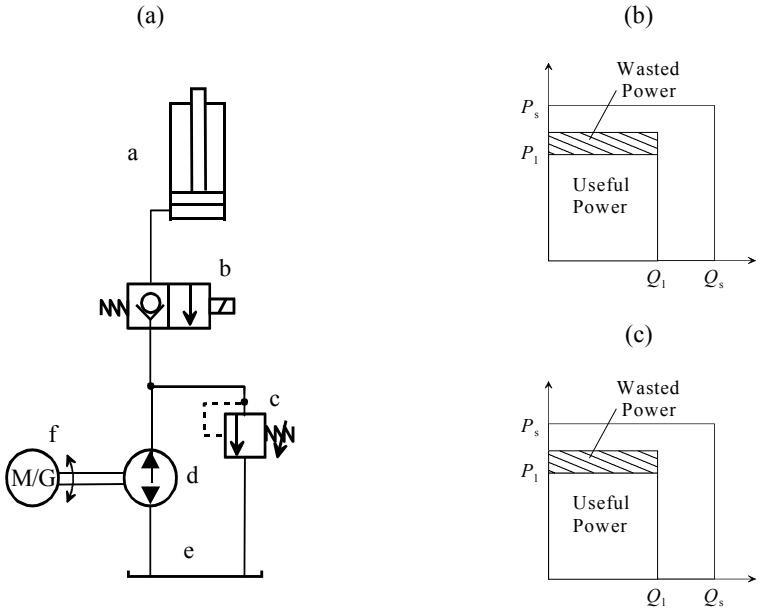

Figure 2.18: (a) Hydraulic circuit of the main lift function with energy regeneration from potential energy. The experimental system consists of a) a single-acting cylinder, b) a two-way normally closed poppet valve, c) a pressure relief valve, d) a pump/motor, e) an oil tank, and f) a variable-speed permanent magnet synchronous machine drive system. (b) Lifting consumption. (c) Lowering consumption.

The electric motor servo drive and a hydraulic pump are used instead of a proportional valve to control the position of the hydraulic cylinder piston. The hydraulic pump takes oil from a tank and delivers it to the rest of the hydraulic circuit. While operating, it raises the oil pressure to the required level determined by the load mass and friction. The two-way normally closed poppet valve (counter balance valve) is included in the system for safety. For the lifting consumption of the hydraulic structure with direct flow

control (see Figure 2.18 (b)), the supply pressure is variable and controlled by feedback from the motor side. In this case, the pump delivers only the needed amount of flow for the actuator, controlled from the motor side. Regeneration from potential energy gives possibilities to "re-use energy". Figure 2.18 (c) illustrates consumption during the lowering motion.

The hydraulic pump produces a flow depending linearly on the rotational speed of the servo motor, which is shown in Figure 2.19 for an internal gear pump.

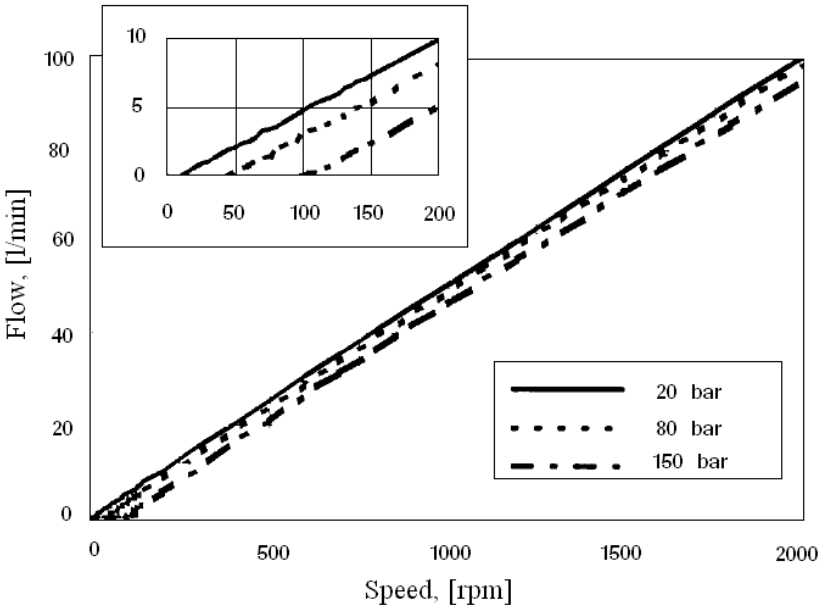

Figure 2.19: Flow versus speed characteristic for internal gear pump (Helduser, 1999).

The oil flow determines the actuator speed, and the actuator force determines the oil pressure needed. While lowering a mass, the potential energy of the load produces a flow that rotates the hydraulic machine as a motor, and the mechanically connected electric machine acts as a generator, which is controlled by a frequency converter.

2.5 Summary

In this chapter, the basic hydraulic and electric components needed in a hydraulic lifting and lowering system and their efficiencies were discussed. Hydraulic flow methods and their efficiencies were illustrated. Based on the information mentioned above, knowledge of problems occurring in working machines was gathered. Information about components was used construct models in Matlab/Simulink in the following Chapter 3.

3 Electro-hydraulic system component modelling

The modelling of the forklift can be divided into two categories: electric and hydraulic. Section 3.1 illustrates equations for hydraulic models, and Section 3.2 those for electric models. Section 3.3 discusses system modelling and analysis. System equations given in the following section will be used for simulations in Chapter 5.

3.1 Hydraulic component model

The hydraulic parts of a forklift are the cylinder and the pump. The modelling of these components will be shown below.

3.1.1 Cylinder model

The theoretical modelling of a hydraulic single-acting cylinder was based on an equation of piston motion and a pressure dynamic equation (Handroos, 2010). The equation for an actuator chamber is derived from the continuity of the mass equation

$$\dot{p}_s = \frac{B_e}{V}(Q_{in}) - \frac{B_e}{V} \cdot \dot{V}, \tag{3.1}$$

where the bulk module B_e = 1400·10^6 in Pa, p_s is the system pressure in Pa, V is the cylinder volume in m^3, and Q_{in} is the input flow in m^3/s.

$$V = V_0 + x_p S_p, \tag{3.2}$$

where the piston area is S_p = 0.0028 m^2. The additional volume describes the dead volume V_0 of the cylinder. The initial end position equals zero, and it gives the initial position of the end of the cylinder tube and the piston. The length of the piston is L_{cyl} = 1.82 m; these data are used for the limited movement of the piston.

The equation of piston motion is derived from Newton's second law:

$$m_t \ddot{x}_p = p_s S_p - F_f(\dot{x}_p) - F_{load}, \tag{3.3}$$

$$m_t = m_p + m, \tag{3.4}$$

where m_t is the total mass, m is the load mass equal to 920 kg, m_p is the mass of the cylinder piston equal to 50 kg and F_f is the friction force, and $x_p, \dot{x}_p$ and $\ddot{x}_p$ are the piston position, velocity and acceleration, respectively.

The cylinder friction equation is (DesignAerospace LLC, 2009)

$$F_{\mathrm{f}}\left(\dot{x}_{\mathrm{p}}\right)=\sigma\dot{x}_{\mathrm{p}}+\mathrm{sign}\left(\dot{x}_{\mathrm{p}}\right)\cdot\left[F_{\mathrm{co}}+F_{\mathrm{so}}\cdot e^{\left(\frac{-\left|\dot{x}_{\mathrm{p}}\right|}{C_{\mathrm{s}}}\right)}\right], \tag{3.5}$$

where σ is the viscous friction, F_{co} is the Coulomb friction, F_{so} is the static friction and C_{s} is the Stribeck friction in the seals. The behaviour of the cylinder is considered as a spring-damping system. For the case shown in Sections 5.3.2 and 5.3.3, the following values were chosen: σ = 5000, F_{co} = 0.01, F_{so} = 0.001 and C_{s} = 1. Equation (3.5) gives the dependency of the friction force on the piston velocity according to Figure 3.1, which illustrates the static friction, viscous friction, Coulomb friction and Stribeck friction.

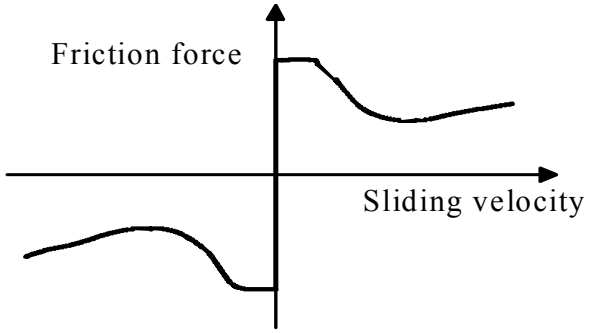

Figure 3.1: Static friction, viscous friction, Coulomb friction and Stribeck friction model based on Equation (3.5) (Handroos, 2010).

Static friction models are applied at zero velocity. It results in no movement at the first moment, and a significant displacement after the threshold level in force is exceeded. Dynamic friction models are used during movement and are also applicable for hydraulic machine modelling (Section 3.1.2, Equation 3.9).

3.1.2 Hydraulic Machine model

The following simple equation was used for simulating the behaviour of the pump (Majumdar, 2002):

$$Q_{\mathrm{p}}=\frac{\Omega\cdot V_{\mathrm{th}}}{2\cdot\pi}\cdot\eta_{\mathrm{vol}}, \tag{3.6}$$

where Q_{p} is the pump output flow in m^3/s, Ω is the rotating angular speed, V_{th} is the theoretical volumetric displacement of the pump in $\mathrm{m}^3/\mathrm{rev}$, and η_{vol} is its volumetric efficiency.

The second-order differential equation for the pump shaft rotation is (DesignAerospace LLC, 2009)

$$J_{\mathrm{p}} \frac{\mathrm{d}}{\mathrm{d}t} \Omega + T_{\mathrm{f,p}}(\Omega) = T_{\mathrm{motor}} - \eta_{\mathrm{vol}} T_{\mathrm{p,th}}, \tag{3.7}$$

where the total equivalent inertia of the pump is $J_{\mathrm{p}} = 1.1 \cdot 10^{-3} \mathrm{kgm}^2$, $\mathrm{d}\Omega/\mathrm{d}t$ is the pump angular acceleration, T_{motor} is the drive torque, $T_{\mathrm{p,th}}$ is the theoretical (ideal) torque required for compressing fluid and $T_{\mathrm{f,p}}$ is the frictional torque. The volumetric efficiency of the pump is equal to $\eta_{\mathrm{vol}} = 0.95$.

The theoretical torque to compress the fluid can be modelled as follows (DesignAerospace LLC, 2009):

$$T_{\mathrm{p,th}} = V_{\mathrm{th}}(p_{\mathrm{s}} - p_{\mathrm{rtn}}), \tag{3.8}$$

where the theoretical volumetric displacement for the internal gear pump is equal to $V_{\mathrm{th}} = 13.3 \cdot 10^{-6}$ m^3/rev, p_{s} is the system pressure and p_{rtn} is the tank pressure in Pa.

The frictional torque can be modelled as follows (DesignAerospace LLC, 2009):

$$T_{\mathrm{f,p}}(\Omega) = T_{\mathrm{v}}\Omega + \mathrm{sign}(\Omega) \cdot \left[T_{\mathrm{co}} + T_{\mathrm{so}} \cdot e^{\left(\frac{-|\Omega|}{C_{\mathrm{s}}} \right)} \right], \tag{3.9}$$

where T_{v} is the viscous friction, T_{co} is the Coulomb friction, T_{so} is the static friction and C_{s} is the Stribeck friction. Figure 3.1 is suitable also for the representation of friction in a hydraulic machine. To match the modelling results with the measured ones, the calculation system was calibrated. This means that the coefficients were adjusted during the process of simulation. The friction depends on the speed of movement, gaps between metal parts, temperature and viscosity of oil. For the case shown in Sections 5.3.2 and 5.3.3, the following values were chosen: $T_{\mathrm{v}} = 0.018$, $T_{\mathrm{co}} = 0$, $T_{\mathrm{so}} = 0.002$ and $C_{\mathrm{s}} = 1$.

3.2 Electrical servo drive component model

The electric part of the forklift can be divided into an electric machine and its control part, a converter. The traditional two-axis space vector model of the permanent magnet synchronous machine is shown in Section 3.2.1, and the model of the converter control principle is given in Section 3.2.2.

3.2.1 Electrical servo machine model

The rotor of a permanent magnet synchronous machine with rotor-surface-mounted magnets can be considered non-salient and assumed to have similar reluctance along any axis through the centre of the machine. Figure 3.2 illustrates the vector equivalent circuits for a PMSM having some damping properties. In most cases, the damping properties in servo motors are determined by the eddy current behaviour in the rotor structures because there are no real damper windings.

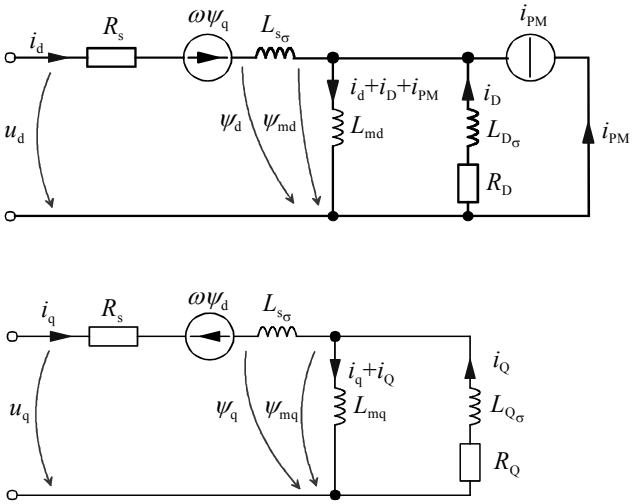

Figure 3.2: Equivalent circuits of direct and quadrature axis circuits of PMSM (Pyrhönen, 2008).

In Figure 3.2, i_d and u_d are the direct-axis components of the stator current and voltage, ψ_q and ψ_d are the quadrature- and direct-axis components of the stator flux linkage, and i_D is the direct-axis current of the damper winding. R_s is the stator resistance. R_D and R_Q are the direct- and quadrature-axis resistances of the damper winding. $L_{s\sigma}$ is the leakage inductance of the stator. L_{md} and L_{mq} are the direct- and quadrature-axis magnetizing inductances. $L_{D\sigma}$ and $L_{Q\sigma}$ are the direct- and quadrature-axis leakage inductances of the damper winding. In a permanent magnet machine with a laminated rotor and surface magnets, the damping effects are small and can often be neglected (Pyrhönen, 2008).

In the following are equations with which the PMSM was described in the simulation:

$$\vec{i} = i_a(t) \cdot e^{je0\pi/3} + i_b(t) \cdot e^{j2\pi/3} + i_c(t) \cdot e^{je4\pi/3} \tag{3.10}$$

The stator d- and q-winding flux linkage components can be expressed as follows:

$$\psi_{sd} = L_{sd} \cdot i_{sd} + \psi_{PM}, \tag{3.11}$$

$$\psi_{sq} = L_{sq} \cdot i_{sq}. \tag{3.12}$$

The voltage for the d- and q-axes can be expressed as follows:

$$u_{sd} = R_s \cdot i_{sd} + \frac{d}{dt}\psi_{sd} - \omega_m \cdot \psi_{sq}, \tag{3.13}$$

$$u_{sq} = R_s \cdot i_{sq} + \frac{d}{dt}\psi_{sq} + \omega_m \cdot \psi_{sd}. \tag{3.14}$$

In the practical case of the experimental test setup, the motor parameters for CFM90M are $R_s = 0.54\ \Omega$ and $L_{sd} = L_{sq} = 0.57 \cdot 10^{-3}$ H, and for CFM112M are $R_s = 0.193\ \Omega$ and $L_{sd} = L_{sq} = 0.31 \cdot 10^{-3}$ H.

The rotor electrical angular speed ω_m is related to the actual mechanical angular speed Ω as follows:

$$\omega_m = p\Omega, \tag{3.15}$$

where $p = 3$ is the number of pole pairs.

The electromagnetic torque T_e of a non-salient pole PMSM can be expressed as

$$T_e = \frac{p}{2}\psi_{PM} i_{sq}. \tag{3.16}$$

The acceleration is determined by the difference of the electromagnetic torque and the load torque acting on J_{eq}, the combined inertia of the load J_p and the motor J_m.

$$\frac{d}{dt}\Omega = \frac{T_{em} - T_L}{J_{eq}}, \tag{3.17}$$

where the total equivalent inertia of the CFM90M is $J_m = 22.3 \cdot 10^{-4}$ kgm^2 and that of the CFM112M is $J_m = 88.2 \cdot 10^{-4}$ kgm^2

The per-phase motor circuit parameters are the voltage constant $K_e = 0.22$ V/rad/s for both machines, and the reference speed $\Omega = 314$ rad/s.

Motor efficiency model

The losses of an electrical machine comprise iron losses, copper losses, and mechanical and additional losses. The electric power loss analysis here is based on testing and redesigning of the PMSMs. The electrical power lost in the stator winding resistance is also known as copper loss. The copper loss varies with the load in proportion to the current squared and the resistance of the stator, and it can be expressed as

$$P_{\mathrm{Cu}} = 3 \cdot R_{\mathrm{s}} \cdot I_{\mathrm{s}}^2 , \tag{3.18}$$

where P_{Cu} is the stator winding copper loss (W), R_{s} is the stator AC resistance (Ω) in the average operating temperature, and I_{s} the stator current (A).

Stray losses are the losses that remain after primary copper and secondary losses, iron losses, and mechanical losses. The largest contribution to the stray losses is due to harmonic energies generated when the motor operates under load. These energies are dissipated as currents in the copper windings, harmonic flux components in the iron parts, and as leakages in the laminate core.

The total iron losses are

$$P_{\mathrm{Fe}} = P_{\mathrm{Feys}} + P_{\mathrm{Feds}} , \tag{3.19}$$

where the core loss in the stator yoke is written as

$$P_{\mathrm{Feys}} = k_{\mathrm{Fey}} P_{15} \left(\frac{B_{\mathrm{ys}}}{1.5} \right)^2 \cdot m_{\mathrm{ys}} \left(\frac{f}{50} \right)^{\frac{3}{2}}, \tag{3.20}$$

where k_{Fey} =1.5 is the correction coefficient, m_{ys} is the mass of the stator yoke (kg), f is the frequency (Hz), B_{ys} = 1.3 (Vs/m^2), and P_{15} = 6.6 (W/kg).

The core loss in the tooth area is calculated with

$$P_{\mathrm{Feds}} = k_{\mathrm{Fed}} P_{15} \left(\frac{B_{\mathrm{d}}}{1.5} \right)^2 \cdot m_{\mathrm{d}} \left(\frac{f}{50} \right)^{\frac{3}{2}}, \tag{3.21}$$

where k_{Fed} =2 is the correction coefficient, m_{d} is the mass of the teeth (kg), and B_{d} = 1.59 (Vs/m^2).

The stator slot openings cause permeance harmonic losses in the rotor surface permanent magnets.

$$k_{\mathrm{v}} = \sqrt{f_{\mathrm{PM}} \cdot 2\pi\mu_{\mathrm{rec}}\mu_0 \frac{\sigma_{\mathrm{PM}}}{2}}, \tag{3.22}$$

$$B_0 = \beta_{\mathrm{v}} \cdot B_{\max}, \tag{3.23}$$

$$\beta_{\mathrm{v}} = \frac{2 f_{\mathrm{PM}} \pi}{\pi D_{\mathrm{r}} \omega}, \tag{3.24}$$

where $B_{\max}$ is the maximum flux density (T), ω is the angular speed (rad/s), and f_{PM} is the frequency on the rotor surface caused by slot openings $f_{\mathrm{PM}} = \omega \cdot Q_{\mathrm{ss}}$, where Q_{ss} is the number of stator slots, $\mu_0 = 4\pi 10^{-7}$ (Vs/Am) is the permeability of the vacuum, μ_{rec} is the permeability of the permanent magnet material, D_{r} is the rotor diameter (m) and $\sigma_{\mathrm{PM}} = 6.7 \cdot 10^5$ is the conductivity of the permanent magnet.

$$a_{\mathrm{Rv}} = \left(\frac{1}{\sqrt{2}}\right)\sqrt{\sqrt{4 + \left(\frac{\beta_{\mathrm{v}}}{k_{\mathrm{v}}}\right)^4} + \left(\frac{\beta_{\mathrm{v}}}{k_{\mathrm{v}}}\right)^2}, \tag{3.25}$$

$$P_{\mathrm{PMEC}} = \left(\frac{a_{\mathrm{Rv}}}{2}\right)\left(1 + \frac{\tau_{\mathrm{u}}}{2}\frac{1}{l}\right)\left(\frac{B_0}{\mu_0\mu_{\mathrm{rec}}}\right)^2\left(\frac{k_{\mathrm{v}}}{\sigma_{\mathrm{PM}}}\right)^2 \pi D_{\mathrm{r}} \alpha_{\mathrm{PM}} l \frac{\left(\sqrt{2} \cdot k_{\mathrm{v}}\right)^2}{\beta_{\mathrm{v}}^2}, \tag{3.26}$$

where τ_{u} is the stator slot pitch, α_{PM} is the chosen effective relative magnet width, l is the core length in a machine with no cooling channels (m), and β is the flux variation (Pyrhönen, 2008).

Mechanical losses include friction in the motor bearings and in the fan for air cooling.

$$P_{\rho} = k_{\rho} D_{\mathrm{r}} \left(l + 0.6\tau_{\mathrm{p}}\right) v_{\mathrm{r}}^2, \tag{3.27}$$

where $k_{\rho} = 10$ Ws^2/m^4 is an experimental factor, v_{r} is the volume of the rotor (m^3), and τ_{p} is the stator pole pitch (m).

There are also some additional losses in the machine. These losses are assumed to be 0.5% of the input power:

$$P_{\mathrm{ex}} = 0.005 \cdot P_{\mathrm{in}}. \tag{3.28}$$

The sum of power losses P_{loss} in the machine is calculated as

$$P_{\mathrm{loss}} = P_{\mathrm{Fe}} + P_{\mathrm{Cu}} + P_{\rho} + P_{\mathrm{PMEC}} + P_{\mathrm{ex}}. \tag{3.29}$$

The input power P_{in} is written as

$$P_{in} = P + P_{loss}, \tag{3.30}$$

where P is the shaft power (W).

The efficiency η_{EM} of the electric motor is obtained by

$$\eta_{EM} = \frac{P}{P_{in}} \ . \tag{3.31}$$

The corresponding efficiency of a generator is calculated vice versa as the ratio of the shaft power (P_{shaft}) to the generator stator electric output power P_s ($\eta_{gen} = P_s/P_{shaft}$). Calculations based on Equations (3.18–3.31) were repeated for fixed torques for all speeds for the $i_d = 0$ control. The results for 4.5 kW PMSM CFM90M and for 10 kW PMSM CFM112M are shown in Figures 5.25 and 5.26, respectively, in Section 5.3.1.

3.2.2 Control principle model

The main principle of the DTC is to control the torque and the modulus of the stator flux linkage directly by controlling the inverter switches using the outputs of the hysteresis comparators and selecting the correct voltage vector from the optimal switching table.

The estimated stator flux linkage is calculated with the integral

$$\boldsymbol{\psi}_s = \int (\boldsymbol{u}_s - r_s \boldsymbol{i}_s) \mathrm{d}t \ . \tag{3.32}$$

The estimated electric torque is calculated from estimated flux linkage components and measured stator currents in the two-axis stationary reference frame (Mohan, 2001).

$$T_e = \frac{3p}{2}\left(\psi_d i_q - \psi_q i_d\right) \tag{3.33}$$

Figure 3.3 illustrates the DTC control principle. In principle, DTC works as a hysteresis control of the magnitude of the stator flux linkage and the torque by directly selecting one of the six non-zero or two zero discrete voltage vectors of the inverter. The switching table helps to choose the appropriate voltage vector. The selected voltage vector is synthesized and then realized in the inverter (VSI) by suitable switching of power switches. In this case, an enhanced version of the DTC is used. It applies a space vector modulator instead of the optimal switching table, but calculates the flux linkage estimate in the same manner as the earlier versions. This system guarantees a constant switching frequency.

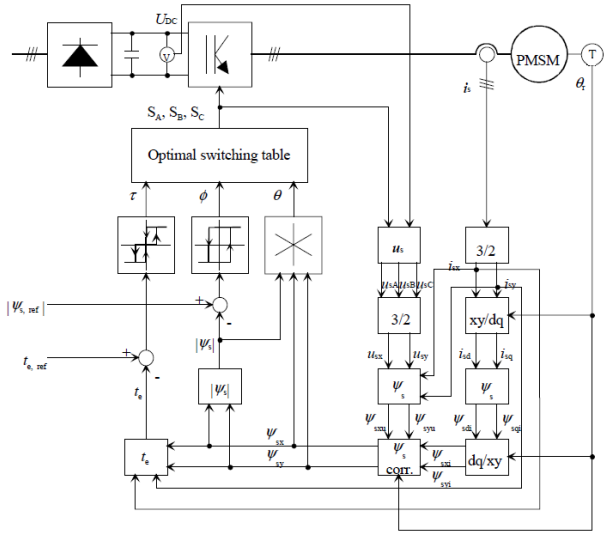

Figure 3.3: Operation principle of the DTC control (Luukko, 2000).

3.3 System modelling

This section provides an introduction to the model for lifting and lowering movements. Modelling and simulations are based on the mathematical presentations given above in Sections 3.1 and 3.2. Two models were established for the evaluation of energy consumption separately during lowering and lifting. To analyse the energy consumption in the cycles, a combined model of separate models was built and will be shown in Section 3.3.3.

3.3.1 Model for lifting movement

Based on the modelling of each component, a system was established for lifting, as shown in Figure 3.4.

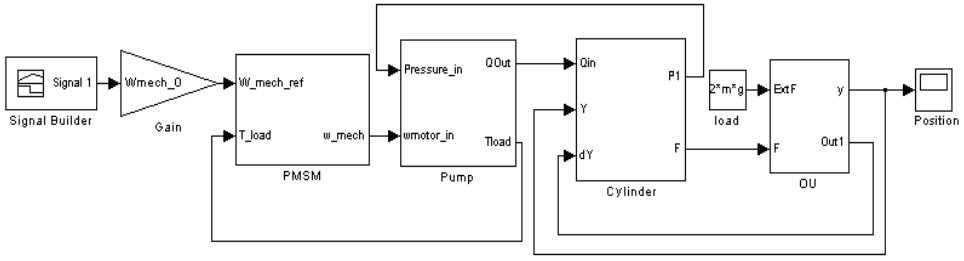

Figure 3.4: Matlab/Simulink model of the test setup for lifting (Minav, 2011e).

Considering the response of the parts in the system, the electric drive control response is much higher than the responses of the hydraulic and mechanical parts. This was taken into account when modelling the electric part of the system by using different sampling times. The reference signal for controlling the system is realized by a signal builder. The signal has acceleration, constant speed and deceleration parts. The PMSM block behaves according to the reference signal (acceleration, constant speed and deceleration according to the actual measured speed signal). The torque is transferred between the hydraulic pump and electric motor with mechanical coupling. Pressure is transferred between the cylinder and the pump. The pump delivers an amount of oil to the cylinder to move the tare and the payload with the motor reference speed $w_{\text{mech-0}}$. The cylinder block Cylinder simulates the moving of the load during lifting (Minav, 2011e).

3.3.2 Model for lowering movement

Figure 3.5 shows the Matlab/Simulink model of the test setup during lowering. The cylinder block simulates the motion of the load and cylinder during lowering.

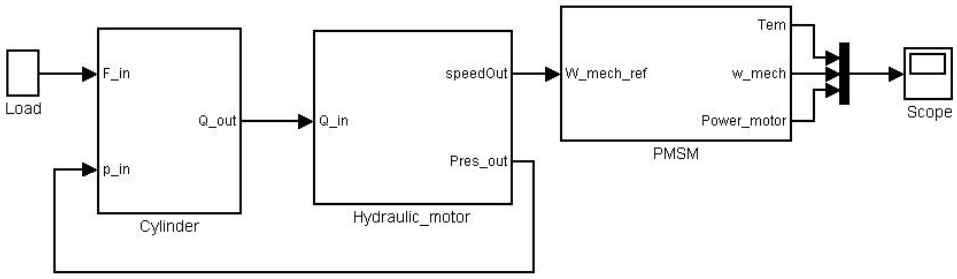

Figure 3.5: Matlab/Simulink model of the test setup for lowering.

The oil flows from the cylinder to the hydraulic machine and the pump acts as a motor. Torque is transferred between the hydraulic motor and the electric motor with mechanical coupling. The PMSM and converter with the implemented DTC control ensure that the speed of the load going down follows the reference speed.

3.3.3 Combined model for a lifting and lowering cycle

The two models discussed above can be combined to construct a full model of a cycle movement: up and down. For this reason, a logic block should be provided to couple the initial values in the direction changing point. Figure 3.6 shows the Matlab/Simulink model of the test setup for the cycle.

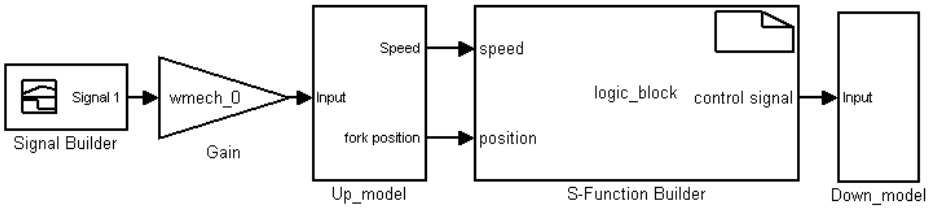

Figure 3.6: Matlab/Simulink model of the test setup for the cycle.

Figure 3.7 shows an flowchart of the algorithm that was used to implement the logic block (see Figure 3.6). The user inserts the speed of the motor and payload. These are the required input data to produce a control signal for a lifting motion. The output information from the "Up" model is the end position of the cylinder (fork position). This information and also the required speed and payload become inputs for the "Down" model. The output information from the "Down" model is the position of the cylinder. Also torque, pressure and speed can be checked. The program was implemented in Matlab 2008a.

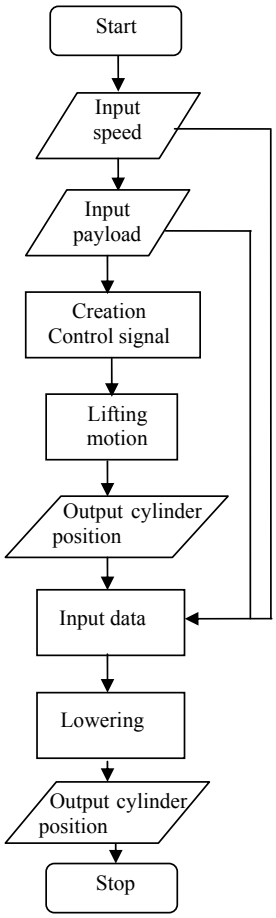

Figure 3.7: Flowchart of the logic block.

The logic block helps to combine the models for lifting and lowering.

3.3.4 Model of flow ripples

This section provides an introduction to the model for testing the compensation of the flow ripple produced by the pump (Figure 3.8). The modelling and simulations are based on the mathematical presentations given in Section 2.2.1, Equations 2.5–2.7.

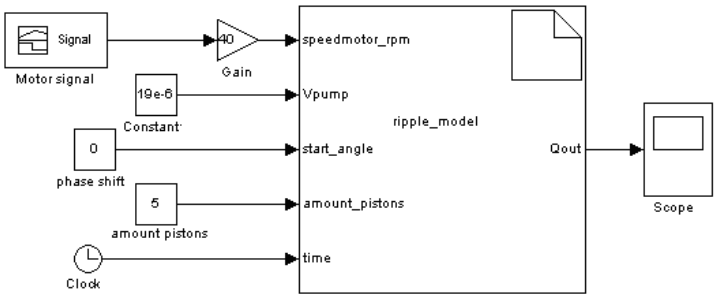

Figure 3.8: Matlab/Simulink model of the test compensation of flow ripples (Minav, 2011a).

The reference signal to control the system is provided by a signal builder. The "pump motor" block contains the equation which produces ideal ripples (Equations 2.5–2.7) realized in the C-language. The main input values of this block are the actual speed, the volumetric displacement of the pump and the number of pistons in the pump. The actual speed is the output from the signal builder block "Motor signal". The "Motor signal" block produces oscillation opposite to the pump flow ripple. It means that we try to make the motor speed "oscillate" to compensate for the flow ripple produced by the pump (Minav, 2011a).

3.4 Summary

In this chapter, the modelling of the forklift was described. Modelling was divided into two categories: electric and hydraulic. Section 3.1 illustrates equations for hydraulic models, and Section 3.2 those for electric models. Section 3.3 discusses system modelling. System equations given in the following section were used for simulations and will be verified by measurements in Chapter 5. In the following chapter 4, fork speed and position controller design, its basic requirements and the structure of software and hardware are introduced.

4 Design of an electro-hydraulic controller

In this chapter, the fork position controller design and its basic requirements are discussed. Secondly, the structure of software and hardware is introduced. As the process may change significantly because of the changing parameters (e.g. variation in the load mass and motor speed) during the working of the forklift, it is likely that some kind of an adaptive control is needed. As this work does not aim at a detailed control design, the traditional PID controller structure is taken as the basis for the work. It is noticed that a constant parameter PID controller does not satisfy the requirements, and therefore, it is further developed in the following study. The results of the capability of smooth control of the fork position and speed, especially during lowering were important practical results for the forklift manufacturer supporting the study.

4.1 Initial requirements

In the experimental setup during switching from lifting to lowering, the slow response of the PMSM drive results in an unacceptable overshoot in the acting speed, which affects the hydraulic part of the system negatively. Figure 4.1 illustrates an example of the response of the system during the lowering movement of the fork. Originally, a fixed PID controller was used to control the speed because of the problem related to it (see Figure 4.1). The main objective of the controller design is to find a suitable speed control method for the proposed system. This, within the bounds of this project, means that the speed should behave smoothly during the lifting and lowering of loads and independently from the mass moved.

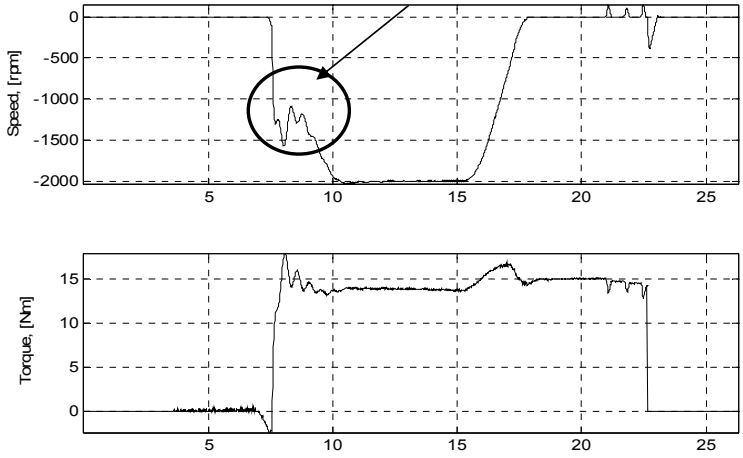

Figure 4.1: Example of a poor slow speed control response during the lowering movement of the fork.

In the test setup the payloads may vary between 0 and 1600 kg, and the fork speed can vary from 0.1 to 0.5 m/s. Based on the information mentioned above to reach the required functionality and dynamic response of the system, the initial requirements for the control system are specified in Table 4.1.

Table 4.1: Initial requirements for the fork control system.

Rise time	Max settling time	Max overshoot	Max steady state error
0.3 s	1 s	7 %	3 %

The key question is the design of the controller for the "down" movement. How can the speed of the movement be controlled so that changing from the upper standstill to the lowering movement takes place smoothly and without oscillation? The following information needs to be taken into account: All hydraulic components include many types of nonlinearities, such as pressure-flow characteristics in control valves, dry friction acting on actuators and moving parts of valves, and the collision of valves against valve seats. All these nonlinearities produce nonlinear phenomena in hydraulics (Hayashi, 2001); also the system in general can be characterized by its slow response, and large uncertainties and disturbances (Merrit, 1967). The target of the research is to control the hydraulic part of the system through electric motor drive control. Following this idea, it was an obvious decision to make the speed controller independent of the system model, and robust for variable conditions, such as a changing speed, direction of movement or payload. To reach this target, a decision was made to use a resolver, since feedback from the motor is the only information source about the load behaviour (hydraulic system). Because of this, a conventional PID controller cannot necessarily reach satisfactory results, as it was shown in Figure 4.1. Burrows (2005) reviewed developments in the control of hydraulic systems. Most of the examples illustrated in his material were based on neural networks and fuzzy control. According to L. Tian (2004) and B. Feng (2009), a self-tuning-parameter fuzzy PID controller provides a control of the system with excellent performance in responsibility, stability and accuracy. One of the advantages of the fuzzy logic is the ability to translate human reasoning using linguistic variables. This makes it possible to take into account the uncertainties and nonlinearities that are otherwise very difficult to model mathematically. The main element of the controller is a PID type fuzzy control technique that utilizes a simple set of membership functions and rules to meet the basic control requirements of such an application. According to sources (Jianxin, 2009; Zheng, 2009; Xiaofeng, 2010), fuzzy control can adapt to inconstant working situations and nonlinear systems, which makes the system strongly robust. It was mentioned above that the ACSM1 drive applies a conventional PID controller, and thus, the decision to use a self-tuning-parameter fuzzy PID controller was made to meet the initial requirements for the controller.

4.2 Design of the forklift control algorithm

The design of the control algorithm can be divided into small targets. The first target is to have an opportunity to easily change the speed and direction of motion. The second target is to guarantee smooth speed control and prevent any overshoots in the system. The third target is to produce position control for the forks (direct electro-hydraulic position control (DEHPC) or simply DPC). The fourth target is to compensate for the ripple of flow produced by the hydraulic pump by using the favourable control properties of the electric motor drive.

4.2.1 Speed, direction and position control

Direct electro-hydraulic position control (DEHPC), or simply DPC, can be divided into logical parts, which are connected in one algorithm: speed, direction and position control. Figure 4.2 shows a functional flowchart for the control programme.

The user decides the direction (block 7 or 5) and the speed of the movement of the fork (block 3). Depending on the speed and height, the programme calculated how many revolutions (N_{cal}, block 15) the motor needs to perform to deliver the correct amount of oil from the tank to the cylinder, where $N_{cal} = N + N_{add}$. A N_{add} additional correction factor was included in the system. An estimated torque (block 11) and acting speed (block 9) are used as feedbacks from the motor side. The converter estimates the motor torque fairly accurately. The estimated torque gives as estimation of the payload on the forks (block 12). This value influences the pressure of the oil in the cylinder (block 13). A high pressure results in extra leakage, and this means that the motor is required to perform additional revolutions (N_{add}) to reach the desired height. When the amount of real revolutions is close to the calculated ones ($N_{cal}=N_{act}$, in block 16), the programme will send a new reference speed signal equal to zero (block 18), and following the deceleration curve (adjustable parameters in ACSM1) the motor and also the system will stop (block 19). Information about the number of real revolutions N_{act} (block 10) is supplied to the system from a resolver. Depending on the direction, a reference signal is changed to be positive (lifting) or negative (lowering). During lowering (block 7), the programme also controls the opening of the normally closed safety valve (block 8). If the user has not given a correct speed reference or has forgotten to insert a height reference, the system will not work before the error is eliminated. The programme was implemented in Matlab 2008a in C code.

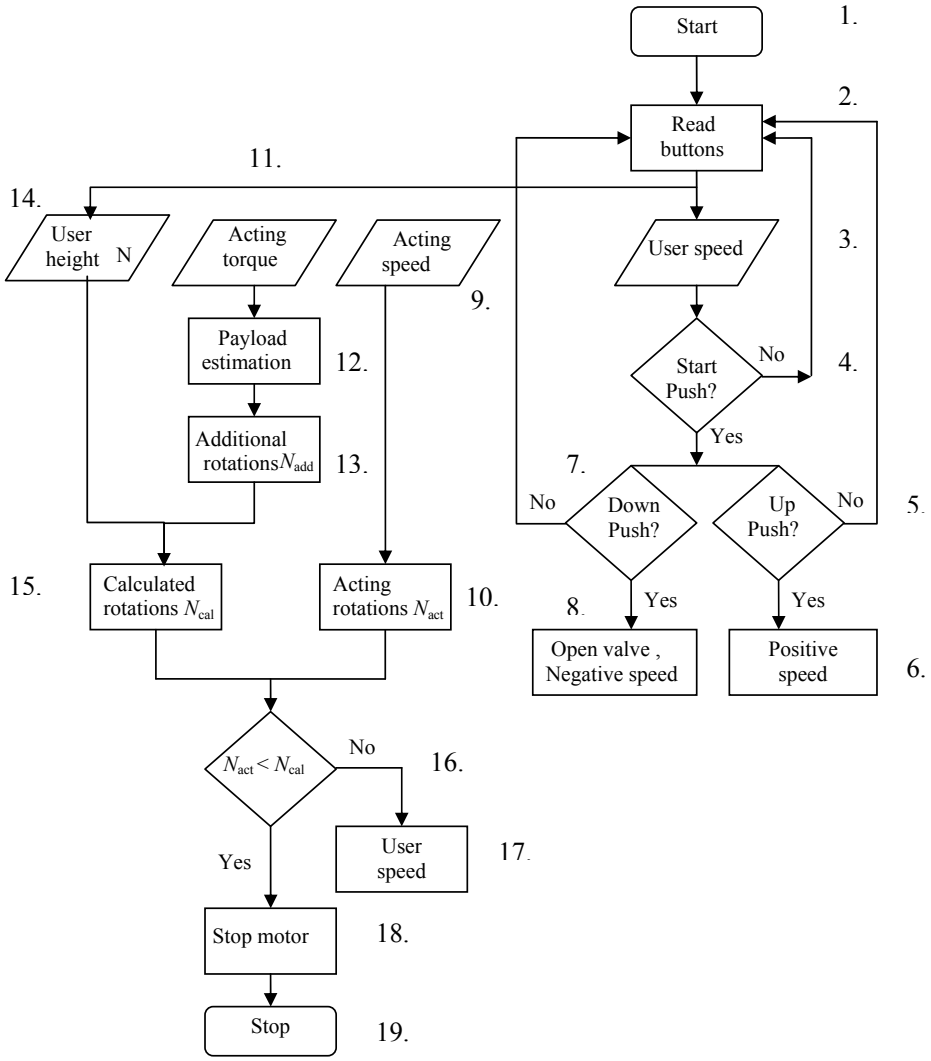

Figure 4.2: Control software functional flowchart.

4.2.2 Self-tuning-parameter Fuzzy PID control for speed

In our case, we have a non-linear system under investigation, and the speed controller must be independent of the system model and robust for variable conditions: changing speed, direction or load. Because of these requirements, a conventional PID controller cannot reach satisfactory results. According to (Tian, 2004, Feng, 2009), a self-tuning-parameter fuzzy PID controller provides a control of the system with excellent

performance in reliability, stability and accuracy. The basic approach is to try to detect when the controller is not properly tuned and then seek to adjust the PID gains to improve the performance. The schematic structure of the self-tuning-parameter fuzzy PID controller is given in Figure 4.3.

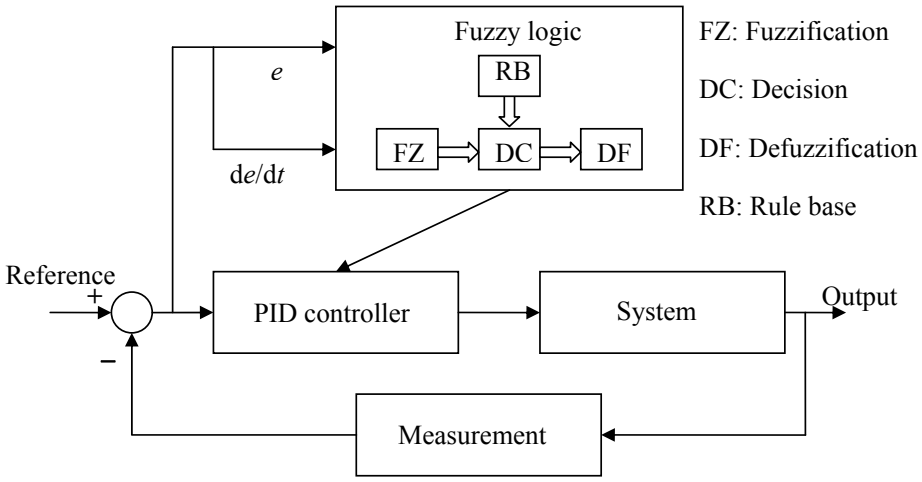

Figure 4.3: Self-tuning-parameter fuzzy PID controller structure (Tian, 2004).

A block diagram of a fuzzy control system is shown in Figure 4.3. The fuzzy controller is composed of the following four elements:

1. *A fuzzification interface,* which converts controller inputs into information that the inference mechanism can easily use to activate and apply rules.

2. *A rule-base or knowledge base* (a set of If-Then rules), which contains a fuzzy logic quantification of the expert's linguistic description of how to achieve good control.

3. *An inference mechanism or decision making mechanism* (also called a "fuzzy inference" module), which emulates the expert's decision-making in interpreting and applying knowledge about how to best control the plant.

4. *A defuzzification interface,* which converts the conclusions of the inference mechanism into actual inputs for the process.

In Figure 4.3, the input is the reference value of speed and the output is the actual speed. Inputs for the fuzzy block are the speed error E and the time derivative of the speed error EC. The PID controller parameters K_p, K_i and K_d are self-tuned according to the following logic rules by a fuzzy interface.

Consider a human in the loop whose responsibility is to control the speed. First, a decision on which information will be used as inputs in the decision-making process must be made.

After all the inputs and outputs are defined for the fuzzy controller, we can specify the fuzzy control system. The linguistic description provided by a control "expert" on how to tune the PID parameters. An example is written as follows:

"Since K_p can speed up the control process, at the beginning of the control process, K_p should be larger in order to reduce the rising time and make the control process faster. In the middle of the control sequence, K_p should be adjusted to its middle value for the consideration of system stability and control accuracy. In the final period, K_p should be given a smaller value, compared with the beginning of the process, in order to reduce the steady-state error" (Tian, 2004).

Next, the linguistic quantification above specifies a set of rules (a rule-base) that capture the expert's knowledge about how to control the speed. The knowledge of the process, which is a fuzzy model, is always described in simple fuzzy linguistic rules instead of precise mathematical functions.

• **If** the steady-state error is significant **then** increase the proportional gain.

• **If** the response is oscillatory **then** increase the derivative gain.

• **If** the response is sluggish **then** increase the proportional gain.

• **If** the steady-state error is excessive **then** adjust the integral gain.

• **If** the overshoot is excessive **then** decrease the proportional gain.

Using the approach above, we could continue to write down rules for the control problem for all possible cases.

Up to this point, we have only quantified, in an abstract way, the knowledge that the human expert has about how to control the speed. The membership function is used to represent of the magnitude of participation of each input graphically. It associates a weighting with each of the inputs that are processed, defines functional overlaps between inputs, and ultimately determines an output response.

Figure 4.4 and Figure 4.5 show the membership functions for inputs and outputs, respectively. Figure 4.4 shows two inputs: the speed error E and the derivation of the error EC. Both E and EC are divided into seven values as {NB, NM, NS, ZO, PS, PM, PB}, where NB∴Negative Big, NM∴Negative Medium, NS∴Negative Small, ZO∴zero, PS∴Positive Small, PM∴ Positive Medium, PB∴Positive Big.

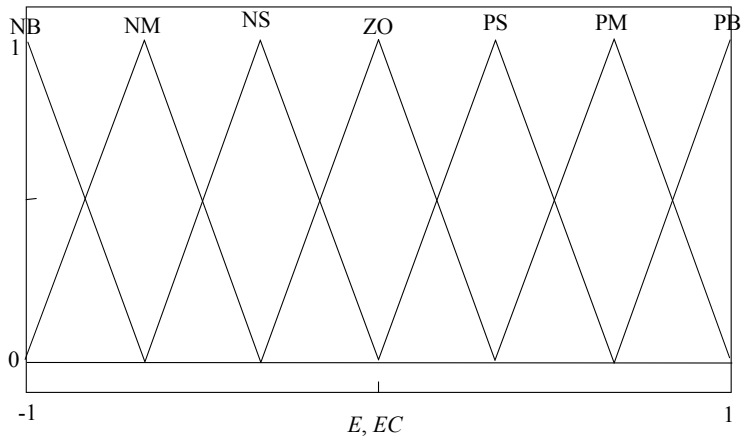

Figure 4.4: Membership function of inputs (Feng, 2009).

The horizontal axis illustrates the scaling gain for the speed error E and its time differential EC. The membership function shows how the scaling gains actually affect the meaning of the linguistics that forms the basis for the definition of the fuzzy controller. Triangle membership functions were chosen as they are the most common and easy to implement in an embedded controller. Each of the triangles represents an area of the effect of rules. Similar interpretations of linguistic values were made in the definition of the membership functions on the outputs. Combinations of letters are used to define the sector (triangle). Figure 4.5 shows outputs K_p, K_i and K_d.

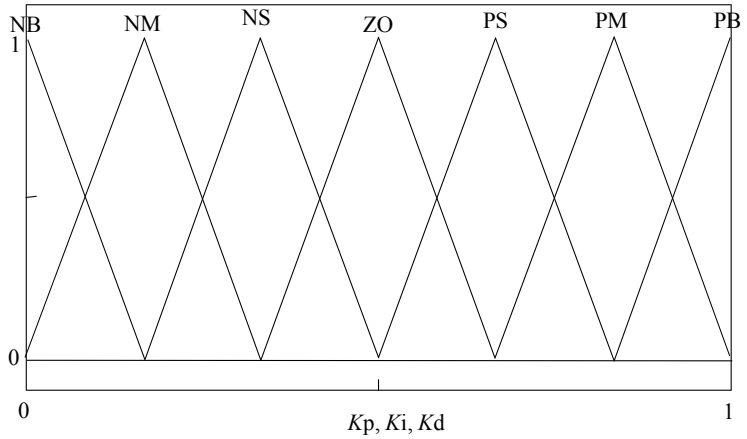

Figure 4.5: Membership function of outputs (Feng, 2009).

By combining the fuzzy sets of inputs for the speed error (7) and the differential of the speed error (7), there are all in all 7×7 = 49 rules for tuning one controller output.

Because we have three outputs (K_p, K_i and K_d), there are 49 × 3 = 147 rules. The rule base for the tuning of the control system is shown in Table 4.2.

Table 4.2: Fuzzy rules for the calculation of the coefficients of the parameters K_p, K_i and K_d of the PID controller (Feng, 2009).

Speed error *E*	Differential of the speed error *EC*						
	NB	NM	NS	ZO	PS	PM	PB
NB	PB/NB/NB	PB/NB/NB	PB/NB/NM	PB/NB/NM	PB/NB/NM	PB/NB/NB	PB/NB/NB
NM	PM/NM/ZO	PM/NM/ZO	PM/NS/NM	PS/NS/NM	ZO/NS/NM	ZO/NM/ZO	ZO/NM/ZO
NS	ZO/PM/ZO	ZO/PM/NS	ZO/PS/NM	NS/PS/NM	NM/PS/NS	NM/PM/NS	NM/PM/ZO
ZO	NS/PM/NS	NS/PM/NS	NS/PS/NS	ZO/ZO/NS	NS/PS/NS	NS/PM/NS	NS/PM/NS
PS	NM/PM/ZO	NM/PM/NS	NM/PS/NM	NS/PS/NM	ZO/PS/NS	ZO/PM/NS	ZO/PM/ZO
PM	ZO/NM/ZO	ZO/NM/ZO	ZO/NS/NM	PS/NS/NM	PM/NS/PS	PM/NM/ZO	PM/NM/ZO
PB	PB/NB/NB	PB/NB/NB	PB/NB/NM	PB/NB/NM	PB/NB/NM	PB/NB/NB	PB/NB/NB

The table illustrates what rule is effective when a specific combination of the speed error *E* and its time differential *EC* is present. For instance, the speed error *E* is "located" in the NS triangle, and the differential of error *EC* in ZO triangle. The combination of this information tells us that the output for K_p follows the NS triangle rule, K_i is follows the PS triangle rule and K_d follows the NM triangle rule.

The *inference process or decision* generally involves two steps:

1. The premises of all the rules are compared with the controller inputs to determine which rules apply to the current situation. This matching process involves determining the certainty that each rule applies.

2. The conclusions (what control actions to take) are determined using the rules that have been determined to apply at the current time. The conclusions are characterized with a fuzzy set that represents the certainty that the input to the plant should take on various values (Passino, 1997).

In this stage, the fuzzy rules combine two or more fuzzy input sets called antecedent sets and associate them with an output. The antecedent sets are combined by means of the usual logical “AND” or “OR”. The “AND” operator is applied, then the membership degree of the output in a rule can be calculated as

$$\mu(z) = \min \{\mu(x);\mu(y)\}. \tag{4.1}$$

Based on the input information (*E, EC*), the triangle membership function is chosen. Figure 4.6 illustrates the process of implementation of the rules and the logical operator “AND”. The result $\mu(z)$ should go through a defuzzification process.

A defuzzification interface converting the data into a crisp output is accomplished by combining the results of the inference process and then computing the "fuzzy centroid" of the area. In the simple example in Figure 4.6, only one rule was used. Usually a maximum of four rules are involved. To search for an output from more complex results, the weight coefficient is used. The weighted strengths of each output member function are multiplied by their respective output membership function center points and summed. Finally, this area is divided by the sum of the weighted member function strengths, and the result is taken as the crisp output. The result is the $\mu(E;EC)$ weight coefficient which depends on E and EC and is used for calculating K_p, K_i and K_d in Equations 4.2–4.4.

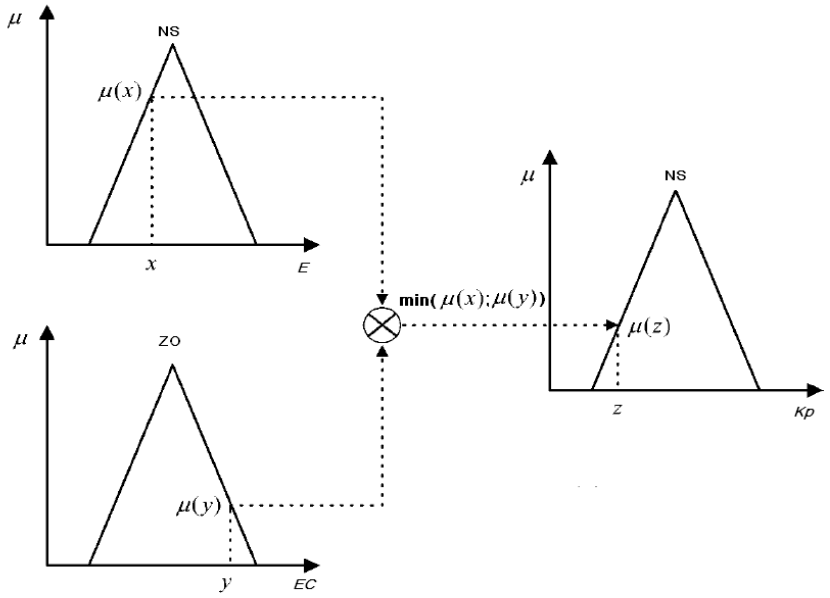

Figure 4.6: Implementing process of a fuzzy rule (Tian, 2004).

New, tuned parameters of the PID controller can be found as follows (Tian, 2004):

$$K_{\mathrm{p}} = K_{\mathrm{pmin}} + \mu K_{\mathrm{p}}(E;EC)\cdot\left(K_{\mathrm{pmax}} - K_{\mathrm{pmin}}\right), \tag{4.2}$$

$$K_{\mathrm{i}} = K_{\mathrm{imin}} + \mu K_{\mathrm{i}}(E;EC)\cdot\left(K_{\mathrm{imax}} - K_{\mathrm{imin}}\right), \tag{4.3}$$

$$K_{\mathrm{d}} = K_{\mathrm{dmin}} + \mu K_{\mathrm{d}}(E;EC)\cdot\left(K_{\mathrm{dmax}} - K_{\mathrm{dmin}}\right), \tag{4.4}$$

where μ is a weight coefficient, K_{pmax} and K_{pmin} are the maximum and minimum limits for the proportional gain, K_{imax} and K_{imin} are the maximum and minimum limits for the integral gain, K_{dmax} and K_{dmin} are the maximum and minimum limits for the derivational gain. The initial values for the self-tuning-parameter of the fuzzy PID were chosen to be the same as for a conventional PID controller (the Zigler-Nichols method was used for finding the coefficients for the conventional PID controller). Appendix D illustrates the Matlab model of PMSM drive with a Fuzzy PID controller. The evaluation and analysis of the fuzzy approach by model, and verification by measurements are shown in Section 5.3.5.

4.2.3 Ripple compensation control

A positive displacement pump flow output ripple can be called pulsation. For our theoretical assumption, we will use the sinusoidal theory of pulsation (Equation 2.7). The produced pulsation can, at least in principle, be removed by adjusting the speed of the motor in synchronism with the flow pulsation of the hydraulic pump. This means that the speed reference signal for the motor should contain an opposite rectified sinusoidal function to the flow pulsation of the pump. Appendix E illustrates the C code of the ripple compensation control. As the torque control in a modern servo drive can be performed very effectively and fast, an electric drive provides an opportunity to compensate for the positive displacement pump pulsation up to certain speeds. Of course, the system torque capability and the inertia limit control the speed ripple.

Before applying the algorithm, the system requires calibration. The top dead centre position of one piston in the pump must be known. If the position of one piston is known, the positions of the remaining four pistons in a five piston pump can be calculated. The top dead centre position of the piston is linked to the position of the rotor, which in servo drives is measured by an accurate resolver. This gives an opportunity to synchronize the reference signal with ripples produced by the pump. Otherwise, the proposed algorithm will oscillate and increase pump pulsation.

A theoretical analysis of speed which can be compensated by the proposed control is shown below. The piston pass frequency is given by

$$f = \frac{n\Omega}{2\pi}, \tag{4.5}$$

where n is the number of pistons and Ω is the rotation angular velocity of the pump.

For example, a five-piston pump produces five strokes per revolution and for instance at 600 rpm the pump rotates 10 revolutions per second and the pump ripple frequency is 50 Hz (Equation 4.5). At 50 Hz, the frequency the period is 20 ms. In principle, there should be enough time to accelerate and decelerate the pump at the lowest operational speeds of the pump.

For rotational motion, Newton's second law can be adopted to describe the relation between torque and angular acceleration:

$$T_{\text{ripple}} = J_{\text{eq}} \cdot \frac{\mathrm{d}}{\mathrm{d}t}\Omega, \tag{4.6}$$

where T_{ripple} is the torque needed for compensation of the ripple, $J_{\text{eq}} = J_{\text{p}} + J_{\text{m}} = 0.0033$ kg/m^2 is the system mass moment of inertia and $\mathrm{d}\Omega/\mathrm{d}t$ is the angular acceleration.

4.3 Structure of software and hardware

Figure 4.7 illustrates the structure of the software and hardware. With this structure, the speed, position and ripple compensation control was implemented. The control of the forklift (electric and hydraulic part) is realized with the help of the dSPACE control panel. The user interface is implemented with a control desk. The control programme algorithms are again implemented in Matlab 2008a. The converter reference speed is delivered through the dSPACE analogue output. The estimated torque and acting speed are delivered to the dSPACE from the ACSM1 converter via analogue signals. In the control of speed and torque, the speed feedback from the resolver is used. DTC is used as the main control principle in the ACSM1 converter.

The output analogue signal also controls the opening of the safety valve for the lowering movement. Also three additional analogue outputs were used to control the speed of the motor. The fuzzy selection of the PID controller parameters K_{p}, K_{i} and K_{d} enable smooth control for different speeds, loads and different directions of operation.

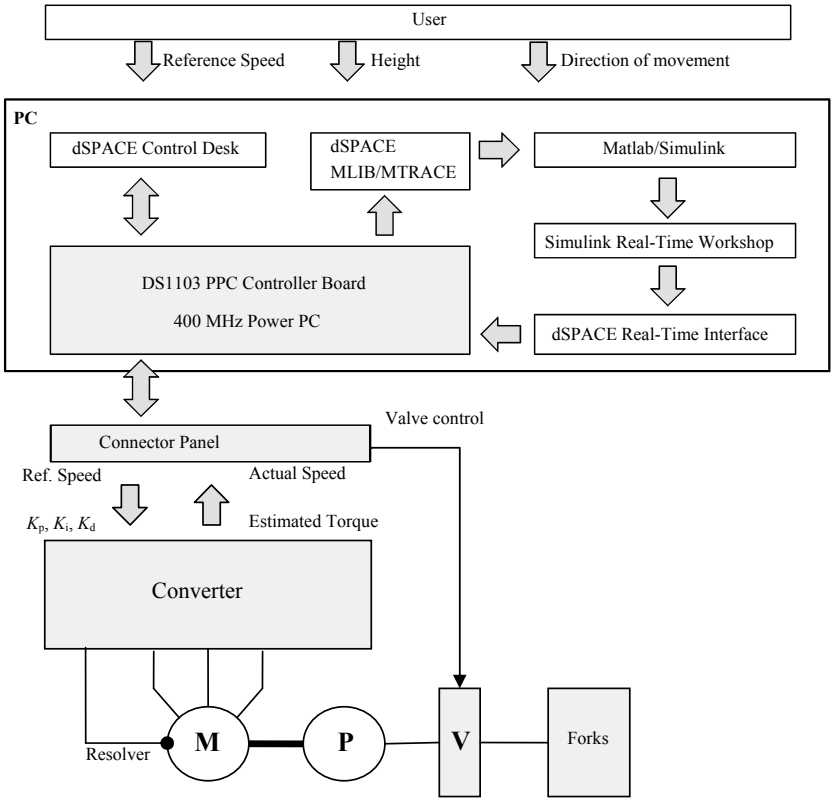

Figure 4.7: Structure of the software and hardware (speed, position control and ripple compensation).

4.4 Summary

In this chapter, the fork movement controller design and the structure of control software were introduced. As this work does not aim at a detailed control design, the traditional PID controller structure was taken as the basis for the work and a double-layer controller is built to control the speed of the fork. In the following chapter, experimental investigation results of the test setup will be given and an analysis of the results will be performed.

5 Experimental tests and analysis

The following section presents experimental investigation of the test setup and an analysis of results.

5.1 Setup description

The experimental investigations were performed at Lappeenranta University of Technology (LUT) in the Laboratory of Electrical Motors and Drives. The test setup is based on a commercial forklift and mainly built aside that. In the study, the original non-regenerative electric drive and hydraulic system of the forklift was replaced by the hydraulic and electric system shown in Figure 5.1. Additional information about the test setup is given in Appendix A.

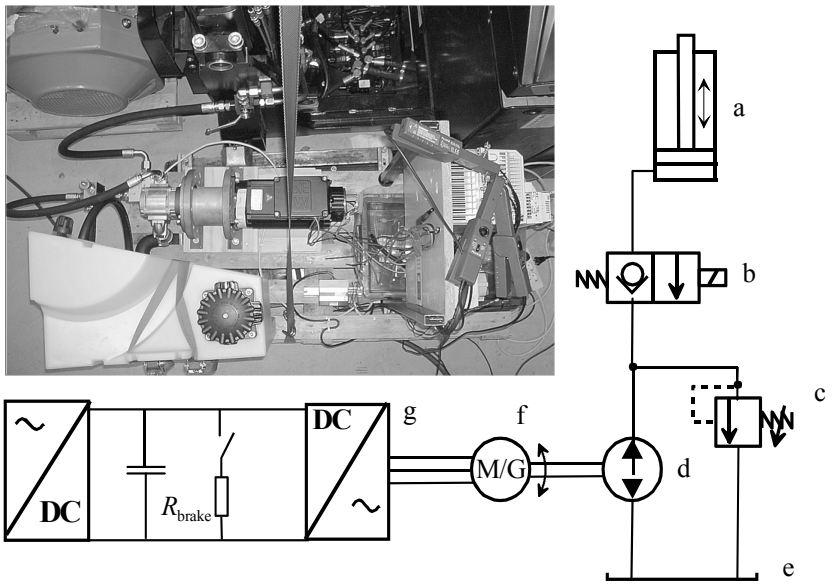

Figure 5.1: Photo and schematics of the electric and hydraulic circuit of the main lift function with energy regeneration from potential energy. The experimental system consists of a) a single-acting cylinder, b) a two-way normally closed poppet valve, c) a pressure relief valve, d) an internal gear pump/motor, e) an oil tank, f) a permanent magnet synchronous motor/generator, g) a frequency converter and a brake resistor R_{brake}.

The experimental test setup uses a speed-controlled electric motor servo drive and a hydraulic pump instead of a proportional valve to control the position of the hydraulic cylinder piston. While operating, the pump raises the oil pressure to the required level determined by the load mass. The two-way normally closed poppet valve included in the system is termed a safety valve. The hydraulic pump produces a flow depending on the rotating speed of the servo motor. The oil flow determines the piston speed, and the

oil pressure determines the actuator force. While lowering a mass, the potential energy of the load produces a flow that rotates the hydraulic machine as a motor, and the mechanically connected electric machine acts as a generator, which is controlled by a frequency converter. The converter rectifies the generated electric energy to the DC link, where an accumulator should be located. In this test case, the electric energy is converted into heat in the brake resistor. The relief valve controls the safety limit of the pressure in the pipes. A control programme was written for the electric drive to control both the electrical and hydraulic parts of the forklift system (Minav, 2008). The test setup was equipped with pressure transducers and electric measurement sensors to measure the efficiencies of different parts of the system. Because of the relatively short lowering period (only a few seconds), recharging of conventional lead acid batteries is inefficient. At the moment, super capacitors seem to be the most suitable solution for fast recharging. Their total cycle efficiency in a charge/discharge cycle is also fairly high, on average approximately 92% (Glavin, 2008).

Benefits of the energy recovery system include reduced electrical energy consumption, an extended operation time between battery charging and an increased utilization rate of the vehicle. With the system developed in this study, the conventional proportional valve can be replaced by a simpler and less costly low-loss valve, as the load speed and torque control are performed by the electric drive.

The experimental setup was tested with payloads of 0 kg, 690 kg and 920 kg for different speeds. The tare weight of the fork system is 250 kg. Two pumps and two motors were tested. In the case of an internal gear pump, the speed of the motor varies from 600 to 3000 rpm, and with an axial piston pump, the speed varies from 400 to 2000 rpm. The experimental setup with a map of the locations of the sensors is shown in Figure 5.2. The axial piston pump and internal gear pump have fixed displacements. The PMSM servo motor is mechanically connected to the hydraulic pump. Depending on the direction of the fork movement has chosen by the user, this combination works either as an electric motor–hydraulic pump or as an electric generator–hydraulic motor combination. An ACSM1- $04x^{4)}x^{5)}$-046A-4 converter was used. The power source of the ACSM1 in the current setup is the electric network, and a brake resistor acts as the "energy storage". The ACSM1 has a resolver as the motor rotor position feedback. When the motor is operating in the generator mode, the regenerated power is fed to the converter DC link. If the other drive modules are not taking enough active power from the DC link at the same time, the braking energy is stored into the DC link capacitors and the DC link voltage increases. The DC link voltage has a limit. Therefore, the regenerative energy should be taken away from the system, if the energy capacity of the common DC system is not sufficient. In the test, this was done simply with a brake chopper and a resistor (ABB: Motion Control program Firmware, 2007).

In the experiments, the rotation speed of the PMSM and the DC voltage in the intermediate circuit are measured. The electric machine torque was estimated by the converter. The information required for calculating the hydraulic energy was taken from two S-10 pressure sensors manufactured by WIKA. They were installed into a pipe

directly after the pump and between the pump and the control valve. Yokogawa PZ4000 Power analysers were used for measuring the phase voltages and currents with a 1MS/s resolution. The speed and height of the forks were measured with a wire-actuated encoder SGW/SGI by SIKO. The pressure, speed and height signals were recorded with a dSPACE DS1103 PPC controller board with I/O.

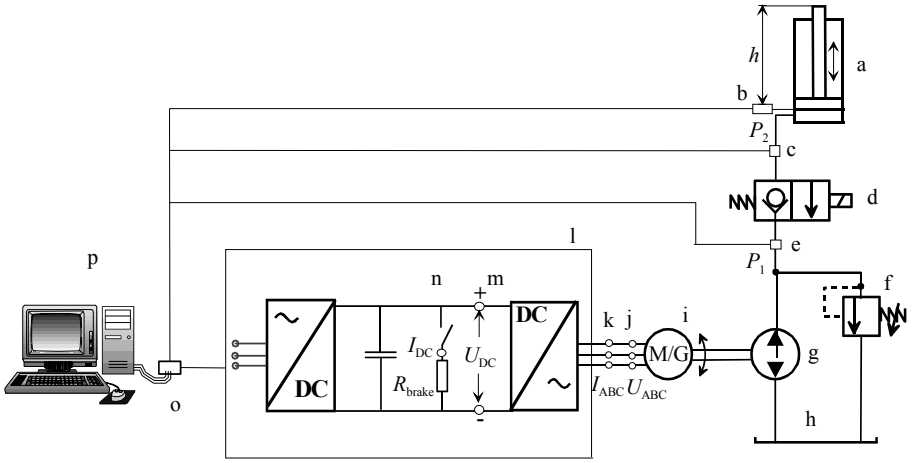

Figure 5.2: Electric and hydraulic circuit of the main lift function with energy regeneration from potential energy. The experimental system consists of a) a single-acting cylinder, b) an actuated encoder SGW/SGI, c) a pressure sensor P2, d) a two-way normally closed poppet valve, e) a pressure sensor P1, f) a pressure relief valve, g) a hydraulic pump/motor, h) an oil tank, i) a permanent magnet synchronous motor/generator, j) phase voltage probes, k) phase current probes, l) a frequency converter and a brake resistor R_{brake}, m) a DC voltage probe, n) a DC current probe, o) the connectional panel dSPACE and p) a computer and dSPACE.

Different sensors used different sampling times, and the data were combined for a complete analysis. Digital low-pass filtering was used to filter noise in the pressure measurements. Because of the large amount of data from different sensors, it was laborious to analyse the results.

There are basically three reasons for errors in a measurement: physical errors in the measuring device, improper or careless use of the measuring device, and ambient conditions. The measurement uncertainty of the Yokogawa power analyser is less than 0.1% of the measurement frequency range. Wika pressure sensors have an uncertainty of 0.25% of the full scale. The repeat accuracy of the wire-actuated encoder SGW/SGI is 0.05 mm, depending on the start direction. It can be assumed that the accuracy is sufficient for this application. The converter torque estimation uncertainty is in the range of a few per cents. Based on the above, it can be assumed that there is a possible error of approximately 1% in the sensor measurements (Minav, 2011b).

By combining all of this information, the cycle efficiency of the system can be calculated. Efficiencies of the lifting and lowering movements were calculated separately. The powers of components were calculated as shown in Table 5.1. The energies of components were calculated by integrating the corresponding powers.

Table 5.1: Definitions of power and energy for calculations (Minav, 2011b).

Equation	Symbol	Measurement method
$E_{pot} = mgh$	E_{pot} – potential energy of the load, J m – mass of load, kg g – gravitational constant h – height of forks, m	h height of fork measured by wire-actuated position encoder SGW/SGI.
$P_{motor} = u_a i_a + u_b i_b + u_c i_c$	P_{motor} – input motor power, W u_a , u_b, u_c – phase voltage, V i_a – phase current, A	u_a phase voltage and i_a phase current measured by probes and Power analyser Yokogawa PZ4000
$P_{shaft} = T_L \Omega$	P_{shaft} – output power of shaft, W T_L – motor torque, Nm Ω – angular speed, rad/sec	Ω angular speed measured and T motor torque estimated by motor control algorithm (ACSM1 software).
$P_{hydr} = p_2 v_c S_p$	P_{hydr} – hydraulic energy output of the pump, W p_2 – pressure, Pa v_c – speed of cylinder piston, m/s S_p– cross area of cylinder, m^2	p_2 pressure measured by Wika pressure sensors S-10 and V_c speed of cylinder piston measured by a wire-actuated encoder SGW/SGI by SIKO.
$P_{brake} = i_{brake}^2 R_{brake}$	P_{brake} – output energy from brake resistor, W i_{brake} – brake current, A R_{brake}– resistance brake resistor, Ω	i_{brake} brake current measured by probes and Power analyser Yokogawa PZ4000. R_{brake} resistance brake resistor measured by a multimeter.

The cycle efficiencies of the system for lifting movements were calculated as shown in Table 5.2:

Table 5.2: Definitions of cycle efficiencies for lifting the load (Minav, 2011b).

Lifting		
System cycle efficiency of lifting $\eta_{\text{up\_sys}}$	$\eta_{\text{up\_sys}} = \frac{E_{\text{pot}}}{E_{\text{motor}}}$	E_{pot} is the potential energy of the load $E_{\text{motor}}$is the input energy to the electric motor
Electric motor cycle efficiency η_{motor}	$\eta_{\text{motor}} = \frac{E_{\text{shaft}}}{E_{\text{motor}}}$	E_{shaft} is the mechanical energy from the motor shaft
Pump cycle efficiency η_{pump}	$\eta_{\text{pump}} = \frac{E_{\text{hydr}}}{E_{\text{shaft}}}$	E_{hydr} is the hydraulic energy output of the pump

The cycle efficiencies of the system for lowering movements were defined as shown in Table 5.3:

Table 5.3: Definitions of cycle efficiencies for lowering the load (Minav, 2011b).

Lowering		
System cycle efficiency of lowering $\eta_{\text{down\_sys}}$	$\eta_{\text{down\_sys}} = \frac{E_{\text{brake}}}{E_{\text{pot}}}$	E_{brake} is the recovered energy
Inverter cycle efficiency η_{inv}	$\eta_{\text{inv}} = \frac{E_{\text{brake}}}{E_{\text{mot}}}$	E_{mot} is the energy taken from the electric generator
Electric generator cycle efficiency η_{gen}	$\eta_{\text{gen}} = \frac{E_{\text{mot}}}{E_{\text{shaft}}}$	E_{shaft} is the output energy from the shaft
Cycle efficiency of hydraulic-mechanical conversion from potential energy to the shaft η_{posh}	$\eta_{\text{posh}} = \frac{E_{\text{shaft}}}{E_{\text{pot}}}$	E_{pot} is the potential energy of the load
Cycle efficiency of the hydraulic motor η_{mot}	$\eta_{\text{mot}} = \frac{E_{\text{shaft}}}{E_{\text{hydr}}}$	η_{mot} is the cycle efficiency of the hydraulic motor
Cycle efficiency of the hydraulic part η_{hydr}	$\eta_{\text{hydr}} = \frac{E_{\text{hydr}}}{E_{\text{pot}}}$	η_{hydr} is the cycle efficiency of the hydraulic part

5.2 Results of experiments

The results will be presented in this section. First, an example of measured data will be shown. Second, the results for an internal gear pump and an axial piston motor will be represented. Finally, these pumps will be compared.

An example of the measured data for internal gear pump is shown in Figures 5.3-5.6. In Figure 5.3, the signal speed is the acting speed of the PMSM in rpm. The signal current is the estimated current of the PMSM in Ampers. The torque is the estimated torque of the PMSM in Nm. U_{dc} is the DC voltage in the DC link of the ACSM1 and RO status shows the position of the relay that controls the counter balance valve (safety valve).

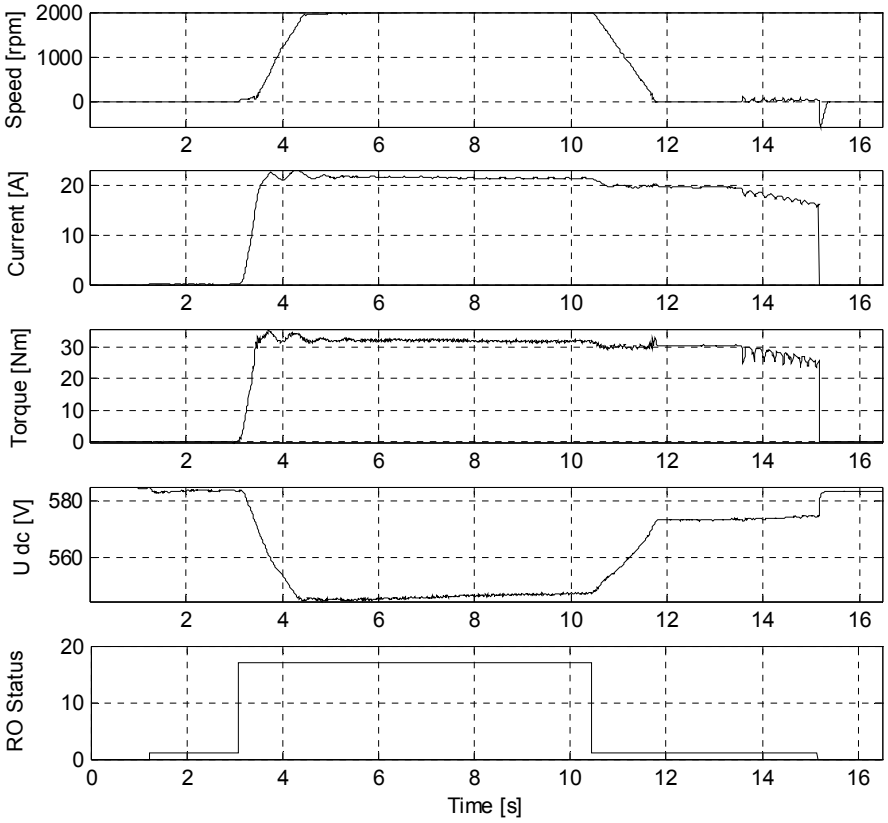

Figure 5.3: Example of the measured data from ACSM1.

Figure 5.4 shows the phase voltage and current measured with probes and the Yokogawa.

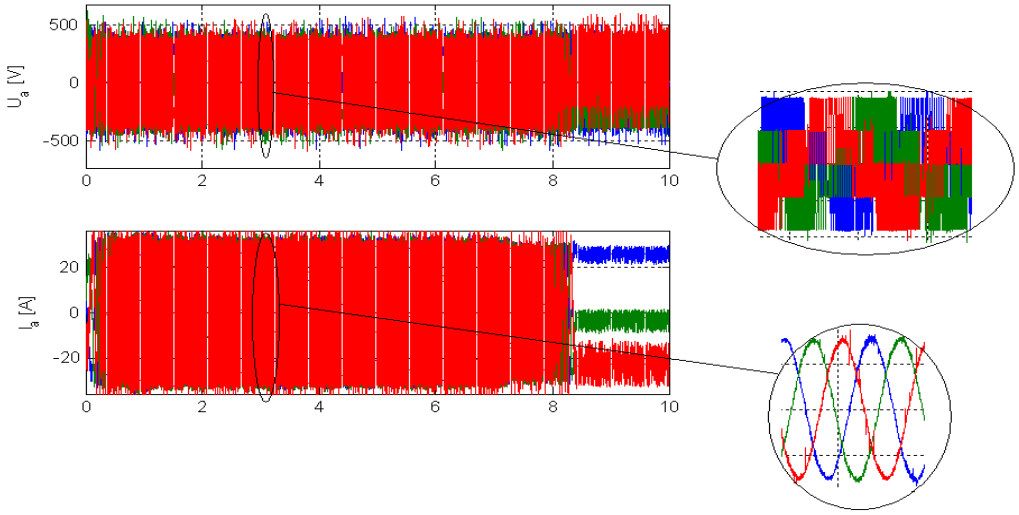

Figure 5.4: Example of the measured data from the Yokogawa.

Figure 5.5 shows an example of measurements of the DC current and DC voltage from the DC link with the Yokogawa for lowering.

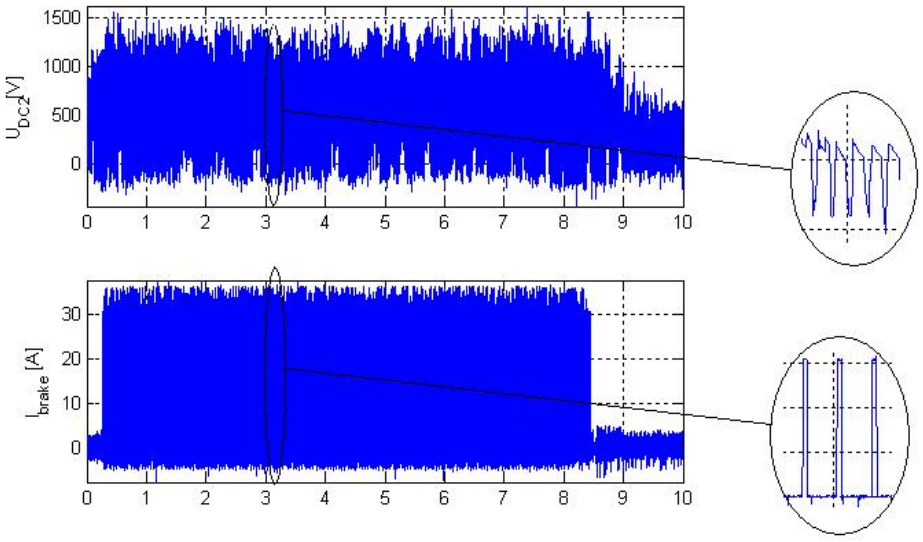

Figure 5.5: Example of the measured data from the Yokogawa during lowering motion.

Figure 5.6 shows an example of the data from the dSPACE for lifting.

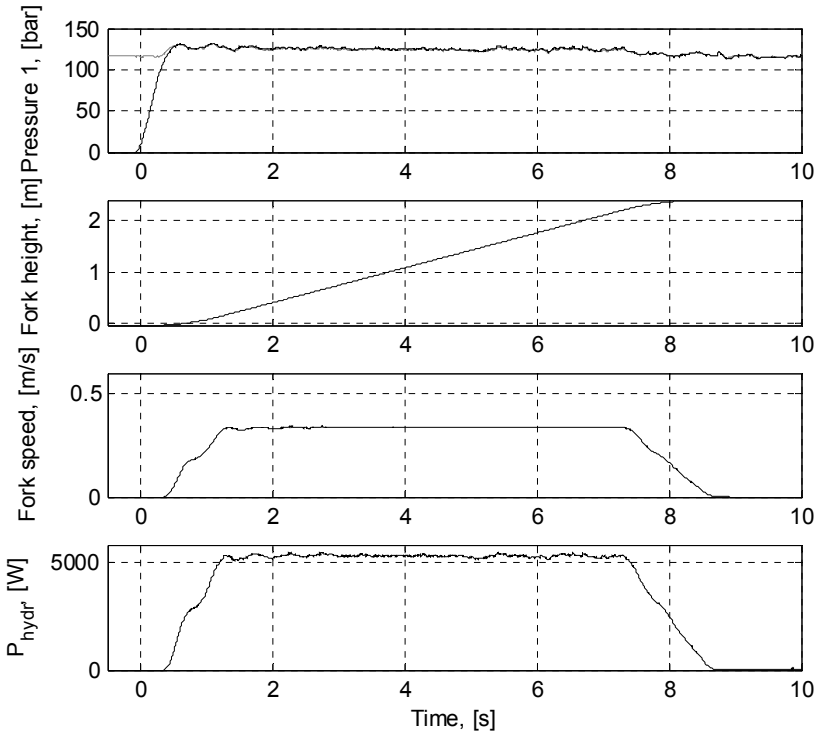

Figure 5.6: Example of the measured data from dSPACE.

In Figure 5.6, the first signal is the pressure measured before and after the valve in bars. The second signal shows the movement of the forks and their height changes. The fork speed was measured in m/s. P_{hydr} is the hydraulic power in W.

5.2.1 Measurements with the internal gear pump

A. *Measured cycle efficiencies for lifting and lowering with different payloads when using the 4.5 kW motor*

Figure 5.7 shows the measurement results for the system cycle efficiency for lifting with payloads of 0 kg, 690 kg and 920 kg for a combination of an internal gear pump and a 4.5 kW PMSM. One should note here that the efficiencies are calculated similarly in each case by dividing the achieved potential energy by the input energy. In this case, there is also a non-zero efficiency for the case where no beneficial work is done for instance when lifting only the tare.

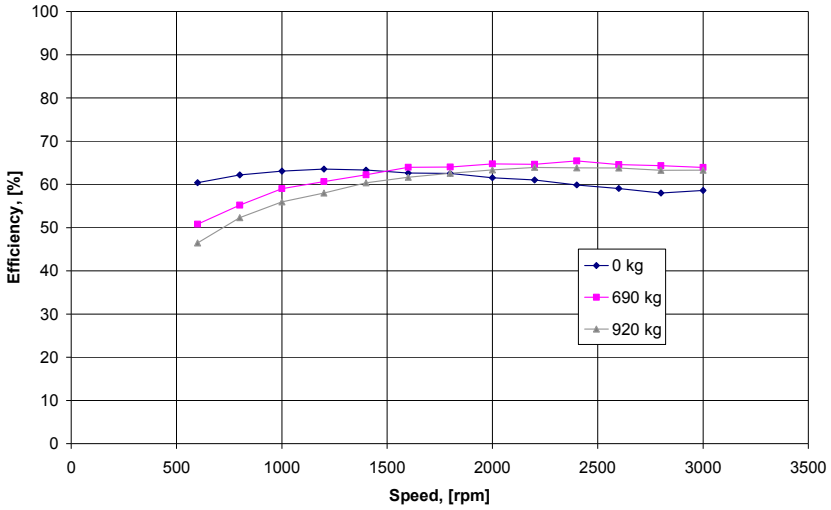

Figure 5.7: System cycle efficiency for lifting with payloads of 0 kg, 690 kg and 920 kg.

The highest system efficiency at zero loads (tare weight only) was roughly 63% and at the 690 kg load 65%. Figure 5.8 shows the system cycle efficiency of the system during lowering with payloads of 0 kg, 690 kg and 920 kg with a combination of an internal gear pump and a 4.5 KW PMSM.

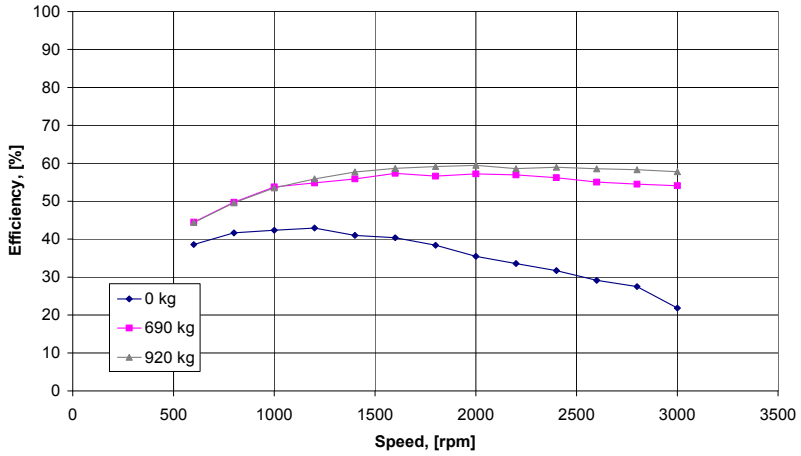

Figure 5.8: System cycle efficiency for lowering with payloads of 0 kg, 690 kg and 920kg.

The cycle efficiency was lowest at the lowest speeds also during lowering. This is mainly due to two reasons: the pump slip, which lets the oil leak, and the copper losses of the electric drive; the cycle efficiency behaviour can be seen to be almost constant at higher speeds.

Figure 5.9 shows the measured 4.5 kW motor cycle efficiencies for lifting and lowering with payloads of 0 kg, 690 kg and 920 kg.

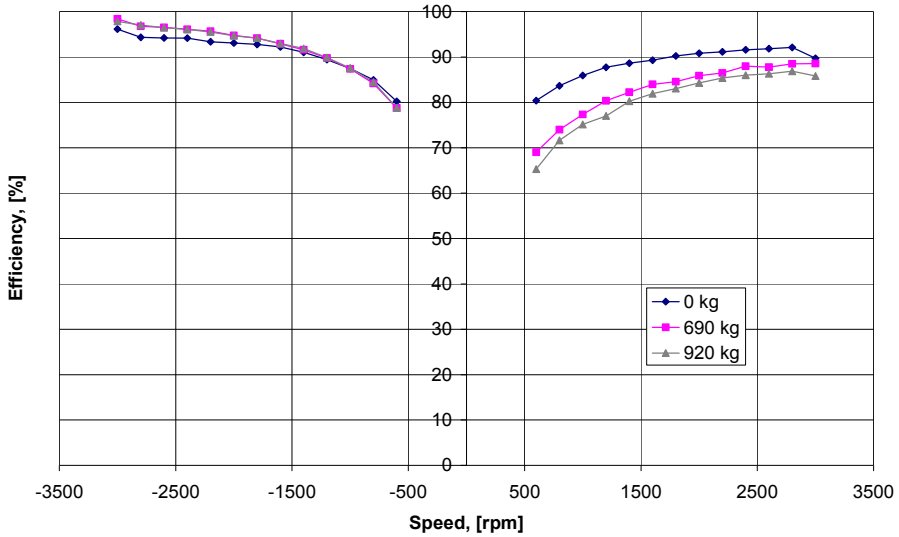

Figure 5.9: Measured motor/generator cycle efficiency for lifting and lowering with payloads of 0 kg, 690 kg and 920 kg.

The results show that with an increasing speed of rotation, the electric machine cycle efficiency will be higher in both the motor and generation modes. In the tests, the lowest motor cycle efficiency was achieved with the load of 920 kg during lifting. At the highest speeds in the motor operation mode, the losses varied between 14% and 10%. For the generation mode, the losses are lower; close to 5%. At the lowest speeds, the losses varied between 35% and 20% for motor operation mode, and from 20% to 10% for the generator mode. This can be explained by high copper losses in the motor and the long lifting time because of the low speed.

Figure 5.10 shows the results of the cycle pump/motor efficiency measurements for lifting and lowering with payloads of 0 kg, 690 kg and 920 kg for 4.5 kW PMSM. This figure shows that the cycle efficiency of the hydraulic pump does not vary considerably as a function of speed or mass to be lifted. The unsymmetrical location of the curves suggested greater losses in the hydraulic motor mode.

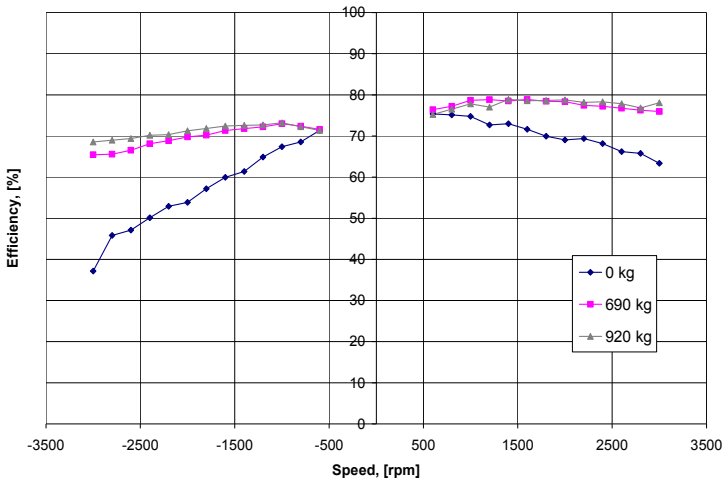

Figure 5.10: Measured pump/motor cycle efficiencies for lifting and lowering with payloads of 0 kg, 690 kg and 920 kg.

B. *Measured cycle efficiencies for lifting and lowering with different payloads with 10 kW PMSM.*

Figure 5.11 shows the measurement results for the system cycle efficiency for lifting with payloads of 0 kg, 690 kg and 920 kg for combination internal gear pump and 10 kW PMSM.

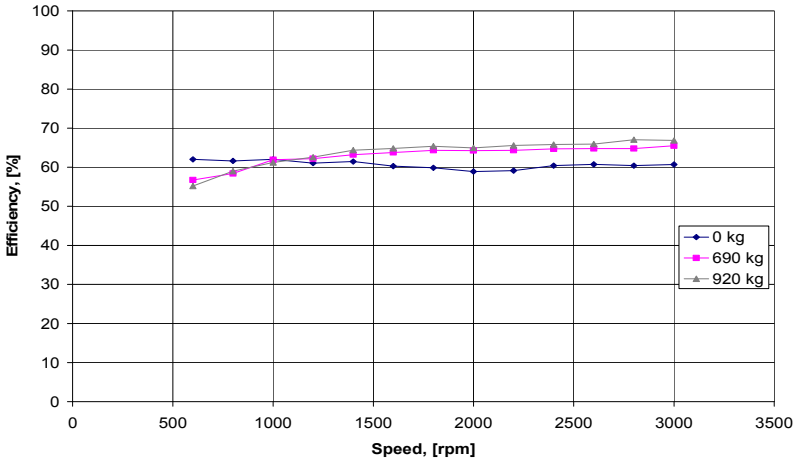

Figure 5.11: System cycle efficiency for lifting with payloads of 0 kg, 690 kg and 920 kg.

The highest cycle efficiency at zero loads (tare weight only) was approximately 62%, and at the 920 kg load it was 67%.

Figure 5.12 shows the system cycle efficiency of the system during lowering with payloads of 0 kg, 690 kg and 920 kg for a combination of an internal gear pump and a 10 KW PMSM.

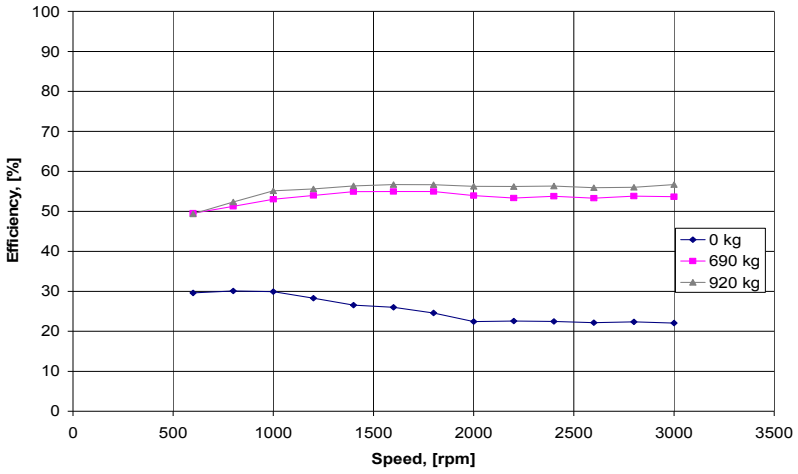

Figure 5.12: System cycle efficiency (E_{out}/E_{pot}) for lowering with payloads of 0 kg, 690 kg and 920 kg.

The lowest cycle efficiency was obtained from the zero load. The lowest cycle efficiency is equal to 22%. The highest cycle efficiency, 57%, was obtained with the maximum tested load 920 kg.

Figure 5.13 shows the measured 10 kW motor cycle efficiencies for lifting and lowering with payloads of 0 kg, 690 kg and 920 kg.

It can be seen that the curves are symmetrical. There is a slight difference between operations. For instance, the motor cycle efficiency with a maximum load is less efficient compared with the generator mode.

According to the test results, increasing the load from 0 to 920 kg degraded the generator cycle efficiency by ten percent units at higher speeds and by three percent units at lower speeds. The maximum motor cycle efficiency reached at the maximum speed of 0.5 m/s (3000 rpm) was 92% and with the zero load and 91% with the 920 kg load. In addition, the maximum generator cycle efficiency reached at the maximum speed of 0.5 m/s (3000 rpm) was 85% and with the zero load and 95% with the 920 kg load.

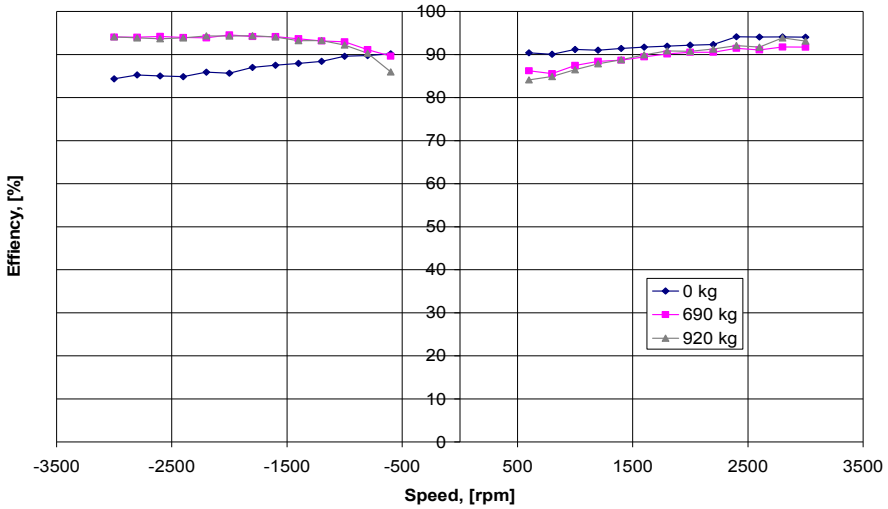

Figure 5.13: Measured motor/generator cycle efficiency for lifting and lowering with payloads of 0 kg, 690 kg and 920 kg.

Figure 5.14 shows the results of the pump/motor cycle efficiency measurements for lifting and lowering with payloads of 0 kg, 690 kg and 920 kg for a 10 kW PMSM.

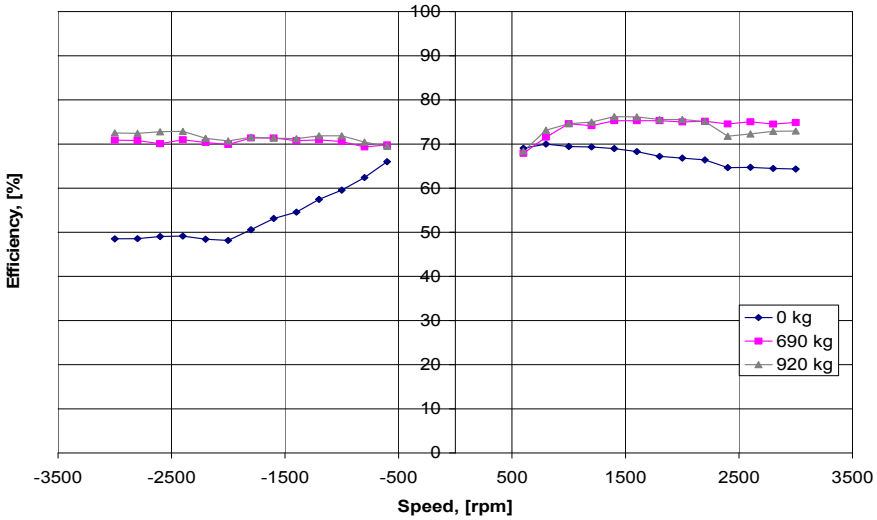

Figure 5.14: Measured pump/motor cycle efficiencies for lifting and lowering with payloads of 0 kg, 690 kg and 920 kg.

Figure 5.14 shows that the cycle efficiency of the hydraulic pump varies considerably as a function of speed or mass to be lifted. The unsymmetrical location of the curves suggested greater losses in the hydraulic motor mode.

5.2.2 Measurements for the axial piston motor

A. *Measured cycle efficiencies for lifting and lowering with different payloads with a 4.5 kW PMSM.*

Figure 5.15 shows the measurement results for the system cycle efficiency for lifting with payloads of 0 kg, 690 kg and 920 kg for a combination of an axial piston motor and a 4.5 kW PMSM.

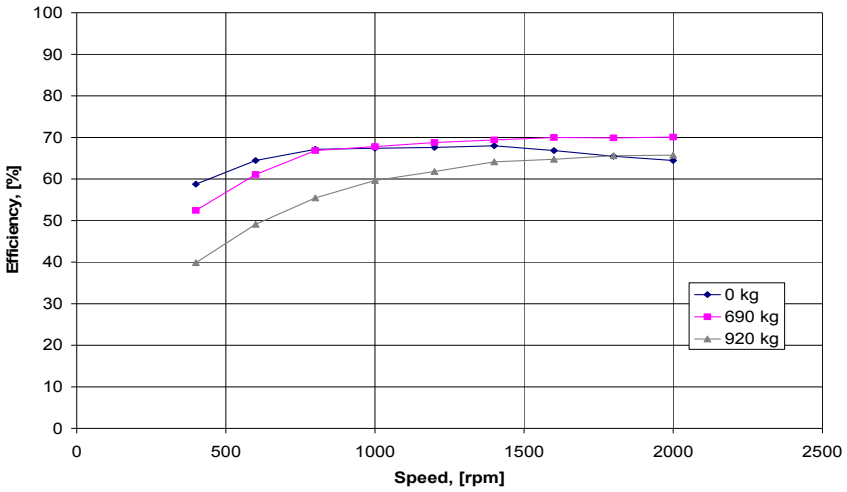

Figure 5.15: System cycle efficiency for lifting with payloads of 0 kg, 690 kg, and 920 kg.

The highest cycle efficiency at zero loads (tare weight only) was roughly 68%, and at the 690 kg load it was 70%.

Figure 5.16 shows the system cycle efficiency of the system during lowering with payloads of 0 kg, 690 kg and 920 kg with axial piston motor and 4.5 KW PMSM combinations.

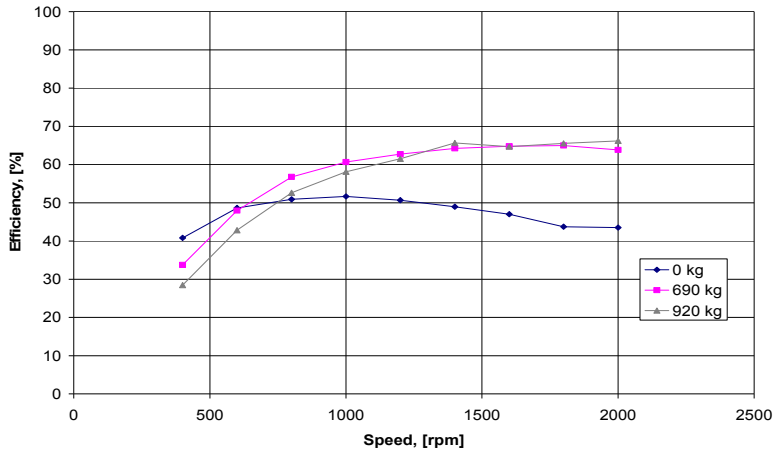

Figure 5.16: System cycle efficiency for lowering with payloads of 0 kg, 690 kg and 920 kg.

Figure 5.17 shows the measured 4.5 kW motor cycle efficiencies for lifting and lowering with payloads of 0 kg, 690 kg and 920 kg.

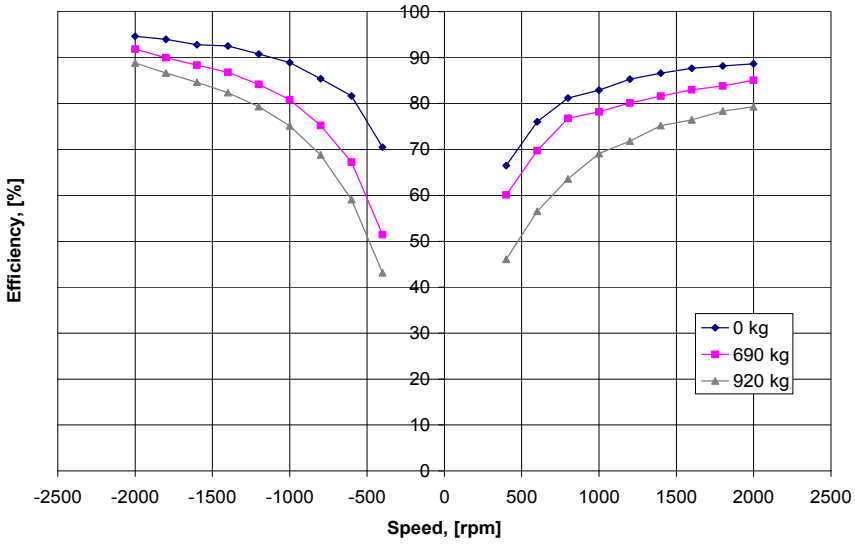

Figure 5.17: Motor/generator cycle efficiency for lifting and lowering with payloads of 0 kg, 690 kg and 920 kg.

The results show that with an increasing speed of rotation, the electric motor cycle efficiency is higher. In the tests, the lowest cycle efficiency was achieved with the load

of 920 kg. At the highest speeds, the losses varied between 21% and 12%. At the lowest speeds, the losses varied between 52% and 73%. This can be explained by high copper losses in the motor and the long lifting time because of the low speed. It can be noticed that the curves for the motor and generator are symmetrical against the vertical axis.

Figure 5.18 shows the results of the pump/motor cycle efficiency measurements for lifting and lowering with payloads of 0 kg, 690 kg and 920 kg for a 4.5 kW PMSM. Figure 5.18 shows that the cycle efficiency of the hydraulic pump does not vary considerably as a function of speed or mass to be lifted. The symmetrical location of the curves indicated greater losses in the zero-load test.

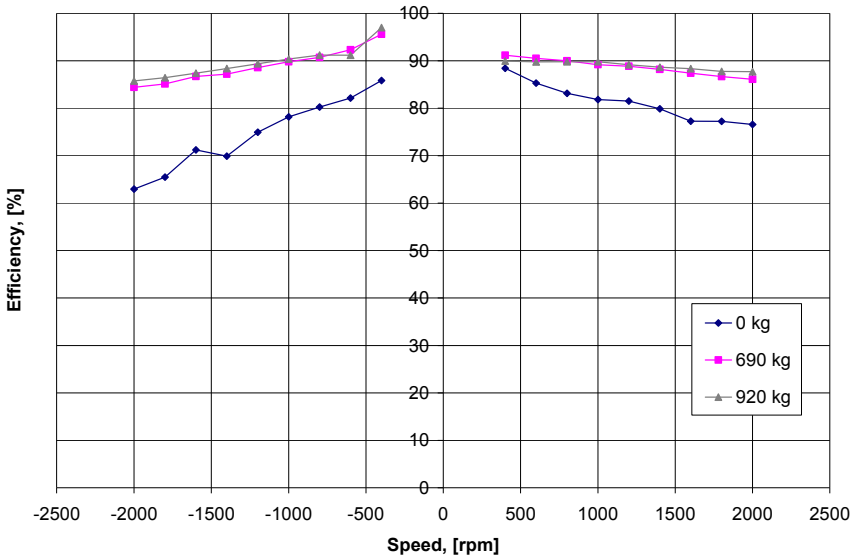

Figure 5.18: Measured pump/motor cycle efficiencies for lifting and lowering with payloads of 0 kg, 690 kg and 920 kg.

B. *Measured cycle efficiencies for lifting and lowering with different payloads with a 10kW PMSM.*

Figure 5.19 shows the measurement results for the system cycle efficiency for lifting with payloads of 0 kg, 690 kg and 920 kg for a combination of an axial piston motor and a 10 kW PMSM. The highest cycle efficiency at zero loads (tare weight only) was approximately 70%, and at the 920 kg load it was 72%.

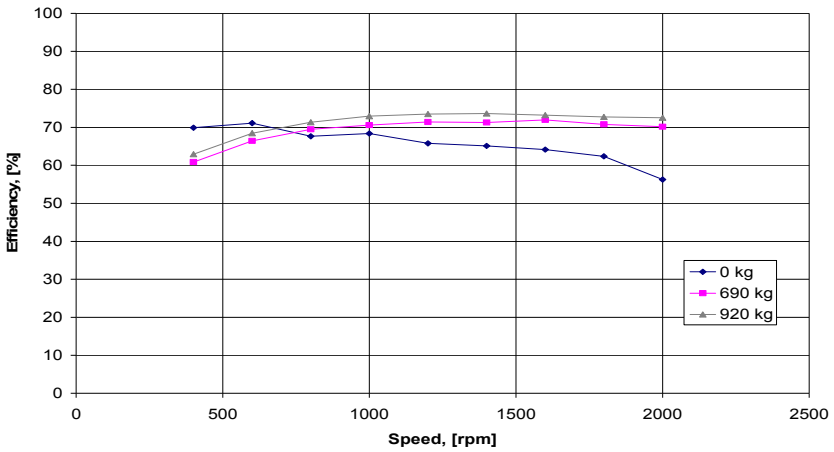

Figure 5.19: System cycle efficiency for lifting with payloads of 0 kg, 690 kg, and 920 kg.

Figure 5.20 shows the system cycle efficiency of the system during lowering with payloads of 0 kg, 690 kg and 920 kg with axial piston motor and 4.5 KW PMSM combinations.

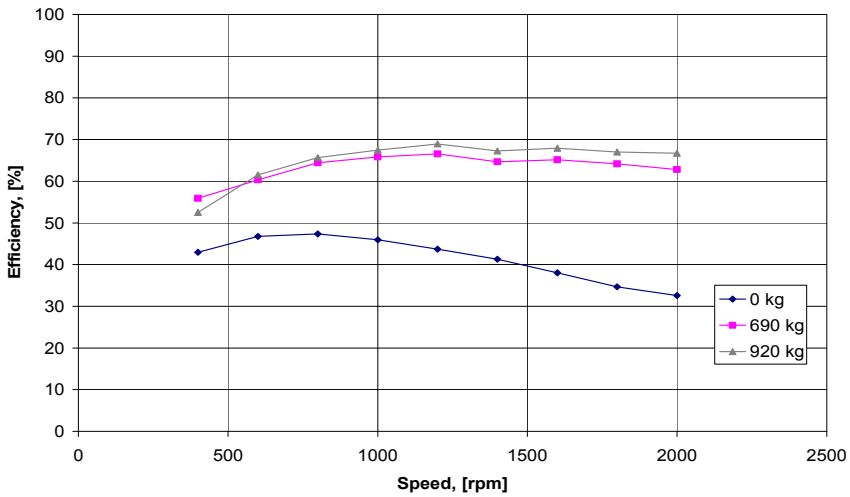

Figure 5.20: System cycle efficiency for lowering with payloads of 0 kg, 690 kg, and 920 kg.

The cycle efficiency 68% was achieved in the 920 kg load test for a maximum speed of 2000 rpm.

Figure 5.21 shows the measured 10 kW motor cycle efficiencies for lifting and lowering with payloads of 0 kg, 690 kg and 920 kg.

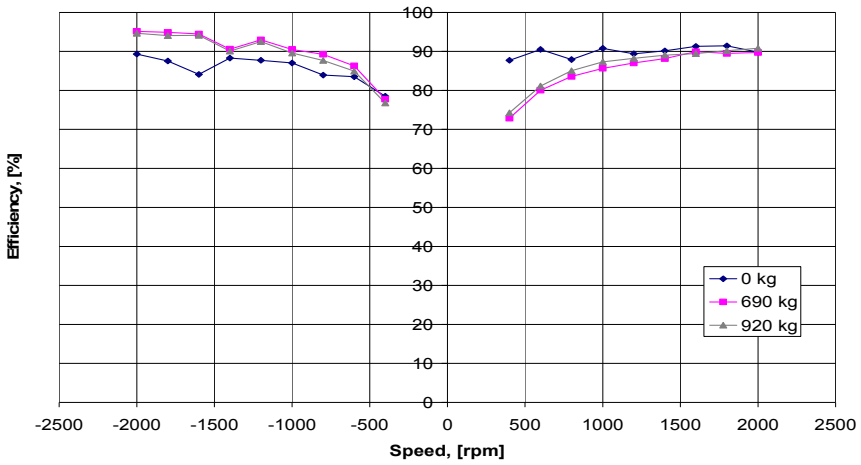

Figure 5.21: Motor/generator cycle efficiency for lifting and lowering with payloads of 0 kg, 690 kg and 920 kg.

Figure 5.22 shows the results of the pump/motor cycle efficiency measurements for lifting and lowering with payloads of 0 kg, 690 kg and 920 kg for a 10 kW PMSM.

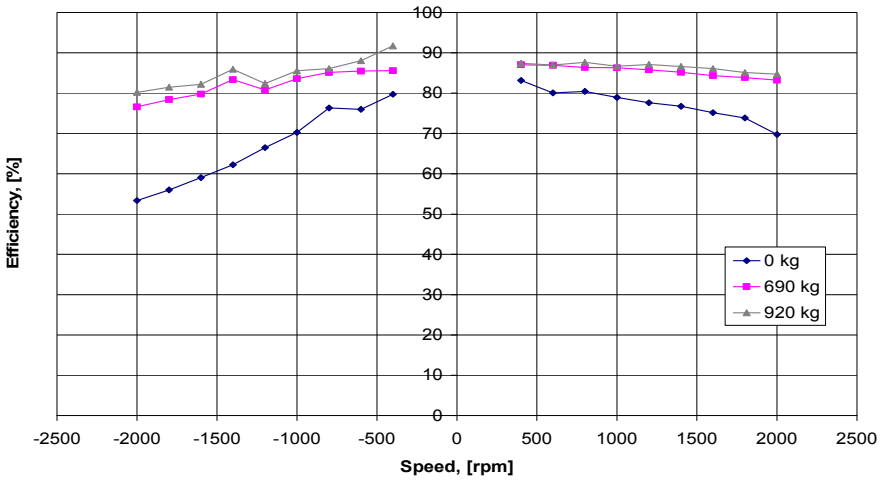

Figure 5.22: Measured pump/motor cycle efficiencies for lifting and lowering with payloads of 0 kg, 690 kg and 920 kg.

Figure 5.22 shows that the cycle efficiency of the hydraulic pump does not vary considerably as a function of speed or mass to be lifted. The curves are located symmetrically against the vertical axes.

5.2.3 Analysis of the cycle efficiencies

Figure 5.23 illustrates cycle efficiencies for a combination presented earlier with an internal gear pump and an axial piston motor with the load of 0 kg. The measurement data for the inverter cycle efficiency for lifting movement were not examined. To estimate the circuit efficiency, the system lifting cycle efficiency was multiplied by the inverter cycle efficiency for downward movement.

It can be seen that combination of a gear pump and a PMSM is not very efficient for lifting a zero load. At the same time, however, the combination of an axial piston motor and a PMSM shows good results for both the lifting and lowering of empty forks. It is interesting that the small PMSM exhibits better regeneration with a zero load compared with the larger 10 kW machine. In lifting, the highest cycle efficiency was achieved with the same configuration of an internal gear pump and a 4.5 kW PMSM. It can be observed that the cycle efficiency lines are not symmetric relative to the vertical y axis.

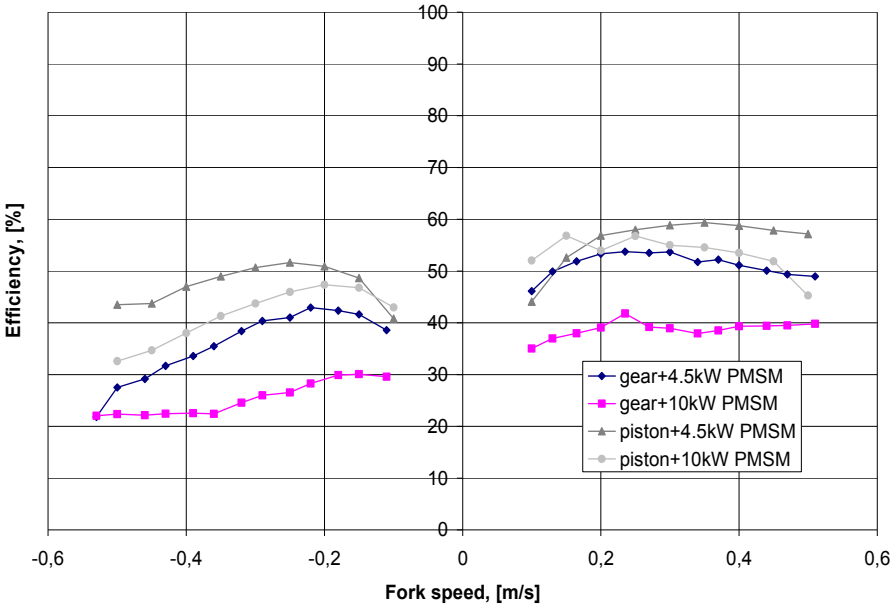

Figure 5.23: Measured system cycle efficiencies for lifting and lowering with payloads of 0 kg.

Figure 5.24 illustrates system cycle efficiencies for a combination presented earlier with an internal gear pump and an axial piston motor with the load of 920 kg.

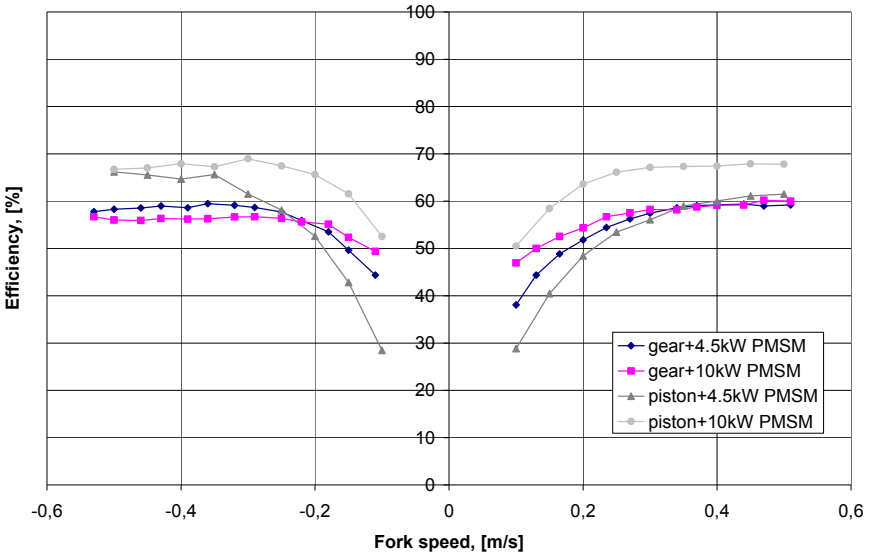

Figure 5.24: Measured system cycle efficiencies for lifting and lowering with payloads of 920kg.

It can be observed that the cycle efficiency lines are symmetric relative to the vertical axis. The highest cycle efficiency for lifting, 68%, was achieved for the axial piston pump and large 10 kW PMSM combination. The same combination gave the best regeneration cycle efficiency of 69%. The system cycle efficiency is quite low for lower speeds. Nevertheless, for speeds above 0.3 m/s, the average lifting cycle efficiency is 60%, and for lowering 55%. It can be concluded that the combination of the axial piston pump is so far the best for these types of applications. Appendix F contains, as an example, cycle efficiency Sankey diagrams for lifting and lowering with 10 kW PMSM and axial piston pump for speed 2000 rpm and payload 920 kg.

5.3 Verification of the models by measurements

The actual simulation work was presented in Chapter 3. The following section verifies the simulation results by comparing them with the measurements.

5.3.1 Verification of the motor model

The next step is verifying the calculated model of the PMSM from Section 3.2.1 with the measured sets of efficiency.

Figure 5.25 shows the calculated efficiency of the PMSM CFM90M with the measured efficiency points with an internal gear pump and an axial piston motor.

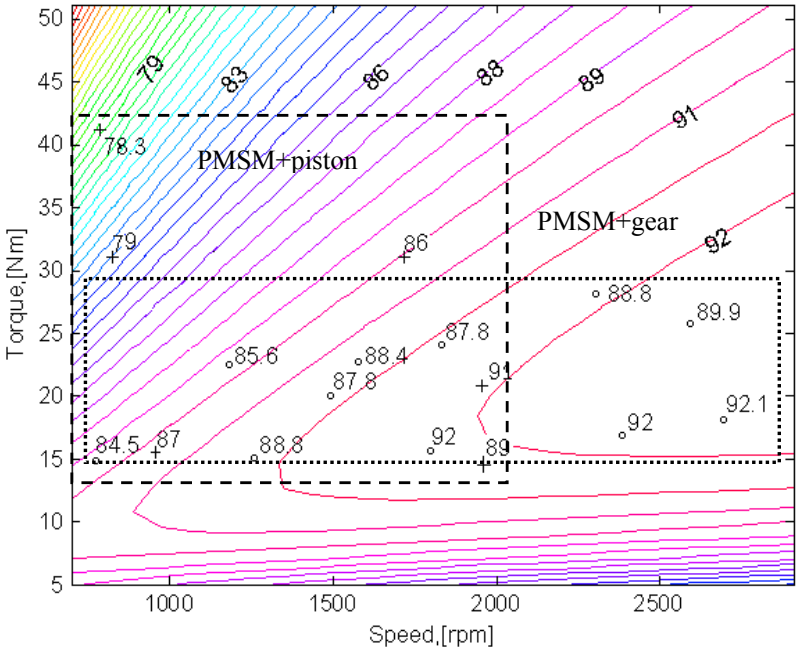

Figure 5.25: Efficiency maps for the CFM90M PMSM. Some measured efficiency points (instantaneous efficiencies measured from the constant speed regions of cycles) in lifting are indicated by + signs when operating with the piston pump and with ○ signs when operating with internal gear pump (Minav, 2011d).

It can be seen that the rated region shows high efficiency.

Figure 5.26 shows the calculated efficiency of PMSM CFM90M with the measured efficiency points with an internal gear pump and an axial piston motor.

Comparing the experimental points with the simulation curves, a conclusion can be drawn that the verified model is trustworthy. It can also be concluded that the motor for the experiments was not chosen correctly, and a new motor needs to be chosen for the current setup so that the system operation point is located in the area of maximum efficiency. This means that the lifting and lowering efficiencies (recovery options) can be improved.

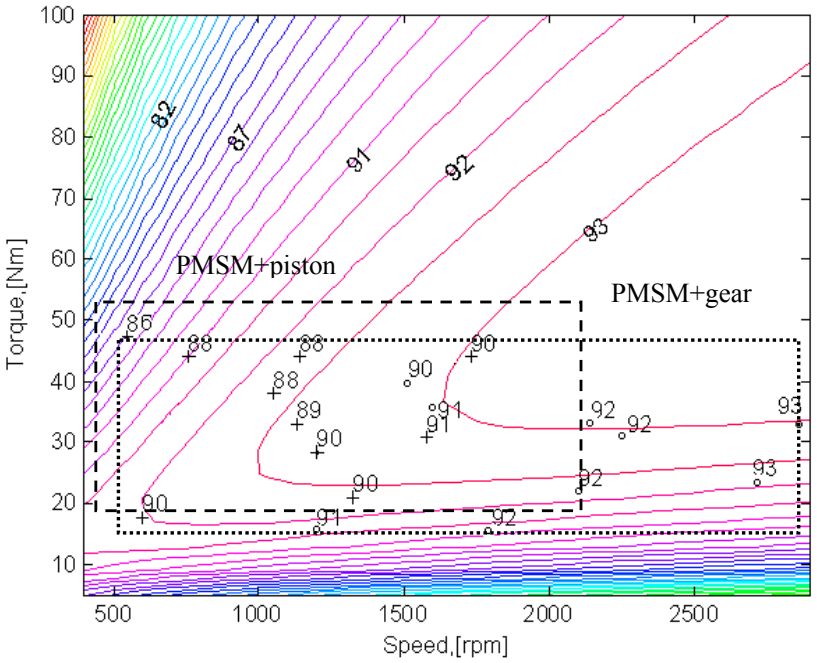

Figure 5.26: Efficiency maps for the 10 kW PMSM (CFM112M). Some measured efficiency points (instantaneous efficiencies measured from the constant speed regions of cycles) in lifting are indicated with + signs when operating with the piston pump and with ○ signs when operating with internal gear pump (Minav, 2011d).

5.3.2 Verification of the Matlab/Simulink lifting model

In order to make the simulation trustworthy, the model should be verified by experiments. The process of verification of the model is discussed below. The first step was to conduct the experiments and record the structured data in time sequences. The second step was to measure the acting speed used as a reference signal for the simulation. The parameters of friction in the model were adjusted until the behaviour of the model was similar to reality. This procedure was repeated for the verification of the lifting and lowering model.

Figure 5.27 illustrates the dynamic simulation results: the speed, torque, pressure and position of the fork for a payload of 920 kg with an internal gear pump and a 4.5 kW PMSM. The speed and the torque have some ripple in this operation, and a better controller or a smoother speed reference should be used.

Figure 5.28 illustrates the measurement results: the speed, torque, pressure and position of the fork for a payload of 920 kg with an internal gear pump and a 4.5 kW PMSM. The speed in Figure 5.27 follows the motor ramp measured from the test setup (Figure

5.28). The pressure and torque grow similarly at the beginning to overcome friction. Subsequently, they stay constant and decrease slightly when the speed is reduced. The plot "Position" (Figure 5.27) demonstrates how the fork moves from its initial zero position to the maximum (plot "Fork height" in Figure 5.28). When comparing Figures 5.27 and 5.28, it can be concluded that the dynamic simulation gives results comparable with the measurement results (Minav, 2011e).

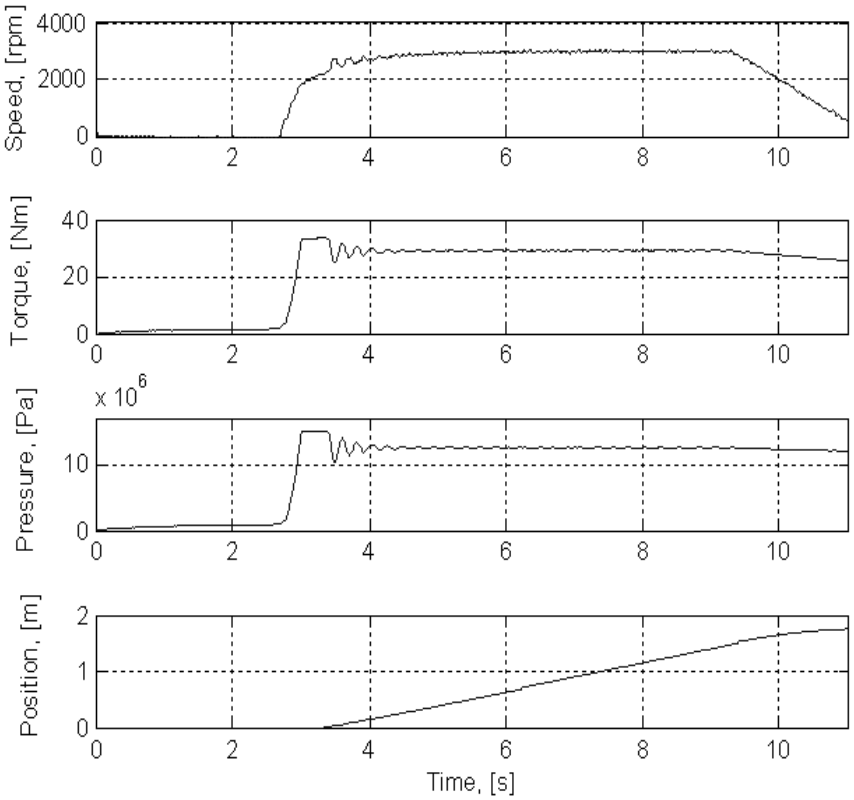

Figure 5.27: Simulated speed, torque, pressure and position for lifting the payload of 920 kg.

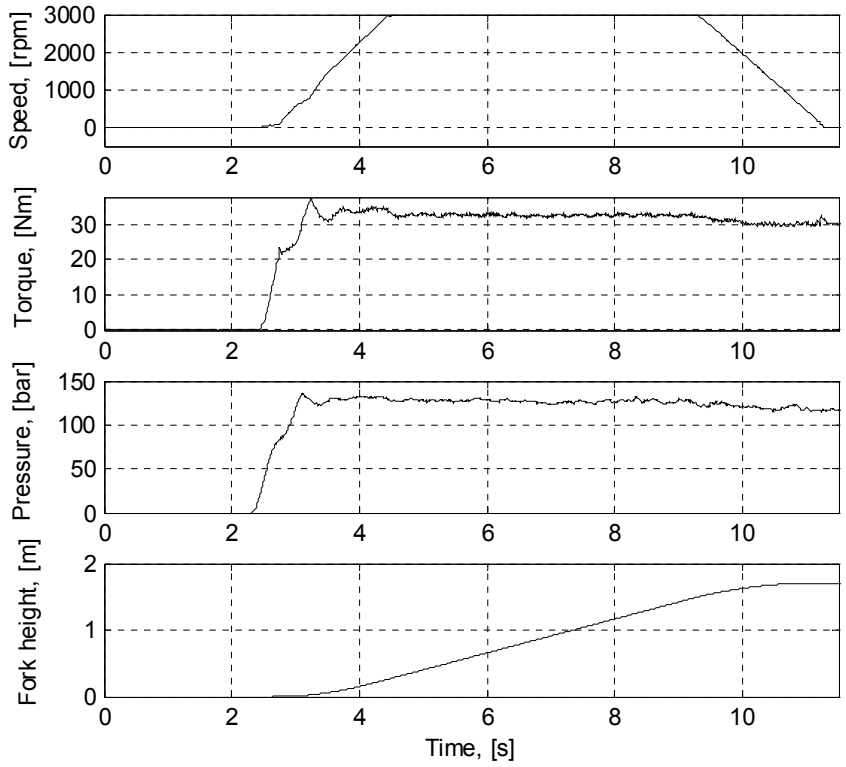

Figure 5.28: Measured speed, torque, pressure and position for lifting the payload of 920 kg.

Table 5.4 illustrates the measured and simulation results for lifting the payload of 920 kg for the combination of an internal gear pump and a 4.5 kW PMSM.

Table 5.4: Comparison of measured and simulation results for lifting the payload 920 kg (Minav, 2011e).

Lifting the payload of 920 kg		
Values	Measurements	Simulation
Height of movement, [m]	1.7	1.67
Speed of rotation, [rpm]	3000	3000
Fork velocity, [m/s]	0.5	0.5
Potential energy, [kJ]	51	51
Hydraulic energy,[kJ]	54	54
Energy from the shaft to hydraulic-mechanical conversion, [kJ]	68	68
Motor energy, [kJ]	80	79
Cycle efficiency of the hydraulic part, [%]	95	95
Electric motor cycle efficiency, [%]	86	85
Cycle efficiency from the shaft to hydraulic-mechanical conversion, [%]	74	75
Hydraulic pump cycle efficiency, [%]	78	80
System lifting cycle efficiency, [%]	63	64

It can be seen that the results from the simulation match the experimental results well.

5.3.3 Verification of the Matlab/Simulink lowering model

Table 5.5 illustrates the measured and simulation results for lifting the payload of 920 kg for the combination of an internal gear pump and a 4.5 kW PMSM.

Table 5.5: Comparison of measured and simulation results for lowering the payload 920 kg.

Lowering the payload of 920 kg		
Values	Measurements	Simulation
Height of movement, [m]	1.81	1.81
Speed of rotation, [rpm]	3000	3000
Fork velocity, [m/s]	0.5	0.5
Potential energy, [kJ]	54	54
Hydraulic energy, [kJ]	50	49
Energy to the shaft, [kJ]	34	35
Generator energy, [kJ]	33	33
Energy from the brake resistor, [kJ]	31	31
Cycle efficiency of the hydraulic part, [%]	92	90
Generator cycle efficiency, [%]	98	93
Cycle efficiency from the hydraulic-mechanical conversion to the shaft , [%]	63	64
Hydraulic pump cycle efficiency, [%]	69	71
Cycle efficiency of inverter, [%]	94	94
System lowering cycle efficiency, [%]	58	57

5.3.4 Verification and analysis of ripple compensation

Energy consumption and the level of noise have become important factors in evaluating the performance of machines and equipment. In order to overcome these weak points in conventional hydraulic systems, new alternative concepts need to be applied. The presented control algorithm proposes an FBN reduction in Section 4.2.3. The following chapter contains simulation results, described in Section 3.3.4 and analysis of the applicability of the results.

Figure 5.29 illustrates the simulation results of calculated reference speed signals for the proposed compensation method for speeds 500, 1000, 1500 and 2000 rpm. This speed signal reference forces the motor speed to oscillate in synchronism with the pump pistons. Such an operation at the same time reduces the fluid flow oscillations.

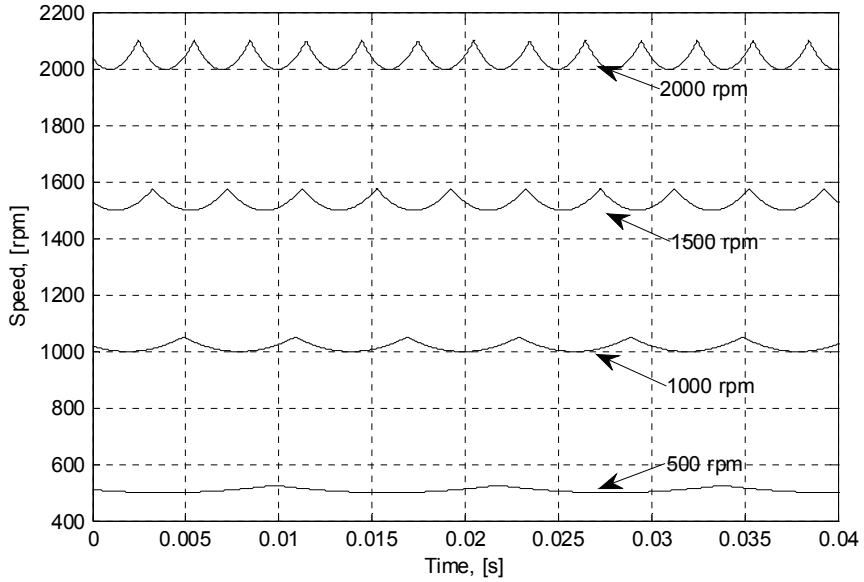

Figure 5.29: Ripple compensation speed reference signals calculated for average speeds of 500, 1000, 1500 and 2000 rpm (Minav, 2011a).

This means for instance that at a speed of 500 rpm, the motor drive needs to accelerate from 500 rpm to 525 rpm (Figure 5.29) during 0.006 seconds to compensate for the fluid flow dip. For the speed of 1500 rpm, the reference signal should vary by 65 rpm during 0.002 seconds; three times faster compared with the 500 rpm compensation signal.

Figure 5.30 illustrates a simulation result of the proposed compensation method at a low speed. The blue line is the original ideal flow delivery of the five-piston axial piston pump; the green line is the result after applying the speed oscillation technique in the motor control.

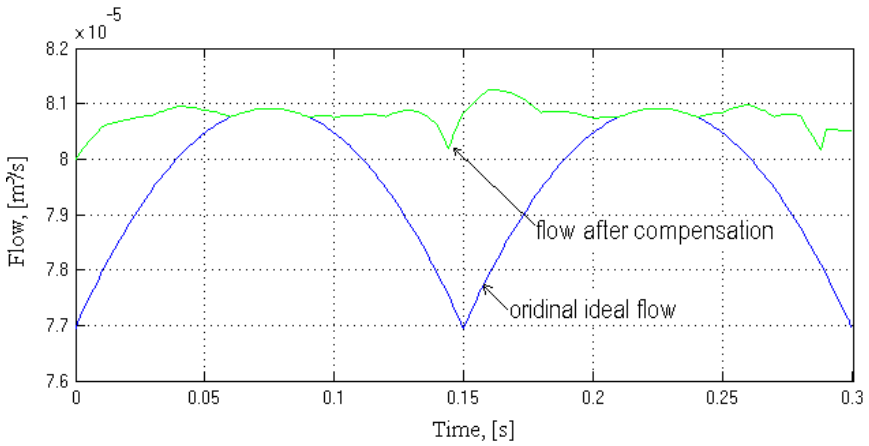

Figure 5.30: Simulation results of the flow for the speed 40 rpm: the blue line is the original ideal flow delivery and the green line is the result of the compensation technique (Minav, 2011a).

Figure 5.30 shows that the flow ripple amplitude has become significantly smaller. Figure 5.31 illustrates a simulation result of the torque reference for the proposed compensation method at a low speed of 40 rpm for the 0 kg payload.

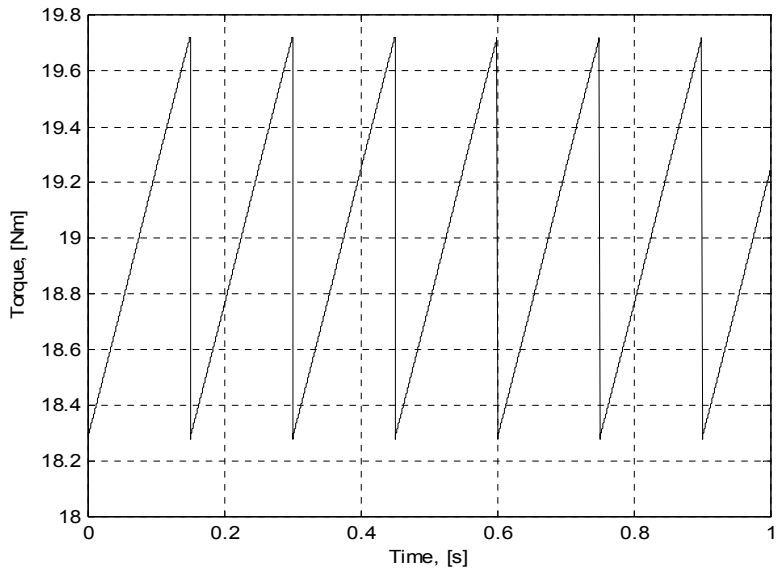

Figure 5.31: Simulation results of the torque reference for the speed 40 rpm for the 0 kg payload.

Table 5.6 illustrates the measured PMSM phase currents and torques with different loads at different speeds. According to Table 5.6, lifting a load of 920 kg required 41 Nm with a speed of 400 rpm. This is the maximum load measured with the experimental test setup. The CFM112M was chosen for the evaluation. The characteristics of the CFM112 M are 31 Nm nominal torque, 35 A nominal current, 108 Nm maximum torque, and 140 A maximum current.

Table 5.6: Measured PMSM torques with different loads in lifting at different rotational speeds (Minav, 2011a).

Speed, [rpm]	Mass of payload, [kg]		
	0 kg	690 kg	920 kg
	Torque, [Nm]		
400	18	35	41
1000	19	35.5	42
2000	22	37	43

Torque limitation was calculated by applying Equation (4.2) in Table 5.7; also the actual and required differentials di/dt given in Table 5.8 was calculated by using Equation (5.1).

$$\frac{\mathrm{d}i}{\mathrm{d}t} = \frac{U_\mathrm{s} - E_\mathrm{s}}{L_\mathrm{d}}, \tag{5.1}$$

where U_s is power supply voltage, E_s is the stator-flux-linkage-produced back emf, where $U_\mathrm{res} = U_\mathrm{s} - E_\mathrm{s}$ is the reserve voltage, L_d is synchronous inductance of a PMSM with no damping 3.1 mH and di/dt is the current differential.

Table 5.7: Estimation of the maximum PMSM torques with different loads in lifting at different rotational speeds when using dynamic ripple compensation.

Speed, [rpm]	Mass of payload, [kg]		
	0 kg	690 kg	920 kg
	Torque, [Nm]		
50	19.2	36.2	43.2
500	38	55	62
1000	95	>100	>100
1500	>100	>100	>100
2000	>100	>100	>100

Dynamic limitation was calculated for the 0 kg payload in Table 5.8 for different speeds.

Table 5.8: Estimation of dynamic limitations with the 0 kg payload in lifting at different rotational speeds.

Speed, [rpm]	Reserve voltage U_{res}, [v]	Maximum available current differential di/dt , [kA/s]	Required differential di/dt , [kA/s]	Required peak current, I_{peak}, [A]	Required peak torque, T_{peak}, [Nm]	Decision (yes/no)
50	319	103	0.052	6.25	18.2	yes
500	283	91.5	1.06	12.75	36.95	yes
1000	243	78.5	5.45	32.7	97.8	yes/no border
1500	203	65.6	16.6	66.3	192.3	no
2000	164	52.7	37.3	111.9	324.5	no

The limit for compensation operation also comes from the torque capability of the motor. As Table 5.7 indicates, at a speed of 2000 rpm to compensate the flow ripple at this speed with any payload the required dynamic torque is more than 100 Nm; it is almost two or three times as high as the standard operation torque at this speed (Table 5.6). Based on Equation (4.6) and Table 5.6, it can be concluded that the motor used in the tests is capable of producing the required torque in a limited speed range. The maximum speed for compensation is reached when the drive speed can no longer follow the speed reference desired (Note: I_{max} = 140 A, T_{max} = 108 Nm for CFM112M). The maximum theoretical speed limit is 1000 rpm for the 0 kg payload based on dynamic estimations (Table 5.7 and Table 5.8). The final answer to the maximum operating speed of the compensation system can only be found by testing.

5.3.5 Verification of the fuzzy control approach

As is was mentioned earlier in Section 4.1, in the experimental setup during switching from lifting to lowering, the slow response of the PMSM drive results in an overshoot in the acting speed, which affects the hydraulic part of the system negatively.

The realized controller was simulated in Matlab 2008a, and system model are shown in Appendix D. A fuzzy control block was used to construct the control rules for the self-tuning PID controller.

For simulation (Figure D.3, Appendix D), the following values were chosen: K_{pmax} = 20, K_{pmin} = 0, K_{imax} =6, K_{imin} = 0 , K_{dmax} = 0.001 and K_{dmin} = 0.

The step responses for the conventional PID control are presented in Figure 5.32 and for the self-tuned-parameter fuzzy PID in Figure 5.33.

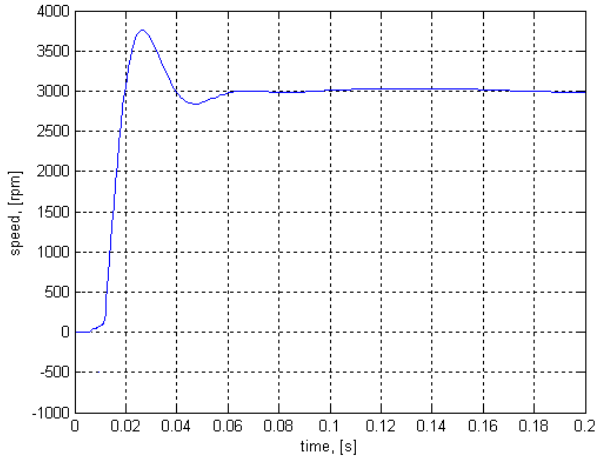

Figure 5.32: Simulated step response for the conventional PID controller.

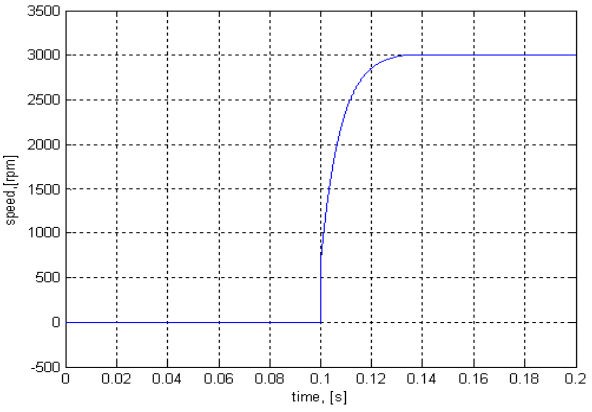

Figure 5.33: Simulated step response for the self-tuned-parameter Fuzzy PID controller.

When comparing Figure 5.32 with Figure 5.33 it can be seen that the step response for the conventional PID controller has an overshoot compared with the Fuzzy-PID controller.

Figure 5.34 and Figure 5.35 show responses to the trapezoidal reference control signal. In Figure 5.34 similar overshoot and long settling time can be seen as above. But this time signal follows the reference signal very well.

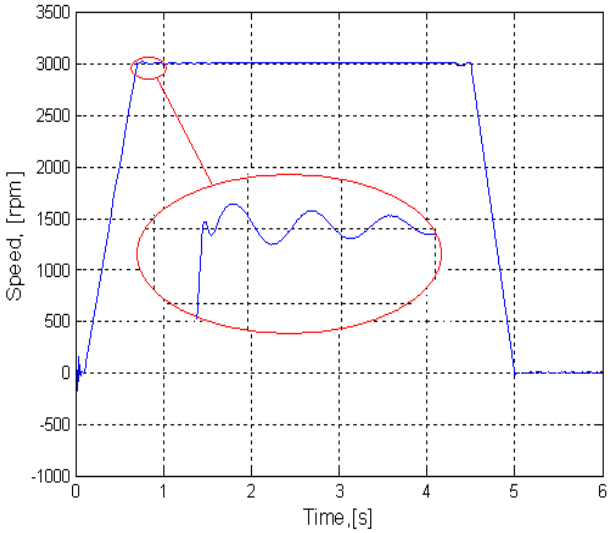

Figure 5.34: Simulated response for the conventional PID controller.

Figure 5.35 is characterized by absence of overshoot and illustrates a very good response to the reference signal. It can be concluded that the Fuzzy PID is working better than the conventional PID.

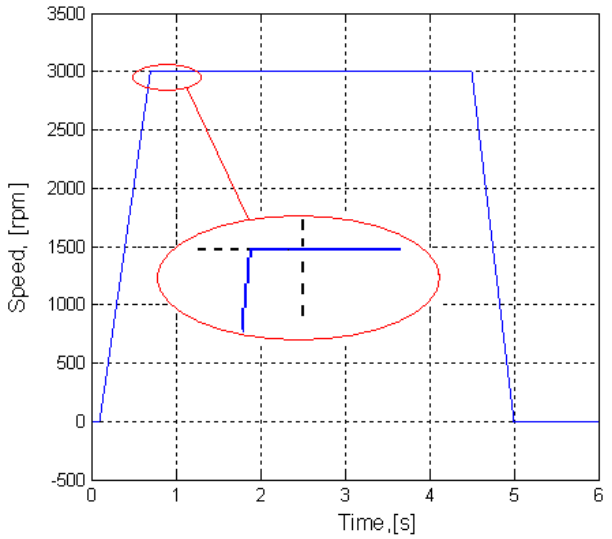

Figure 5.35: Simulated response for the self-tuned-parameter Fuzzy PID controller.

Figure 5.36 illustrates a simulated step response of the system during lifting with the self-tuning-parameter fuzzy PID control. A translational delay was introduced into the model to check the response of the system.

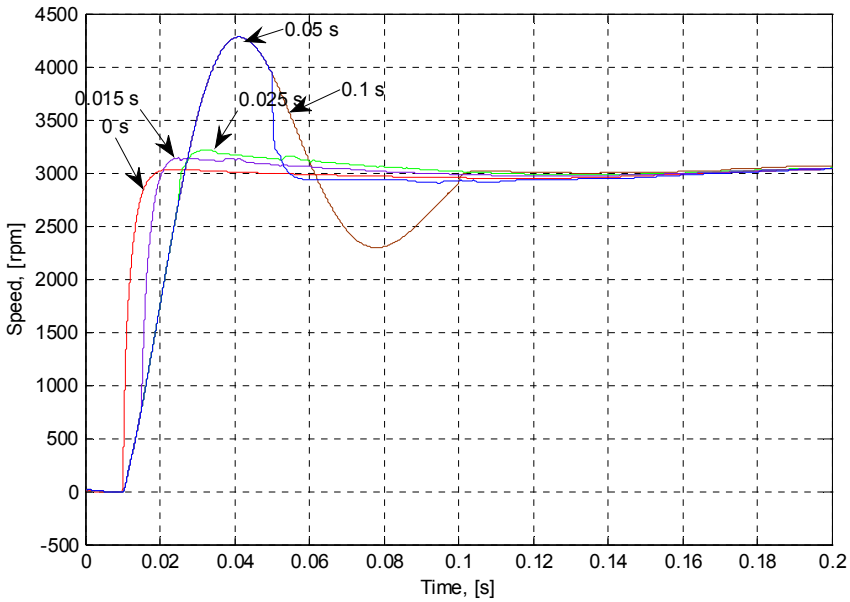

Figure 5.36: Simulated step response of the self-tuned fuzzy PID control with time delay.

According to Figure 5.36, with a time delay over 25 milliseconds the systems produces an overshoot, which is not acceptable. The expected delay in the system is 20 milliseconds because of the time sampling and usage of analogue cables for the delivery of signals.

Figure 5.37 illustrates an example of the measured response of the system during the lifting movement of the fork. A conventional fixed PID controller was used to control the speed (Figure 5.37, red line): slow response in lifting and oscillation during steady speed. To attain the requirements of this project regarding the speed control, the self-tuning-parameter Fuzzy PID control described above was applied. Figure 5.37 (blue line) illustrates an example of the response of the system during the lifting movement of the fork. The self-tuning-parameter Fuzzy PID controller was used to control the speed.

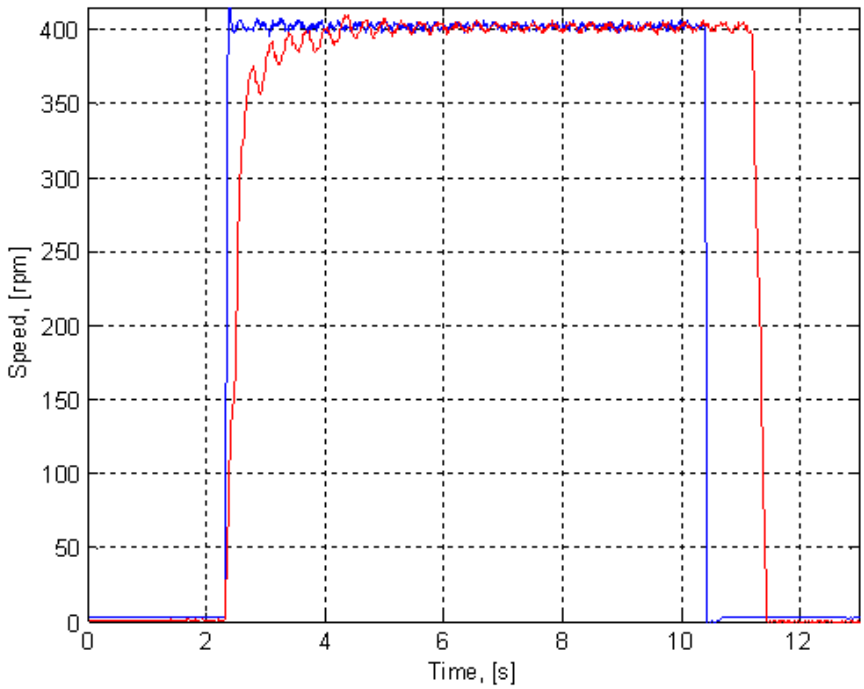

Figure 5.37: Measured 400 rpm speed with fuzzy approach (blue line) during lifting and with a conventional PID controller (red line) with a payload of 0 kg.

Figure 5.38 shows the measured 400 rpm speed with the fuzzy approach (blue line) during lowering and with the conventional PID controller (red line) with a payload of 0 kg. The self-tuning-parameter Fuzzy PID control demonstrates a good response to the reference signal; no overshoot during lowering motion of the fork and less ripple in the speed are observed. At the same time, with the conventional PID, all negative features mentioned above are present during lowering in Figure 5.38 (red line). It can be concluded that the self-tuning-parameter Fuzzy PID control meets the expectations and initial requirements.

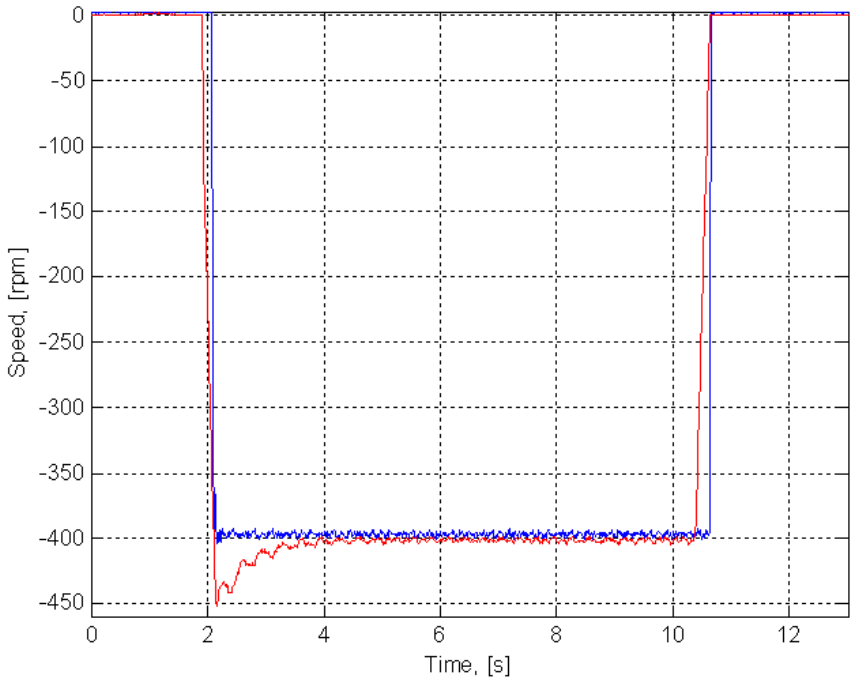

Figure 5.38: Measured 400 rpm speed with the fuzzy approach (blue line) during lowering and with the conventional PID controller (red line) with a payload of 0 kg.

5.4 Analysis of the applicability of the results

The following section contains an analysis of the influence of different factors on the energy recovery in an electro-hydraulic forklift in order to analyse the reasons for poor energy utilization in conventional forklift systems and to find strategies to improve their energy efficiency; an analysis of the applicability of experimental results was made, and finally the system energy consumption was examined.

5.4.1 Analysis of effect of the PMSM sizing on energy efficiency

By and large, the most significant contributors to the described hydraulic lifting system efficiency are the pump and the electrical machine. A permanent magnet synchronous servo motor was chosen for the application because of its high efficiency and high overload capability especially in the power range used in the work. The first servo motor used in the tests was a 4.5 kW PMSM (CFM90M) servo motor by SEW with 14.5 Nm nominal torque, 10.1 A nominal current, 52.2 Nm maximum torque, and 40 A maximum current. The CFM90M operated properly and did not overheat in the tests despite high overloading because of the low duty cycle value. However, the PMSM

efficiency could still be improved, and hence, a slightly larger motor CFM112M was chosen for the next evaluations. The characteristics of the CFM112 M are the following: 31 Nm nominal torque, 35 A nominal current, 108 Nm maximum torque, and 140 A maximum current. Figure 5.39 shows the calculated efficiency results for the SEW CFM90M PMSM and CFM112M with some measured efficiency points (Minav, 2010b).

(a) (b)

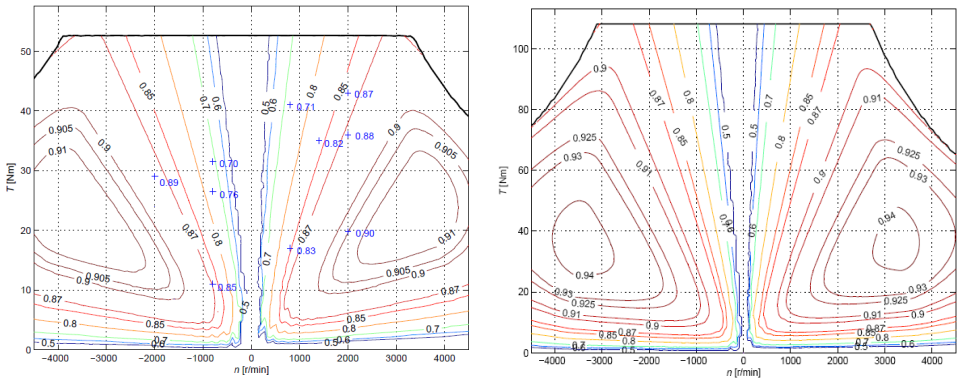

Figure 5.39: Efficiency charts for CFM90M PMSM (a) and CFM112M (b). Some measured efficiency points in lifting and lowering are indicated with + signs (room temperature) (Minav, 2010b). (Fig. courtesy of P. Immonen)

In this design, typically for permanent magnet synchronous machines, the efficiency contours are closed and have areas at 90% and above. Also, the efficiency islands are typically just above the corner point speed and at power levels in the vicinity of the rated power. An efficiency chart was calculated based on information on the device components. Figure 5.39a shows the results for the ACSM104x[4)]x[5)]-046A-4 for operation with CFM90M, and Figure 5.39b for CFM112M. Figure 5.40 (a, b) shows the efficiency of the inverter at different rotational speeds and torques. The chart also includes some measured efficiency points of the inverter calculated from the measurements. In the experiments, we used a bent-type axial piston hydraulic motor with a fixed displacement, as the hydraulic machine is capable of working also as a pump. This type of a pump is usually capable of very high pressures of up to 400 bar. These types of machines are highly efficient; this can be seen in the performance curve of Figure 2.5. Axial piston pumps have high efficiencies compared with other pump types. Depending on where the operating point of a hydraulic unit is located on its performance curve, the relationship between flow and hydraulic losses in a system varies.

Hydraulic losses in piping systems are composed of pipe friction losses, valves, elbows and other fittings, entrance and exit losses, and losses from changes in the pipe size by a

reduction in the diameter. Because the pump internal leakage increases as the operating pressure increases and fluid viscosity decreases, these variables should be taken into account in the calculation of the pump or motor efficiency (Majumdar, 2002). In our test setup, the power losses vary between 5–10% depending on the operation mode. A single-acting cylinder is used in the experimental setup. The overall cylinder efficiency is mostly dependent on the frictional losses encountered by the piston and the rod during its stroke.

(a) (b)

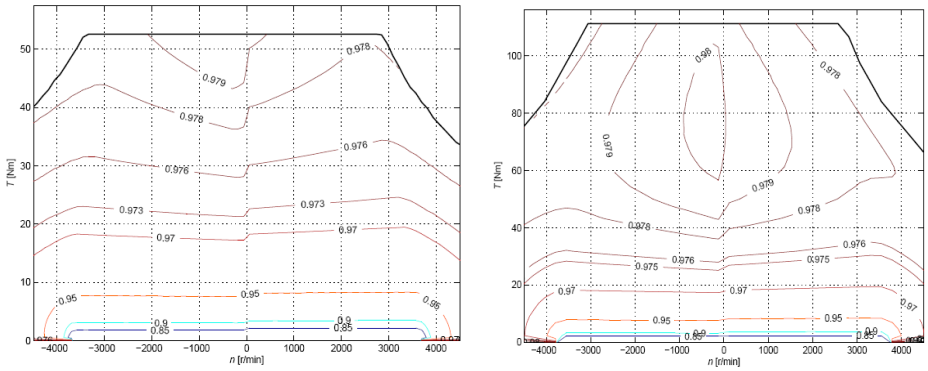

Figure 5.40: Efficiency charts for the 46 A RMS, 400 V ACSM1 converter driving the servo motor CFM90M (a) and CFM112M (b) used in the tests (Minav, 2010b). (Fig. courtesy of P. Immonen)

Frictional losses depend on the pressure difference across the seal, sliding velocity, seal material, temperature, time, wear, and direction of the movement. It is known that the total seal friction of a hydraulic cylinder is 2–5% of the total cylinder force (Majumdar, 2002). The maximum per unit friction occurs when the pressure and speed approach zero. With a positive velocity, the friction force is higher than with a negative velocity. This can be seen especially at high pressure levels. At higher velocities, the friction force should increase because of viscous friction. Based on the information above, the cylinder efficiency was assumed to be 95% (Merritt, 1967). A mechanical gear is embedded in the fork construction. Its efficiency varies between 98% and 99%. Mechanical gears do not significantly affect the system efficiency, but the efficiency will be taken into account in calculating the system efficiency of the test setup. Based on the suggestions given in (Airila, 2004) the efficiency of the mechanical gears was assumed fixed and equal to 99%. This high value can be justified by the fact that the gearing system in the hoisting armature is very simple containing just one chain and a low speed chain wheel which do not seem to heat at all according to the practical measurement results. The development of efficiency charts for the hydraulic drive requires data from the manufacturers about the components included in the system.

The simulated vehicle is defined by standard drive cycles, given motor/generator continuous rating points, and the estimated behaviour of the hydraulics components, all of which have relatively accurate efficiency charts. From this, the performance of the drive can be assessed (Minav, 2010c). Depending on the system architecture, the electric motor/generator, the inverter, and the hydraulic pump/motor will have operating points that follow particular trajectories (shown in Figures 5.39, 5.40, and 2.3). The efficiencies of valves and pipes are combined as one value. Because of the increasing speed and load, the amount of losses (in per cent) is increasing. The efficiency of the cylinder was estimated to be 95% (Minav, 2010c). The system efficiency of the proposed hydraulic system was calculated as

$$\eta_{SYS} = \eta_{inv} \cdot \eta_{EM} \cdot \eta_{HM} \cdot \eta_{VP} \cdot \eta_{G} \cdot \eta_{C}, \tag{5.2}$$

where the subscript INV denotes the inverter, EM the electric machine, HM the hydraulic machine, VP the pipes and valves, G the mechanical gears, and C the hydraulic cylinder. An example of the calculation of the theoretical efficiency is shown below. Tables 5.9 and 5.10 represent a calculation of practical and theoretical efficiencies of the CFM90M PMSM when lifting and lowering a payload of 920 kg (Minav, 2010c).

Table 5.9: Calculation of theoretical efficiencies of CFM90M when lifting a 920 kg payload at different constant speeds (Minav, 2010b).

Speed, [rpm]	400	1000	2000
Inverter efficiency, [%]	97.7	97.8	97.8
Motor efficiency, [%]	55	75	86
Pump efficiency, [%]	83	94	93
Valve & pipe efficiency, [%]	93	92	91
Gear efficiency, [%]	99	99	99
Cylinder efficiency, [%]	95	95	95
System efficiency, [%]	39.0	59.7	66.9

Based on the manufacturer's data and the theoretical model, an experimental verification was made with the test setup. Table 5.11 shows a comparison of the theoretical and empirical efficiencies with a 920 kg payload. Such a comparison is, of

course, not very accurate as the empirical cycle efficiencies contain start and stop operations. Nevertheless, the differences in the efficiencies are not very high as the tables show.

Table 5.10: Calculation of theoretical efficiencies of CFM90M when lowering a 920 kg payload at different constant speeds (Minav, 2010b).

Speed, [rpm]	400	1000	2000
Inverter efficiency, [%]	97.7	97.7	97.7
Motor efficiency, [%]	60	77	88
Pump efficiency, [%]	50	91	92
Valve & pipe efficiency, [%]	93	92	91
Gear efficiency, [%]	99	99	99
Cylinder efficiency, [%]	95	95	95
System efficiency, [%]	25.6	59.2	67.7

Table 5.11: Comparison of theoretical and empirical efficiencies with a 920 kg payload for CFM90M (Minav, 2010b).

Lifting			
Speed, [rpm]	Theoretical system efficiency, [%]	Empirical system cycle efficiency*, [%]	Difference, [% units]
400	39.0	38.95	-0.05
1000	59.7	58.27	-1.4
2000	66.9	64.19	-2.8
Lowering			
Speed, [rpm]	Theoretical system efficiency, [%]	Empirical system cycle efficiency, [%]	Difference, [% units]
400	25.6	28.46	2.8
1000	59.2	58.11	-1.1
2000	67.7	66.18	-1.5

*) Includes the estimated theoretical efficiency of the inverter for lifting. The DC link current could not be measured because of the physical limits of the converter structure. Instead, the DC current of the external brake resistor circuit was measured during lowering.

It can be seen that the larger differences are concentrated on the results obtained at the lower speeds.

A comparison of the theoretical efficiencies with the 920 kg payload is given in Table 5.12 for the two electrical machines lifting and lowering the payload.

Table 5.12: Comparison of theoretical system efficiencies of two motors with a 920 kg payload (Minav, 2010b).

Lifting			
Speed, [rpm]	Theoretical system efficiency with CFM90M, [%]	Theoretical system efficiency with CFM112M, [%]	Difference, [% units]
400	39.0	55.68	16.68
1000	59.7	69.08	9.42
2000	66.9	71.59	4.65
Lowering			
Speed, [rpm]	Theoretical system efficiency with CFM90M, [%]	Theoretical system efficiency with CFM112M, [%]	Difference, [% units]
400	25.64	46.66	21.02
1000	59.23	66.88	7.65
2000	67.70	70.00	2.31

According to Table 5.12, by choosing a larger motor, the system efficiency for lifting and lowering a load can be improved by 20 percentage points at a low speed, while for a high speed, an improvement of at least three percentage points on average can be reached. Measurement data for the inverter efficiency for the lifting movement were not available because of the compact structure of the DC link, which made current measurements impossible. To estimate the circuit efficiency, the system lifting efficiency was multiplied by the inverter efficiency for downward movement (Minav, 2010b).

Because of the theoretical results obtained with the CFM112, a new set of measurements were carried out for the test setup. Table 5.13 shows a comparison of the empirical system cycle efficiencies of two motor sizes when lifting and lowering a 920 kg payload (Minav, 2010b).

It was found that because of larger copper losses in the CFM90 at lower speeds, the CFM112 provided a significant efficiency improvement in the case of lifting and lowering a 920 kg load. At 2000 min^{-1}, the process takes so short a time that the lower copper losses and large friction in the CFM112 make the efficiency with the CFM90 and the CFM112 equal in the generating mode (Minav, 2010b).

The system energy efficiency of an electro-hydraulic forklift was studied. Evaluation of the hydraulic system and the electric part of the working machine and verification of the theoretical approach by practical results assisted in determining the effect of the PMSM on the efficiency of the system. The energy recovered in the tests showed that the PMSM has a significant impact on the efficiency of the system.

Our theoretical investigation predicted a possible improvement, which was then proven empirically. By choosing an appropriate motor, the system cycle efficiency could be improved by 0 to 20 %-units in different operating conditions (Minav, 2010b).

Table 5.13: Comparison of empirical system cycle efficiencies of two motor sizes when lifting and lowering a 920 kg payload (Minav, 2010b).

Lifting			
Speed, [rpm]	System cycle efficiency with CFM90M, [%]	System cycle efficiency with CFM112M, [%]	Difference, [% units]
400	38.95	57.76	18.81
1000	58.27	72.95	14.69
2000	64.19	72.50	8.31
Lowering			
Speed, [rpm]	System cycle efficiency with CFM90M, [%]	System cycle efficiency with CFM112M, [%]	Difference, [% units]
400	28.46	52.52	24.06
1000	58.11	67.47	9.36
2000	66.18	66.70	0.52

5.4.2 Analysis of the hydraulic machine

Hydraulic pumps and motors are used to convert mechanical energy into hydraulic energy and vice versa. Figure 2.5 gives the performance curves of the efficiencies of continuous-travelling positive displacement machines. Theoretically, any hydraulic pump could be used as a hydraulic motor with certain restrictions (Minav, 2010d).

Figure 2.3b shows an internal gear pump construction. Figure 5.41 shows the total efficiency at the speed of 1450 rpm, provided by the manufacturer of the internal gear pump used in the tests. The total maximum efficiency of the pump decreases from 88% at operating pressures above 100 bar. An increasing pressure decreases the volumetric efficiency because there is more internal leakage in the machine. However, owing to the frictional torques, the efficiency is lower also in the lower pressure areas.

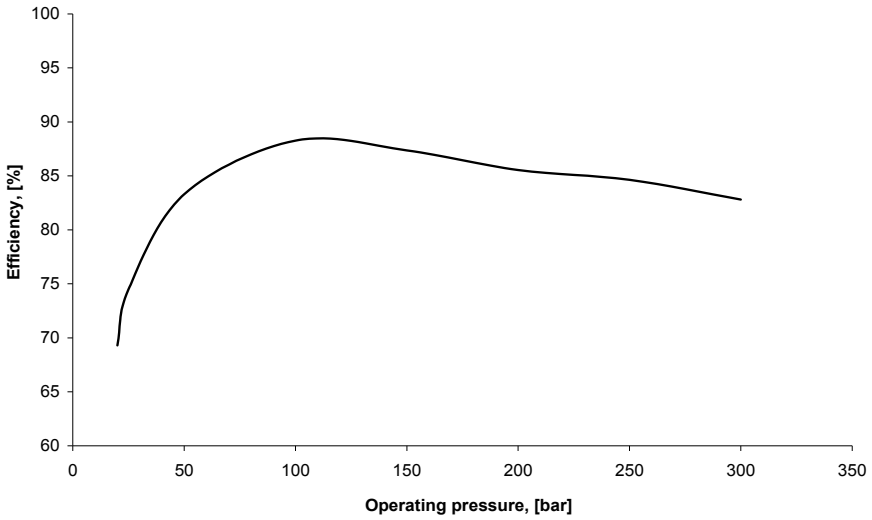

Figure 5.41: Total constant-speed efficiency curve of the internal gear pump at the speed of 1450 rpm (Eckerle, 2007).

A piston pump is yet another important application in high-pressure hydraulic systems. Figure 2.4b illustrates a bent axis axial piston type motor. Piston type machines can be used at working pressures up to 200 bar and above. Figure 5.42 shows the total efficiency of an axial piston machine operating either as a motor or as a pump, as reported by the manufacturer. The figure illustrates the pump characteristic curve, and the same device when used as a motor at the operating pressure of 100 bar.

The rated displacements of the axial piston pump and the internal gear pump are 19 cm^3/rev and 13.3 cm^3/rev, respectively. Both pumps have a fixed displacement .The PMSM servomotor manufactured by SEW-Eurodrive (CFM90M: T_n = 14.5 Nm, I_n = 10.1 A, T_{max} = 52.2 Nm, I_{max} = 40 A) directly connected to the hydraulic machine was used to analyse the behaviour of the hydraulic machine.

The theoretical efficiency behaviour of the internal gear machine as a function of operating pressure was shown in Figure 5.41. Figure 5.10 shows the empirical results for the internal gear pump. The static pressures p_s corresponding to the loads and the expected efficiencies given by the manufacturer were calculated as shown in Tables 5.14 and 5.15 for the internal gear pump and the axial piston motor by using the following equation:

$$p_s = mg/S_p, \tag{5.3}$$

where m is the payload, g is the gravitational constant, and S_p is the cross-sectional area of the cylinder piston.

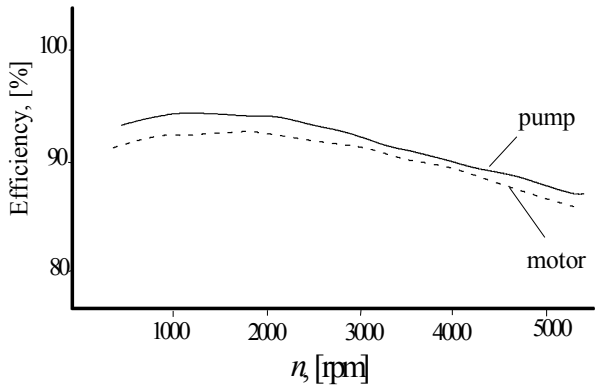

Figure 5.42: Total efficiency of an axial piston pump and motor at a 100 bar pressure (Parker, 2007).

According to Figure 5.41 and Table 5.14, the efficiency of the internal gear pump at the speed of 1450 rpm should grow from 84 to 88% with an increasing load. The experimental results illustrated in Figure 5.10 do not exactly match the steady-state curves given by the manufacturer. This is natural because the values of Figure 5.37 are for the steady state, while Table 5.14 gives the efficiencies taking transient behaviour into account.

Table 5.14: Pressures and efficiencies for an internal gear pump at the speed of 1450 rpm calculated from constant-speed powers (Minav, 2011c).

Load, [kg]	Static pressures corresponding to the load, [bar]*	Expected theoretical efficiency, [%]	Acting pressure required for lifting of the load, [bar]**	Empirical cycle efficiency, [%]***
920	121	88	124	83.2
690	104	87	103	84.1
500	89	86	95	81.6
0	46	84	48	73.8

*) calculated pressure for keeping the load still (without friction)
**) measured data for the speed of 1400 rpm
***) calculated cycle efficiency from cycle measured data at a constant speed of 1400 rpm

The calculated static pressures corresponding to the loads and the expected theoretical efficiencies taken from Figure 2.5 are shown in Table 5.15. The theoretical behaviour illustrated in Figure 5.42 is given for an axial piston machine. The maximum efficiencies are in the range of 90–92% according to the manufacturer's graphs for 100 bar. It can be noticed that Figure 5.42 is almost identical to the results shown in Figure 5.18, even though Figure 5.42 gives constant-speed efficiencies and Figure 5.18 cycle efficiencies for the pump.

Table 5.15: Pressures and efficiencies for an axial piston pump for the speed of 1000 rpm calculated from constant-speed powers (Minav, 2011c).

Load, [kg]	Static pressures corresponding to the load, [bar]*	Expected theoretical efficiency, [%]	Acting pressure required for lifting of the load, [bar]**	Empirical cycle efficiency, [%] ***
920	121	90	124	91
690	104	89	106	89.6
500	89	88	90	88.5
0	46	84	46	82

*) calculated pressure for keeping the load at a standstill
**) measured data for the constant speed of 1000 rpm during the work cycle
***) calculated cycle efficiency from the measured cycle data at a constant speed of 1000 rpm

The cycle efficiency of the internal gear hydraulic machine was on average 80% for pumping and 70% for motoring with a non-zero load (Figure 5.10). The axial piston machine cycle efficiency was 90% for lifting and 85% on average for the lowering movement with a non-zero load (Figure 5.18). A significant difference can be seen in the zero-load tests for both machines. The losses increase from 15% to 38% (lowering) and from 10% to 25% (lifting) with an increasing speed for the zero-load cases for the axial piston hydraulic machine (Figure 5.18). The experimental results of the axial piston machine are close to the manufacturer's data (Table 5.15). The experimental cycle efficiency curves of the axial piston machine are almost symmetrical in both motoring and pumping. This brings more advantages for this type of a system. The same cannot be said about the internal gear pump, which behaved less efficiently (Minav, 2011c).

5.4.3 Analysis of the energy storage

In general, the basic idea of an energy regeneration system is to reduce the energy consumption by converting potential or dynamic energy into other types of energy, such as hydraulic, rotating dynamic or electric energy. In the field of mobile machines, there are three well-known types of energy regeneration systems based either on a hydraulic accumulator (Ding, 2007; Lin, 2010b; Yang, 2007; Hui, 2010), a battery, a combination with an SC (Inoue, 2008; Iannuzzi, 2008; Xiao, 2008) or a flywheel system (Boyes, 2000). Single energy storage components do not always meet the requirements for storing the energy recovered in work machines. It is the reason why several topologies combining different technologies have been proposed for storing regenerative energy (Wang, 2010; Lin, 2010a).

Combination of a lead-acid battery and a supercapacitor in a forklift

The concept of this combination provides benefits over separate storage devices. An SC bank makes it possible to store energy fast and to use the recovered energy later. Both a

lead-acid battery and an SC can be connected in parallel at the DC bus, but in such a case, the limited variation in the voltage radically limits the amount of energy to be stored in the SC. The simplest way to benefit from the fast recharge capability of an SC is to connect the lead-acid battery and the SC in a system according to Figure 5.38, where the normal energy consumption is taken from the battery but the recovered energy is stored in the SC. The SC capacitance must be chosen as described above. In such a case, the converter control system must be capable of operating at different DC voltages, but this does not pose any major problems, as most present-day converters are able to operate under varying DC voltages. The only prerequisite is to select the voltage tolerance of the main circuit components according to the DC link maximum voltage requirements. The schematic of setup A is illustrated in Figure 5.43a. In setup A, the battery and the SC are connected in parallel and separated with a power diode. Figure 5.43b illustrates setup B, where the SC is connected to the system with a DC-DC converter. (Minav, 2011f)

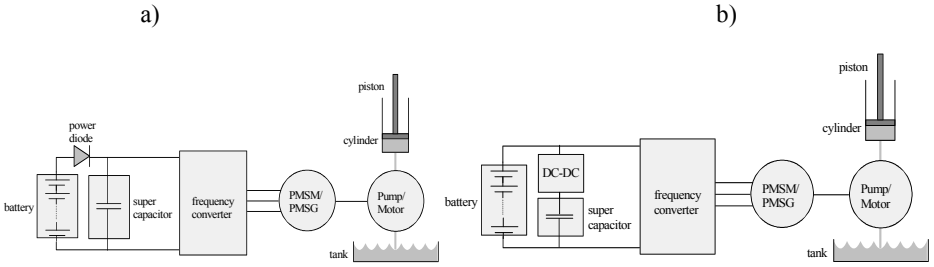

Figure 5.43: Schematics of energy efficient forklift control systems with a lead-acid battery and a supercapacitor as energy storages; a) setup A: variable DC voltage with no DC-DC converter but a varying DC voltage level, b) setup B: DC-DC converter for the supercapacitor, constant DC voltage. (Minav, 2011f)

Combination of a lead-acid battery and a hydraulic accumulator in a forklift

In hydraulic systems, hydraulic accumulators are often used as energy storages, to absorb shocks or to provide backup fluid flow in emergency situations. The task in this case is, however, to store a significant amount of energy. The concept of the proposed combination provides benefits over separate storage devices. The fact that hydraulic energy does not have to be converted into electric energy and back reduces the amount of losses. However, two hydraulic to mechanic conversions are needed, which easily reduces the efficiency below that of electric storages.

Figure 5.44 shows the proposed setup C, a combination of a lead-acid battery and a hydraulic accumulator. According to Figure 5.44, the normal energy consumption is taken from the battery, but the recovered energy is stored into the hydraulic accumulator. The capacitance (volume) of the hydraulic accumulator has to be chosen

such that the maximum energy recovered can be stored into the hydraulic accumulator with an acceptable pressure difference.

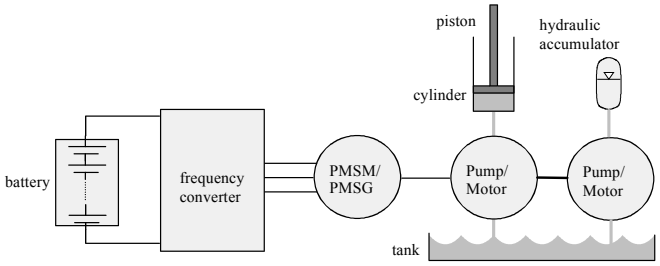

Figure 5.44: Setup C: schematic of an energy efficient forklift control system with a lead-acid battery and a hydraulic accumulator as energy storages. Using a hydraulic accumulator requires an extra energy conversion from hydraulic to mechanic and again from mechanic to hydraulic energy. (Minav, 2011f)

Experimental setups

Two separate test arrangements were prepared for practical reasons. Firstly, an electro-hydraulic forklift without energy storages was measured. The recovered energy was used in a brake resistor (Figure 5.2). Secondly, the SC charge-discharge efficiency was measured separately by using a bidirectional DC-DC converter.

Test setup for measuring SC and DC-DC converter cycle efficiencies

The laboratory test setup for measuring the SC charge-discharge efficiencies during forklift operation (according to current and voltage measurements) is presented in Figure 5.45. It consists of a three-phase diode rectifier, a bidirectional DC-DC converter, a brake resistor R_{brake} in the system DC link, and the SC energy storage. The DC link current i_{DC} and the SC current i_{SC} are measured with Tektronix TCPA 300 AC/DC current probes, and the DC link voltage u_{DC} and the SC voltage u_{SC} are measured with Tektronix P5200 high-voltage differential probes. A dSPACE ds1103 platform is used to acquire the measurement signals and to supply the SC current reference signal $i_{\text{SC,ref}}$ for the DC-DC converter. The system has two modes of operation, SC charge and SC discharge. During the SC charge, the system obtains its energy from the rectified 400 V three-phase supply grid. During the SC discharge, energy is consumed in R_{brake} in order to keep the u_{DC} below the allowable level of 630 V.

The tested SC was of the type BMOD0063 P125 by Maxwell with a rated voltage of 125 V, a maximum voltage of 130 V, and a continuous current of 150 A (the peak value of the current for one second being 750 A). The rated capacitance is 63 F. (Minav, 2011f)

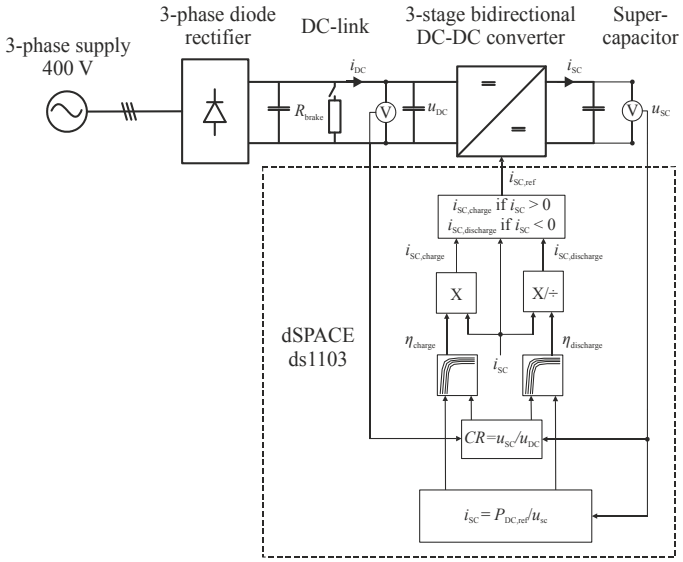

Figure 5.45: Test setup to measure supercapacitor charge-discharge efficiencies (Minav, 2011f). (Fig. courtesy of A.Virtanen).

In order to obtain the desired power $P_{DC,ref}$ from the measurements with setup 1 (Figure 5.2) to the system DC link, the efficiency charts for the DC-DC converter charge and discharge operations were used. The efficiency charts were measured as a function of SC current and conversion ratio of u_{SC} and u_{DC}, and are presented in Figures 5.46 and 5.47, respectively. When the load of the forklift is lowered (the SC is charged), i_{SC} is multiplied by the corresponding charge efficiency η_{charge} of the DC-DC converter. When the load of the forklift is lifted (the SC is discharged), i_{SC} is divided by the corresponding discharge efficiency $\eta_{discharge}$ of the DC-DC converter. (Minav, 2011f)

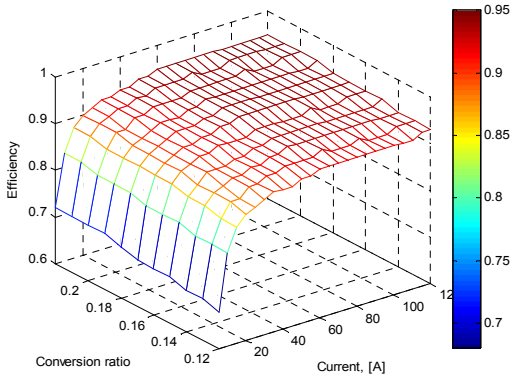

Figure 5.46: DC-DC converter charge efficiency (lowering operation) (Minav, 2011f). (Fig. courtesy of A.Virtanen).

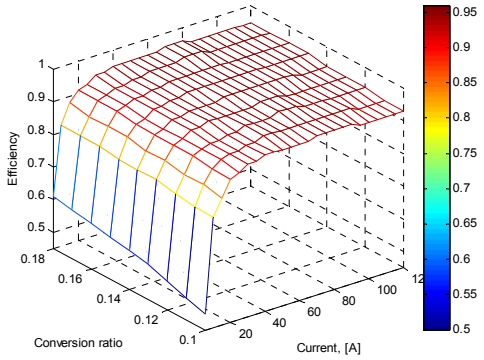

Figure 5.47: DC-DC converter discharge efficiency (lifting operation) (Minav, 2011f) (Fig. courtesy of A.Virtanen).

Electro-hydraulic efficiency measurements

In order to determine the behaviour of the three different systems (setups A, B, and C) of Figures 5.43 and 5.44, cycle efficiency charts for the lifting and lowering operations are used. The cycle efficiency curves have been calculated from the measured data by using equations shown in Tables 5.1, 5.2 and 5.3. The electro-hydraulic cycle efficiency of lifting is defined as a ratio of the input energy from the motor to the potential energy of the load, and for lowering as a ratio of the recovered energy to the potential energy. The curves of electro-hydraulic cycle efficiency are presented as a function of fork speed, and are presented in Figure 5.48.

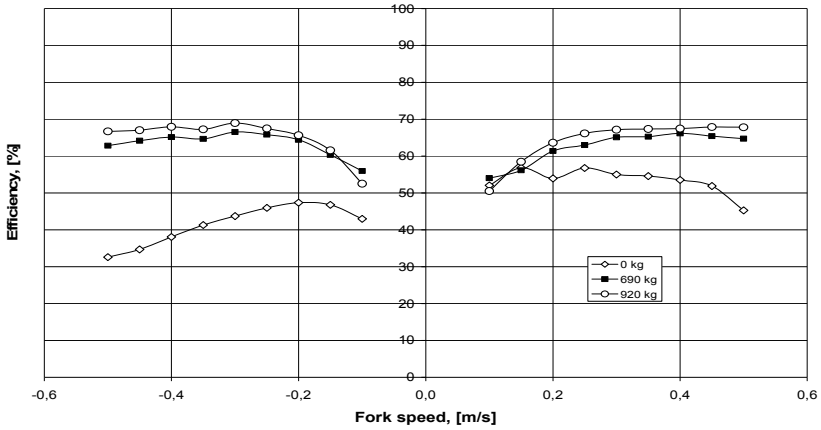

Figure 5.48: Measured electro-hydraulic cycle efficiency for lifting (positive speed, discharging) and lowering (negative speed, charging) payloads of 0, 690 and 920 kg (setup in Figure 5.2) (Minav, 2011f).

Figure 5.48 illustrates the efficiencies for the 10 kW PMSM together with the axial piston motor with loads of 0, 690, and 920 kg for different speeds. When the load of the forklift is lowered (negative fork speed), potential energy is recovered. When the load of the forklift is lifted (positive fork speed), energy recovered from the lowering movement can be used for lifting.

SC and DC-DC converter cycle efficiency measurements

The measured cycle efficiencies for the SC and the DC-DC converter with the SC current of 30 A to 100 A are given in Figure 5.49. The currents 30, 40, and 50 A correspond with the payload weights of 0, 690 and 920 kg, respectively. It can be seen that the cycle efficiency of the SC itself is quite high, which leads to the idea of using the system of Figure 5.43a instead of the system in Figure 5.43b. The SC cycle efficiency is given as the charge-discharge efficiency (Minav, 2011f).

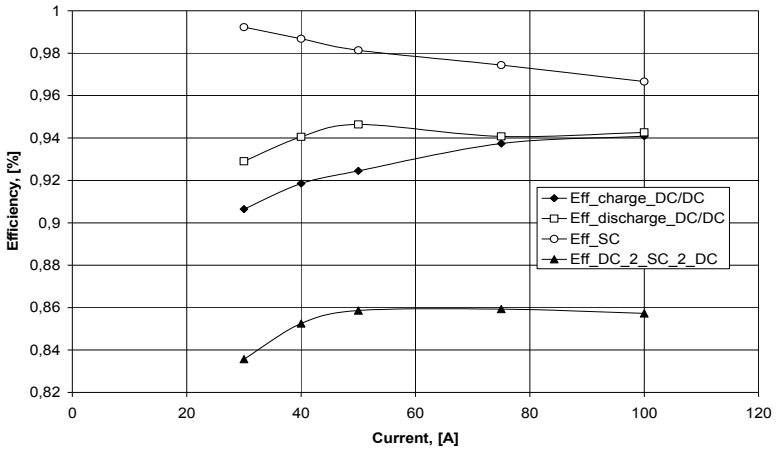

Figure 5.49: Measured cycle efficiencies for the SC and the DC-DC converter (Minav, 2011f).

5.4.4 Analysis of energy consumption

The energy-saving ratio Γ_s describes how much energy can be saved when the new energy-saving method is applied:

$$\Gamma_s = (E_{old} - E_{new})/E_{old} = E_{brake}/E_{motor}, \tag{5.4}$$

where E_{old} is the energy consumption of the forklift without recovery and E_{new} is the energy consumption of the forklift with the energy recovery method. E_{brake} is the energy converted into heat in the 'energy storage' brake resistor and E_{motor} is the input energy of the motor, calculated from the measured motor power against time (Minav, 2010a).

The total cycle efficiency of the system for setup A (Equation 5.5, Figure 5.43a), setup B (Equation 5.6, Figure 5.43b), and setup C (Equation 5.7, Figure 5.44) was calculated as shown below:

$$\eta_{tot\_cycle} = \eta_{up\_sys}\, \eta_{sc}\, \eta_{d}\, \eta_{down\_sys} \tag{5.5}$$

$$\eta_{tot\_cycle} = \eta_{up\_sys}\, \eta_{dc\text{-}sc\text{-}dc}\, \eta_{down\_sys} \tag{5.6}$$

$$\eta_{tot\_cycle} = \eta_{up\_sys}\, \eta_{hyd\_accu}\, \eta_{pump}^{2}\, \eta_{down\_sys}\,, \tag{5.7}$$

where η_{tot_cycle} is the total cycle efficiency of the studied systems, η_{up_sys} is the measured system cycle efficiency for lifting, η_{sc} is the measured cycle efficiency from the SC (setup A, Figure 5.43a), η_{d} is the diode efficiency, $\eta_{dc\text{-}sc\text{-}dc}$ is the measured cycle efficiency from the DC link to the SC and back to the DC link (setup B, Figure 5.43b), η_{down_sys} is the measured system cycle efficiency for lowering (first test setup, Figure 5.2), η_{hyd_accu} is the theoretical efficiency of the hydraulic accumulator (setup C, Figure 5.44), and η_{pump} is the measured cycle efficiency of the axial piston motor (Figure 5.18). Figure 5.50 shows the calculated cycle efficiencies with setups A, B, and C, respectively (Minav, 2011f).

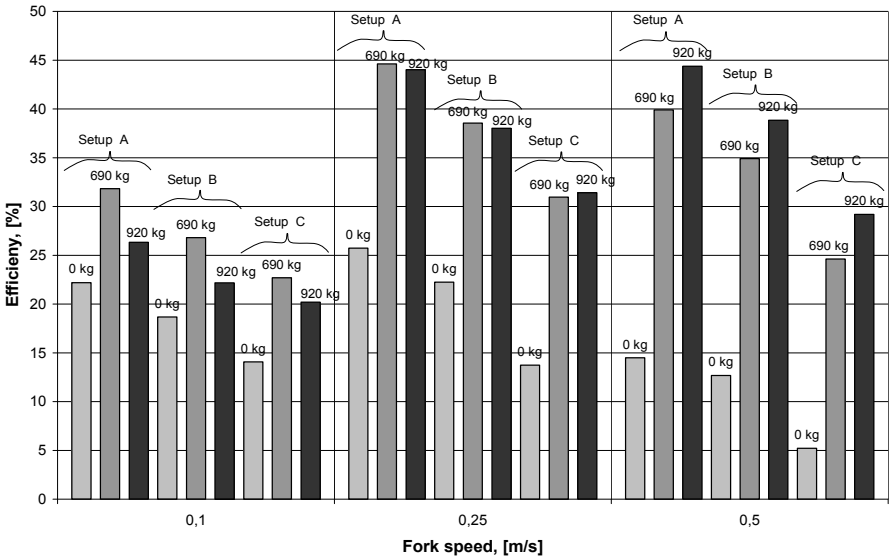

Figure 5.50: Calculated lifting and lowering cycle efficiencies with different payloads (setups A and B in Figure 5.43, setup C in Figure 5.44), setup A with the SC and varying DC voltage, setup B with the SC and DC-DC converter (constant DC voltage), and setup C with a hydraulic accumulator (Minav, 2011f).

It can be seen that the combination of the axial piston motor and the PMSM equipped with suitable energy storage has very good energy efficiency. The simple system of setup A seems to be the most energy efficient because unlike setup B, it does not include a DC-DC converter.

E_{new} for calculating the energy-saving ratio for setup A (Equation 5.8, Figure 5.43a), setup B (Equation 5.9, Figure 5.43b), and setup C (Equation 5.10, Figure 5.44) is given as

$$E_{new}=E_{old}-(E_{brake}\cdot\eta_{sc}\cdot\eta_{d}) \tag{5.8}$$

$$E_{new}=E_{old}-(E_{brake}\cdot\eta_{dc\text{-}sc\text{-}dc}) \tag{5.9}$$

$$E_{new}=E_{old}-(E_{brake}\cdot\eta_{hyd\_accu}\cdot\eta_{pump}^{2}). \tag{5.10}$$

Figure 5.51 shows the calculated energy-saving ratios for setups A, B, and C, respectively. It can be concluded that the ”electrical” setups A and B showed a better cycle efficiency and energy-saving ratio compared with the “hydraulic” setup C.

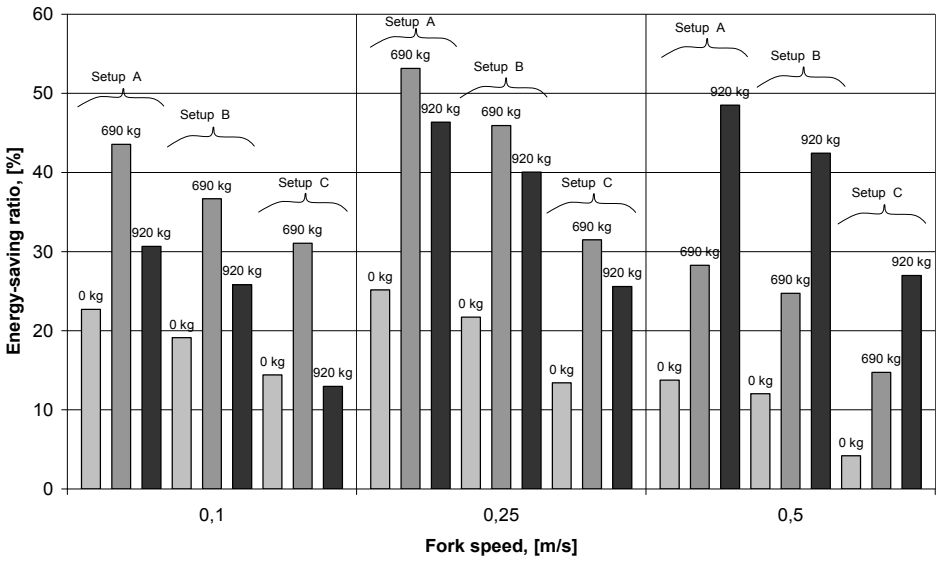

Figure 5.51: Calculated energy-saving ratios for different payloads (setups A and B in Figure 5.43; setup C in Figure 5.44) (Minav, 2011f).

Figure 5.52 illustrates the energy-saving ratio of the electro-hydraulic forklift system with an internal gear pump and an axial piston motor with a 4.5 kW PMSM (CFM90M), respectively, for different payloads and different lifting velocities of the forks.

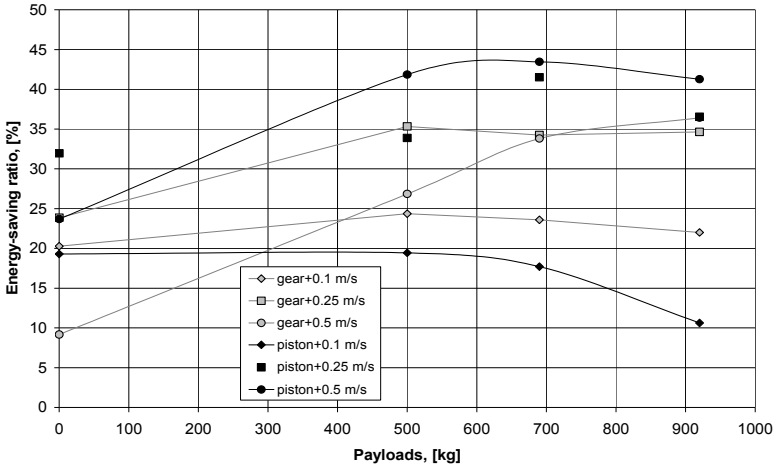

Figure 5.52: Energy-saving ratio of the electro-hydraulic forklift system with an internal gear pump and an axial piston motor with a 4.5 kW PMSM (CFM90M) for the lifting and lowering of the same payload (Minav, 2011c).

The figure shows one lifting cycle: lifting and lowering of the same load. According to Figure 5.52, the system based on the axial piston pump performs better at higher speeds. Both hydraulic machines showed lower efficiencies at low speeds (Minav, 2011c).

Table 5.16 illustrates the measured energy consumption for two sets of proposed systems with a 4.5 kW PMSM (CFM90M) for one lifting-lowering cycle with the 920 kg load.

Table 5.16: Consumption of energy for a lifting-lowering cycle with a 920 kg payload with 4.5 kW PMSM (Minav, 2011c)

Pump type	Motor speed, [rpm]	Fork velocity, [m/s]	Lifting consumption of energy, [kJ]	E_{brake} recovered energy, [kJ]	Energy-saving ratio, [%]
Internal gear pump	600	0.10	25.9	5.7	22
	1400	0.25	45.6	15.8	34.6
	3000	0.50	85.8	31.3	36.4
Axial piston pump	400	0.10	31.6	3.4	10.6
	1000	0.25	47.5	17.4	36.5
	2000	0.50	83.9	34.6	41.3

For instance, this means that the 920 kg load was lifted at the fork velocity of 0.5 m/s (3000 rpm for the internal gear pump and 2000 rpm for the axial piston motor), and the 920 kg payload was lowered at the same speed.

Figure 5.53 illustrates the energy-saving ratio of the electro-hydraulic forklift system with an internal gear pump and an axial piston motor with a 10 kW PMSM (CFM112M), respectively, for different payloads and different lifting velocities of the forks. The figure shows one lifting cycle: lifting and lowering of the same load for different cases. According to Figure 5.53, the system based on the axial piston pump performs better at higher speeds. Both hydraulic machines showed lower efficiencies at low speeds.

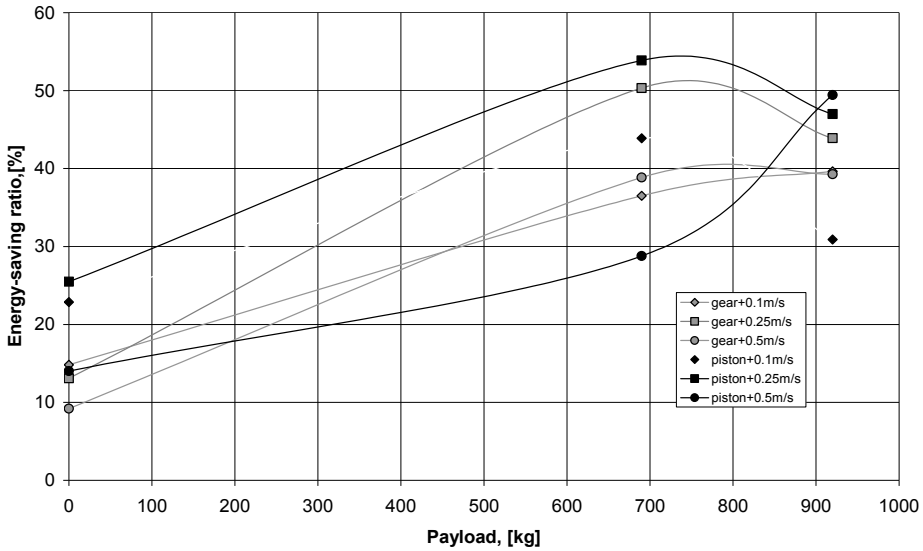

Figure 5.53: Energy-saving ratio of the electro-hydraulic forklift system with an internal gear pump and an axial piston motor for lifting and lowering of the same payload with a 10 kW PMSM (CFM112M).

Table 5.17 illustrates the measured energy consumption for two sets of proposed systems for one lifting-lowering cycle with the 920 kg load with a 10 kW PMSM (CFM112M).

Table 5.17: Consumption of energy for a lifting-lowering cycle with a 920 kg payload with a 10kW PMSM (CFM112M) (Minav, 2011c).

Pump type	Motor speed, [rpm]	Fork velocity, [m/s]	Lifting consumption of energy, [kJ]	E_{brake} recovered energy, [kJ]	Energy-saving ratio, [%]
Internal gear pump	600	0.10	18.8	7.5	39.6
	1400	0.25	40.8	17.9	43.9
	3000	0.50	69.3	27.2	39.3
Axial piston pump	400	0.10	23.3	7.2	30.9
	1000	0.25	42.4	19.9	46.9
	2000	0.50	71.2	35.2	49.4

Compared with Tables 5.16 and 5.17, the energy-saving ratio for lifting a load of 920 kg is 49.4%. This means that an axial piston pump with a 10 kW PMSM is the best combination. According to Figure 5.53, the best energy-saving ratio, 53%, was achieved with a 690 kg payload and a lower speed equal to 0.25 m/s.

A work cycle was constructed to represent a typical usage situation in storehouse operation (Hänninen, 2011). Driving the forklift around the storehouse was excluded in this case. The work cycle consists of four lifting and lowering operations, depicted in Figure 5.54.

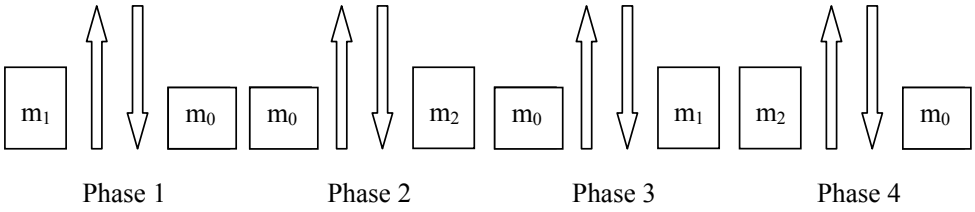

Figure 5.54: Work cycle.

Table 5.18 illustrates the measured consumption of energy and the energy-saving ratio for a lifting-lowering work cycle (Figure 5.54) for four sets of proposed systems with 4.5 kW PMSM (CFM90M) and 10 kW PMSM (CFM112M).

Table 5.18: Consumption of energy for a lifting-lowering work cycle.

System	Conventional energy consumption, [kJ]	Regenerative energy consumption, [kJ]	Energy-saving ratio, [%]
Internal gear pump and 4.5 kW PMSM	236.9	171.3	27.7
Internal gear pump and 10 kW PMSM	166.6	100.9	39.4
Axial piston motor and 4.5 kW PMSM	205.5	124.3	39.5
Axial piston motor and 10 kW PMSM	201.1	125.8	37.5

To produce the work cycle, some assumptions were made: the lifting speed ≅0.5 m/s, the lifting and lowering height is Δh = 3.5 m (area of the second cylinder), Δt per phase ≅ 20 s, m_1= 920 kg, m_2= 690 kg, m_0 is tare. Also consumption of energy during lifting was assumed to be constant for conventional and regenerative setups, and equal to the energy consumed (measured) by the motor (E_{motor}). Consumption of energy during lowering was assumed to be zero for the conventional truck. For the regenerative test setup, regenerative energy is equal to the energy put to the brake resistor (measured) (E_{brake}).

5.5 Conclusions and applicability of the test results

It was shown that the potential energy recovery and load control by an electric drive are feasible in an electro-hydraulic forklift. The cycle efficiency behaviour of electro-hydraulic system components and the overall efficiencies of the forklift system were determined. The maximum recovery efficiency of the system in lowering was 66.2% and the minimum was 28.5% at different loads. The energy recovery is also efficient with a permanent magnet machine drive, and thus, such an approach could be suggested for real equipment.

The opportunities to store and reuse energy recovered from a hydraulic system of a forklift were studied. Some of the easily available practical energy storages (lead-acid battery, supercapacitor and hydraulic accumulator) were described, and the proposed setups were analysed from the energy efficiency perspective. The energy saving ratio was calculated for different test setups. Its value typically varied in the range of 30 to 50 per cent. The cycle efficiency and energy-saving ratio for different payloads and speeds were calculated for the proposed setups A (SC and varying DC voltage with no DC-DC converters), B (SC and DC-DC converter with constant DC voltage), and C (hydraulic

accumulator). The simplest setup A with as few energy conversions as possible seems to be the most energy efficient solution (Figure 5.43).

The calculated energy-saving ratios also showed that the best result was achieved with the axial piston machine at higher speeds (Figure 5.52). The best forklift drive energy saving ratio of 43% was achieved in experimental tests with a 690 kg load and a speed of 2000 rpm (0.5 m/s) for the axial piston machine based system for a 4.5 kW PMSM (CFM90M). Table 5.16 shows that the axial piston machine improves the energy saving features of the system by two to five percentage points. Based on the results, energy can be recovered efficiently from the hydraulic forklift system with an axial piston hydraulic machine controlled by a permanent magnet electric motor drive. The same drive equipped with an internal gear pump performs less efficiently from the energy recovery point of view.

Based on the results, energy can be recovered efficiently from the hydraulic forklift system with an axial piston hydraulic machine controlled by a permanent magnet electric motor drive. The same drive equipped with an internal gear pump performs less efficiently. When comparing the energy consumption of a conventional system without energy recovery and the proposed experimental system, the energy saving is 53% (achieved with an axial piston motor and a PMSM (CFM112M)).

According to Table 5.18, the energy-saving ratio reached was 40% with a work cycle shown in Figure 5.54. This means that the recovered energy from lowering alone is not enough for the lifting movement, but this energy can be used to reduce the energy use from the battery.

6 Conclusions

This doctoral thesis studies the electrical control of hydraulic systems, providing a systems-engineering approach. All of the important components of a hydraulic lifting system are studied and their common operation analysed. The emphasis, however, is on the electric control of such a system. As an example, an electro-hydraulic forklift using an electric servo drive in the control of the lifting position is studied. The method proposed in this research makes it possible to minimize the energy losses in the electro-hydraulic system by recovering potential energy. The proposed structure is highly compatible with the existing solutions.

The key results of the work can be summarized as follows:

1. A control structure for a hydraulic lifting cylinder system is proposed. The hydraulic system is controlled directly by an electric drive. This type of a structure is characterized by its high energy efficiency.

2. Two positive displacement pumps and two different size PMS machines were tested. Possible energy efficient combinations were observed.

3. A model of the test setup is proposed. The realized model is verified with a number of experimental results.

4. An algorithm is provided for the speed and position control of the hydraulic cylinder. This algorithm allows controlling the position of the load without any feedback from the physical position of the cylinder piston.

5. Self-tuned parameter fuzzy PID control is applied to control the speed. The flow of the pump is controlled by the electric motor drive.

6. An algorithm of ripple compensation caused by the hydraulic pump is provided.

The results of this thesis are intended to be used both in practical development work and in further research. The proposed power supply is practice oriented and provides a very suitable, compact and inexpensive solution for modern mobile machine applications.

The results of this work can be applied to other types of hydraulic machines with lifting functions. This thesis also aims at providing a basis for future investigations on the new control design in hydraulic systems.

6.1 Suggestions for further work

This work can be extended to other types of working machines, which were reported at the beginning of the thesis. Some modification is required to be able to apply this recovery technique to other working machines.

The position control could be optimized and automated. For this purpose, sensors could be used to identify the end (maximum and minimum) positions of movement.

Additional tests should be carried out with new axial piston machines, especially designed to work both as a pump and a motor. Also the latest digital hydraulic components provide good opportunities for this kind of an application.

Also a detailed analysis of long-term testing is needed for the proposed system, and research verified by measurements is required to be able to define what kind of an energy storage method will be the best for this application.

References

Aarniovuori, L. (2010). *Induction motor drive energy efficiency- simulation and analysis.* Doctoral thesis, Acta Universitatis Lappeenrantaensis 396, Lappeenranta University of Technology.

Aarniovuori, L. Laurila, L. Niemelä, M. and Pyrhönen, J. (2010). DTC IM drive losses – simulation and measurements. In *Proceedings of the XIX International Conference on Electrical Machines*, Rome, Italy, Sept. 6-8, 2010.

ABB: *Motion Control program Firmware.* (2007), [Online], [Accessed 13 November 2007] http://www.abb.com.

Ahn, K. K., Ho, T. H. and Dinh, Q. T. (2008). A study on energy saving potential of hydraulic control system using switching type closed loop constant pressure system. In *Proceedings of the 7th JFPS International Symposium on Fluid Power,* TOYAMA 2008 September 15–18, 2008.

Airila, M. (2004). *Koneenosien suunnittelu* [Machine part design]. Juva: WSOY. (in Finnish).

Akers, A., Gassman, M. and Smith, R. (2006). *Hydraulic power system analysis*. Boca Raton: Taylor & Francis Group

Andersen, T. O., Hansen, M. R., Pedersen, H. C. and Conrad, F. (2005). Regeneration of potential energy in hydraulic forklift truck. *In Proceedings of the 6th International Conference on Fluid Power Transmission and Control*, pp. 302–306, Hangzhou.

Anon (1973). *Principles of Hydraulics.* Morden, Surrey: Trade & Technical press Ltd.,

Artemis: *Digital Displacement technology.* (2010), [Online], [Accessed 6 June 2011] http://www.artemisip.com.

Backé, W. (2005). What makes new ideas in fluid power succeed? *In Proceedings of the 6th JFPS International Symposium on Fluid Power*, TSUKUBA 2005, November 7–10, pp. 21–30.

Bergmemann, M. (1990). Noise problems of hydraulic piston pumps with odd and even numbers of cylinders. *In Proceedings of the BHRA 9th International Symposium on Fluid Power*, Cambridge, England.

Berkner, P. (2008). How, Why, and When to apply electric motors to mobile hydraulic systems. *In Parker Hannifin 2008 Global Mobile Sales Meeting & Symposium* Whitepaper # 0001., [Online], [Accessed January 10, 2010]. Available at: http://www.allaboutmotion.com.

Boyes, J. D. and Clark, N. H. (2000). Technologies for energy storages flywheels and super conducting magnetic energy storage. *In Power Engineering Society Summer Meeting*, IEEE 2000, Seattle, USA, Vol. 3, pp. 1548–1550.

Burrows, C. R. (2005). Control and condition monitoring in electro-hydraulic systems. *In UKACC Control 2004 Mini Symposia.* [Online]. Available at: http: //www.ieee.com.

Casoli, P., Vacca, A. and Berta, G. L.(2008). Optimization of relevant design parameters of external gear pumps. *In Proceedings of the 7th JFPS International Symposium on Fluid Power,* TOYAMA 2008, September 15–18, 2008.

Chen, Z., Liu, X. D. and Yang, D. P. Dynamic Sliding Model Control for Direct Torque Control of PMSM based on Expected Space Vector Modulation. *In Proceedings of the 2010 Second International Conference on Industrial and Information Systems,* Dalian, China, July 10–11.

de Silva Clarence, W. (2005). *Mechatronics: an integrated approach.* Boca Raton: CRC press.

DesignAerospace LLC (2009), [Online], [Accessed 15 January 2010], available at: www.daerospace.com, 2009.

Ding, Z., Zhao, D. and Zuo, J. (2007). Modeling and Simulation about an Electric car's regenerative braking system. *In Proceedings of the 2007 IEEE International Conference on Mechatronics and Automation*, August 5–8, Harbin, China.

Eckerle (2007) *Hydraulic division. EIPS 2 Internal gear pumps*.[Online]. [Accessed 20 April 2008], available at: http: //www.eckerle.com.

EPA (2011). *Clean Air Nonroad Diesel - Tier 4 Final Rule* [Online], [Accessed 14 January 2010] available at: http://www.epa.gov/nonroaddiesel/2004fr.htm.

Feng, B., Gong, G. and Yang, H. (2009). Self-tuning-parameter fuzzy PID temperature control in a large hydraulic system. *In Proceedings of the IEEE/ASME International Conference on Advanced Intelligent Mechatronics*, Singapore.

Glavin, M. E., Chan, P. K. W., Armstrong, S. and Hurley W. G. (2008). A Stand-alone photovoltaic Supercapacitor Battery Hybrid Energy Storage System. *In Proceedings of the Power Electronics and Motion Control Conference.* Poznan, Poland.

Gulez, K., Adam, A. A. and Pastaci, H.(2008). Torque Ripple and EMI Noise Minimization in PMSM Using Active Filter Topology and Field-Oriented Control. *Transactions on Industrial Electronics*, Jan. 2008 Vol. 55, Issue 1.

Gysen, B. L. J., van der Sande, T. P. J. , Paulides, J. J. H., Lomonova, E. A. (2010). Efficiency of a regenerative direct-drive electromagnetic active suspension. *In Proceedings of the Vehicle Power and Propulsion Conference (VPPC),*Lille, France, 1–3 September.

Handroos, H. (2010) Lecture notes for PhD course: *Modelling and simulation of mechatronics machines.*

Hänninen, H., Kauranne, H., Sinkkonen, A. and Pietola, M. (2011). Study on energy usage of reach truck equipped with energy recovery system. *In Proceedings of the Twelfth Scandinavian International Conference on Fluid Power*, Finland, Tampere, 18–20 May.

Harrison, A. M. and Edge, K. A. (2000). Reduction of axial piston pump pressure ripple. *In Proceedings of the Institution of Mechanical Engineers, Part I: Journal of Systems and Control Engineering*, Vol. 214, No. 1

Hayashi, S. (2001). Nonlinear phenomena in hydraulic systems. In *Proceedings of the 5th international conference on fluid power transmission and control*. Hangzhou, China.

Helduser, S. (1999). Electric-hydrostatic drive—an innovative energy-saving power and motion control system. *In Proceedings of the Institution of Mechanical Engineers, Part I: Journal of Systems and Control Engineering*, Vol. 213, No. 5.

Hui, S. and Junqing, J. (2010). "Research on the system configuration and energy control strategy for parallel hydraulic hybrid loader." *Journal Automation in Construction*, Vol. 19, Issue 2, March 2010, pp. 213–220.

Iannuzzi, D. (2008). Improvement of the Energy Recovery of Traction electrical drives using supercapacitors. *In Proceedings of the 13th International Power Electronics and Motion Control Conference*. Accessed 9 November 2008 [Online]. Available at: http//: www.ieee.org.

Imanishi, E. and Nanjo, T. (2010). Dynamic Simulation of flexible Multibody system with Electric-hydraulic drive system. *In Proceeding of the 1st Joint international conference on Multibody System Dynamics*. Lappeenranta, Finland.

Infineon (2010). [Online], [Accessed 10 May 2010], available at: http://www.infineon.com.

Inoue, H. (2008). *Introduction of PC200-8 Hybrid Hydraulic Excavators*. [Online]. Available at: http://www.komatsu.com/CompanyInfo/profile/report/pdf/161-E-05.pdf.

Ivantysynova, M. (2008). Innovations in pump design-what are future directions. *In Proceedings of the International symposium on fluid power.* Toyama.

Jelali, M. and Kroll, A. (2004). *Hydraulic Servo-systems, modeling, identification and control*. London: Springer.

Jianxin, L. and Ping, T. (2009). Fuzzy logic Control of Integrated hydraulic actuator unit using high speed switch valves. *In Proceedings of the International conference on computational intelligence and natural computing*. Wuhan, China.

Johansson, J., Ölvander, J. and Palmberg, J.-O. (2007). "Experimental Verification of Cross-Angle for Noise Reduction in Hydraulic Piston Pumps." *Journal of systems and control engineering*. Vol. I3 (2007), pp. 321–330.

Kauranne, H., Kajaste, J. and Vilenius M. (2006). *Hydraulitekniikan perusteet.* [Fundamentals in Hydraulic technology]. Helsinki: WSOY. (in Finnish).

KERS (2010). [Online], available at: http://www.formula1.com.

Kunze, G. (2010). *Mobile construction machinery-trends and new developments.* ATZonline. April 2010. [Online]. available at: http: //www.atzonline.com.

Li, W. and Joós, G. (2008). A power electronic interface for a battery supercapacitor hybrid energy storage system for a wind application. *In Proceedings of the 39th IEEE Power Electronics Specialists Conference*. Rhodes, Greece.

Liang, X. (2002). *On improving energy utilization in hydraulic booms.* Doctoral thesis, Helsinki University of Technology.

Liang, X. and Virvalo, T.(2001). What's wrong with energy utilization in hydraulic cranes. *In Proceedings of the 5th international conference on fluid power transmission and control.* Hangzhou, China.

Lilan, Y. and Sunyi, C. Y. (2007). Working Principle and Design of Axial Piston Pump. *In Proceedings of the 5th international symposium on fluid power transmission and control*. Beidaihe, China.

Lin, T., Wang, Q., Hu, B. and Gong W. (2010a). Development of hydraulic powered hydraulic construction machinery. *Journal Automation in construction*. Vol. 19, issue 1, January 2010, pp. 11–19.

Lin, T., Wang, Q., Hu, B. and Gong, W. (2010b). Research on the energy regeneration systems for hydraulic excavators. *Journal Automation in construction.* Vol. 19, issue 8, December 2010, pp. 1016–1026.

Linjama, M. (2009a). Energy saving digital hydraulics. *In Proceedings of the Second Workshop on Digital Fluid Power*, 12–13 November 2009, Linz, Austria.

Linjama, M. and Huhtala, K. (2009b). Digital pump-motor with independent outlets. *In Proceedings of the 11th Scandinavian International Conference on Fluid Power*, 2–4 June 2009, Linköping, Sweden.

Linjama, M. and Tammisto, J. (2009c). New alternative for digital pump-motor-transformer. In: Scheidl R. & Winkler B. (eds.). *Proceedings of the Second Workshop on Digital Fluid Power*, 12–13 November, Linz, Austria, pp. 49–61.

Linjama, M. and Vilenius, M. (2005). Energy-efficient motion control of a digital hydraulic joint actuator. *In Proceedings of the 6th JFPS International Symposium on Fluid Power*, TSUKUBA, November 7–10.

Lomonova, E. A. (2010). Advanced actuation systems — State of the art: Fundamental and applied research. *In Proceedings of the International Conference on Electrical Machines and Systems (ICEMS)*, Incheon, Korea (South), 10–13 October.

Luukko, J. (2000). *Direct torque control of permanent magnet synchronous machines - analysis and implementation*. Doctoral thesis. Acta Universitatis Lappeenrantaensis 97, Lappeenranta University of Technology.

Luukko, J., Niemelä, M. and Pyrhönen, J. (2007). "Estimation of rotor and load angle of direct-torque-controlled permanent magnet synchronous machine drive." *Electric Power Applications, IET*. Volume 1, Issue 3 pp. 299–306

Majumdar, S. R. (2002). *Oil Hydraulic Systems principles and maintenance.* New York: McGraw-Hill.

Manring, N. D. (2000). The discharge flow ripple of axial-piston swash-plate type hydrostatic pump. *Journal of dynamic systems, measurements, and control.* June 2000, Vol. 122, pp. 263–268.

Manring, N. D. (2003). The theoretical flow of an external gear pump. *Journal of dynamic systems, measurements, and control.* September 2003, Vol. 125, pp. 396–404.

Mattila, J. (2000). *On Energy-efficient motion control of hydraulic manipulator.* Doctoral thesis, Publications 312, Tampere University of Technology.

Maxwell Technologies. *Ultra capacitors.* (2010). [Online], available at: http://www.maxwell.com.

McCloy, D. (1980). *Control of fluid power: analysis and design*. Chichester, New York. Horwood, Halsted press. 505 pages.

Mecrow, B. C. and Jack, A. G. (2008). Efficiency trends in electric machines and drives. *Journal Energy Policy*, Volume 36, Issue 12, December 2008, pages 4336–4341.

Mehta, V. (2006). *Torque ripple attenuation for axial piston swash plate type hydrostatic pump noice consideration*. Doctoral thesis. University of Missouri-Columbia

Merritt, H. E. (1967). *Hydraulic control systems*. New Jersey : John Wiley & Sons, 354 pages.

Miller, J. M. (2008). *Propulsion Systems for Hybrid Vehicles*. London: IET.

Minav, T. (2008). *Electric energy recovery system for a hydraulic forklift*. Master's Thesis, Lappeenranta University of Technology.

Minav, T. A., Filatov, D. M., Laurila, L. I. E., Pyrhönen, J. J. and Vtorov, V. B. (2011e). Modelling of an electro-hydraulic forklift in Matlab Simulink. *Journal International Review on Modelling and Simulations*, in press.

Minav, T. A., Immonen, P. A., Pyrhönen, J. J. and Laurila, L. I. E. (2010b). Effect of PMSM Sizing on the Energy Efficiency of an Electro-Hydraulic Forklift. *In Proceedings of the ICEM 2010*, Italy, Roma.

Minav, T. A., Pyrhönen, J. J., Laurila, L. I. E. and Vtorov, V. B. (2011c). "Direct pump control effects on the energy efficiency in an electro-hydraulic lifting system." *International review of Automatic Control (IREACO),* Vol.4, n.2.

Minav, T., Immonen, P., Laurila, L., Vtorov, V., Pyrhönen, J. and Niemelä, M. (2011b). Electric energy recovery system for a hydraulic forklift – theoretical and experimental evaluation. *Journal Power applications IET*, Vol.5, Issue 4.

Minav, T., Laurila, L. and Pyrhönen, J. (2010a). Energy Recovery Efficiency Comparison in an Electro-hydraulic Forklift and in a Diesel Hybrid Heavy Forwarder. *In Proceedings of the SPEEDAM 2010*. Pisa, Italy, 2010.

Minav, T., Laurila, L., and Pyrhönen, J. (2011d). Permanent Magnet Synchronous Machine Sizing: Effect on the Energy Efficiency of an Electro-hydraulic Forklift. *Transactions on Industrial Electronics*, in press.

Minav, T., Laurila, L., Immonen, P., Haapala, M, and Pyrhönen, J. (2009). Electric energy recovery system efficiency in a hydraulic forklift. *Proceedings of the EUROCON 2009*. St. Petersburg, Russia.

Minav, T., Virtanen, A., Laurila, L., and Pyrhönen, J. (2011f). Storage of energy recovered from an industrial forklift. *Journal Automation in Construction*, submitted.

Minav, T.A., Laurila, L. I. E., Pyrhönen, J. J. (2011a). Axial Piston Pump Flow Ripple Compensation by adjusting the pump speed with an electric drive. *In Proceedings of the SICFP 2011*, Finland, Tampere.

Mohan, N. (2001). *Advanced Electric Drives: Analysis, Control and Modeling using Simulink*. MNPERE Minneapolis.

Mohan, N. (2003). *Electric Drives – an integrative approach*. MNPERE, pp. 15–17.

Noguchi, T. (2007). Trends of permanent-magnet synchronous machine drives. *IEEJ Transactions on Electrical and Electronic Engineering*, 2: 125–142. doi: 10.1002/tee.20119.

Parker, Hydraulic Motor/pump Series F11/F12 (2007). [Online], [Accessed 8 October 2008], available at: http://www.parker.com.

Passino, K. M. and Yurkovich, S. (1997). *Fuzzy Control*. Addison-Wesley-Longman, Menlo Park, CA.

Paulides, J. J. H., Kazmin, E. V., Gysen, B. L. J. and Lomonova, E. A.(2008). Series Hybrid Vehicle System Analysis Using an In-Wheel Motor Design. In *Proceedings of the IEEE Vehicle Power and Propulsion Conference (VPPC),* September 3–5, Harbin, China.

Pump School (2007). Viking Pump Inc.[Online], [Acsess 9 November 2007], available at: http://www.pumpschool.com.

Pyrhönen, J. (2010). Lecture notes for PhD course: *Electrical drives*.

Pyrhönen, J., Jokinen, T., and Hrábovcová, V. (2008). *Design of rotating electrical machines*, Chichester; John Wiley & Sons.

Rahmfeld, R. and Ivantysynova, M. (2001). Displacement Controlled Linear Actuator with Differential Cylinder - A Way to Save Primary Energy in Mobile Machines. *In Proceedings of 5th International Conference on Fluid Power Transmission and Control (ICFP'2001)*, Hangzhou, China, pp. 316–322.

Rexroth manual. (2010). *MODULE - 3A Model A10V0 Piston Pump Manual.* [Online], [Accessed 15 October 2010], available at: http: //www.boschrexroth.com/.

Roccatello, A. and Nervegna, N. (2009). Mechanical modelling of a bent axis pump. *International Journal of Fluid Power*, Vol. 10, No 2, pp. 57–72.

Ruggeri, M. and Guidetti, M. (2008). Variable load sensing and anti/stall electronic control with sliding mode and adaptive PID. *In Proceedings of the 7th JFPS International Symposium on Fluid Power*, TOYAMA, September 15–18, 2008.

Ruuskanen, V., Immonen P., Nerg J. and Pyrhönen, J. (2011). Determining Electrical Efficiency of Synchronous Machines with Different Electrical Control Methods. *Electrical engineering*, in press.

Rydberg, K.-E. (2005). Energy Efficient Hydraulic Systems and Regenerative Capabilities. *In Proceedings of the Ninth Scandinavian International Conference on Fluid Power SICFP'05*. Linköping.

Rydberg, K.-E. (2007). Design of Energy Efficient Hydraulic Systems - System Concepts and Control Aspects. *In Proceedings of the 5th International Symposium on Fluid Power Transmission and Control*. Beidaihe, China.

Sebastian, T. (2002). *Temperature effect on torque production and efficiency of PM motor using NdFeb magnets*. [Online], [Accessed 18 April 2009], available at: http www.ieee.org.

Semikron. (2009). *Behaviour of IGBTs and MOFETs during overload and short-circuit operation*. [Online], [Accessed 23 November 2009], available at: http http://www.semikron.com.

SEW Eurodrive. (2006). *The DS/CM synchronous servomotors from SEW-Eurodrive*. [Online]. [Accessed 23 November 2007].available at: http: //www.eurodrive.com.

SEW Eurodrive. (2007). *Engineering-Practical Implementation*. [Online].[Accessed 13 November 2007] Available at http://www.sew-eurodrive.com.

Siivonen, L., Linjama, M., Huova, M. and Vilenius, M. (2009). Jammed on/off valve fault compensation with distributed digital valve system. *International Journal of Fluid power*. Vol. 10 No 2.pp 73-82.

Sun, H. and Jing, J. (2010). Research on the system configuration and energy control strategy for parallel hydraulic hybrid loader. *Journal Automation in Construction*.in press.

Tian, L. (2004). Intelligent self-tuning of PID Control for the Robotic Testing System for Human Musculoskeletal joints test. *Annals of Biomedical Engineering*, Vol. 32, No. 6.

Wagner. (2010). *Tier IV emissions regulations: Knowing the facts*. [Online]. Available at: http: //www.wagnerequipment.com.

Wang, D., Guan, C., Pan, S., Zhang, M. and Lin, X. (2009). Performance analysis of hydraulic excavator powertrain hybridization. *Journal Automation in Construction*, Vol. 18, Issue 3, May 2009, pp. 249–257.

Wang, L. (2008). *Active Control of Fluid-Borne-Noise*. Doctoral thesis, 232 pages. Unoversity of Bath.

Watton, J. (1989). *Fluid power systems: Modeling, simulation, analog, and microcomputer control*. New York: Prentice Hall.

Watton, J. (2007). *Modelling, Monitoring and Diagnostic Techniques for Fluid Power Systems.* London: Springer.

Williason, C. and Ivantysynova, M. (2008). Pump mode prediction for four/quadrant velocity control of valveless hydraulic actuators. *In Proceedings of the 7th JFPS International Symposium on Fluid Power*, TOYAMA, September 15–18, 2008.

Wu, Y., McMahon, R. A., Zhan, Y. and Knight, A. M. (2006). Impact of PWM schemes on induction motor losses. *In Proceedings of the Industry Applications Conference 2006*. 41st IAS Annual Meeting. Conference Record of the 2006 IEEE, Volume 2, pp. 813–818.

Xiao, Q., Wang, Q. F. and Zhang, Y. T. (2008). Control strategies of power system in hybrid hydraulic excavator. *Journal Automation in Construction*. Vol. 17, Issue 4, May 2008, pp. 361–367.

Xiaofeng, L., Wenguang, L., Xu, Y. and Ke, W. (2010). Research on energy-saving control for hydraulic excavator based on FNN. *In Proceedings of the International conference on measuring technology and mechatronics automation*. Changsha, China. March 13–14.

Xu, H. and Li, Z. (2010). Design of Flux-Weakening Control system of PMSM Based on Fuzzy Theory. *In Proceedings of the International Conference On Computer Design And Appliations* (ICCDA 2010), Qinhuangdao, China, June 25–27.

Yang, H., Sun, W., and Xu, B. (2007). New Investigation in Energy Regeneration of Hydraulic Elevators. *IEEE/ASME Transactions on Mechatronics Journal*, Vol. 12, No. 5, October 2007.

Yao, B. and Liu, S. (2002). Energy-saving control of hydraulic systems with novel programmable valves. *In Proceedings of the 4th world Congress on Intelligent Control and Automation*, Shanghai, China, June 10–14.

Yoon, J. I., Kwan, A. K. and Truong, D. Q. (2009). A Study on An Energy Saving Electro-Hydraulic Excavator. *In Proceedings of the ICROS-SICE International Joint Conference 2009.* Fukuoka, Japan.

Zheng, J., Zhao, S., Wei, S. and Zheng, J. (2009). Adaptive Fuzzy PID control for Switched Reluctance Motor Direct Drive Servo Hydraulic Press. *In Proceedings of the International Conference on Measuring Technology and Mechatronics Automation.* Zhangjiajie, Hunan, China. April 11–12.

Appendix A: Description of the test setup

The experimental investigations were performed at Lappeenranta University of Technology (LUT) in the Laboratory of Electrical Motors and Drives. The test setup is based on a commercial forklift (Figure A.1) and the tested pump drive system was built aside the forklift.

Figure A.1: Photo of a conventional forklift.

In the study, the original non-regenerative electric drive and hydraulic system of the forklift was replaced by the hydraulic and electric system. Figure A.2 illustrates a photo of the test setup in laboratory.

Figure A.2: Photo of conventional forklift and the test setup bench.

Figure A.3 shows photo and schematics of electric and hydraulic circuit of the main lift function with energy regeneration from potential energy.

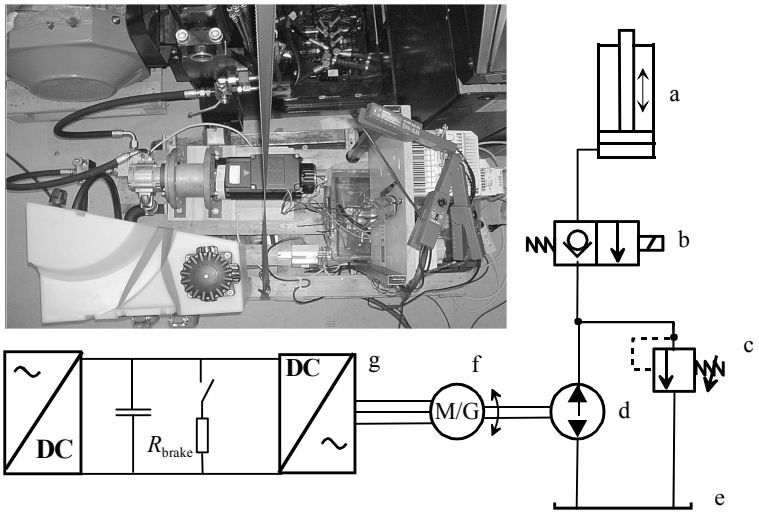

Figure A.3: Photo and schematics of electric and hydraulic circuit of the main lift function with energy regeneration from potential energy. The experimental system consists of a) a single-acting cylinder, b) a two-way normally closed poppet valve, c) a pressure relief valve, d) a pump/motor, e) an oil tank, f) a permanent magnet synchronous motor/generator, g) a frequency converter and a brake resistor R_{brake}.

Table A.1 illustrates the main components and their manufacturer data.

Table A.1 Main components and their manufacturer data.

Component		Manufacturer data
Pump	Internal gear	Eckerle internal gear pump, type EIPS 2, displacement 13.3 cm^3/rev
	Axial piston	Parker axial piston motor series F11, displacement 19 cm^3/rev
Motor	4.5 kW PMSM	CFM90M PMSM by Sew-Eurodrive: T_n = 14.5 Nm, I_n = 10.1A, T_{max} = 52.2 Nm, I_{max} = 40 A
	10 kW PMSM	CFM112M PMSM by Sew-Eurodrive: T_n = 31 Nm, I_n = 35 A, T_{max} = 108 Nm, I_{max} = 140 A
Frequency converter		ACSM1-04x[4)]x[5)]-046A-4 manufactured by ABB
Brake resistor R_{brake}.		25.5 Ω

Figure A.4 illustrates the physical dimensions of a conventional forklift.

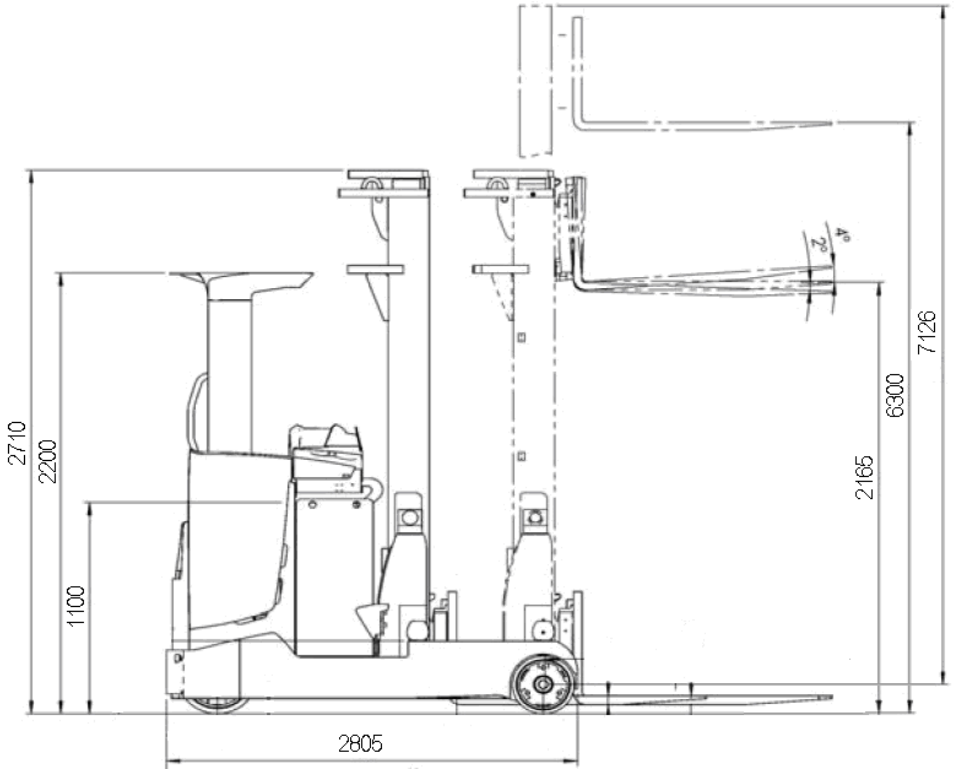

Figure A.4: Physical dimensions of Rocla HS16F forklift.

The experimental setup with a map of the locations of the sensors is shown in Figure A.5. In the experiments, the rotation speed of the PMSM and the DC voltage in the intermediate circuit are measured. The electric machine torque was estimated by the converter. The information required to calculate the hydraulic energy was taken from two S-10 pressure sensors manufactured by WIKA. They were installed into a pipe directly after the pump and between the pump and the control valve. Yokogawa PZ4000 Power analysers were used for measuring the phase voltages and currents with a 1MS/s resolution. The speed and height of the forks were measured with a wire-actuated encoder SGW/SGI by SIKO. The pressure, speed and height signals were recorded with a dSPACE DS1103 PPC controller board with I/O.

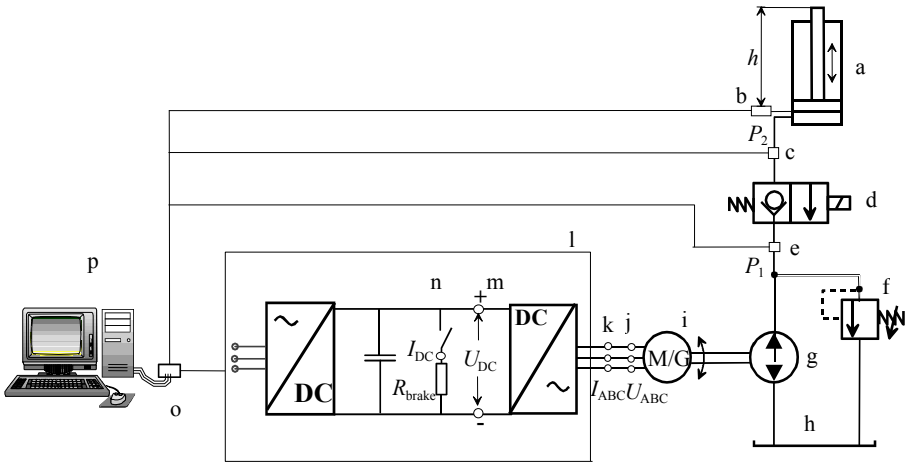

Figure A.5: Electric and hydraulic circuit of the main lift function with energy regeneration from potential energy. The experimental system consists of a) a single-acting cylinder, b) an actuated encoder SGW/SGI, c) a pressure sensor *P*2, d) a two-way normally closed poppet valve, e) a pressure sensor *P*1, f) a pressure relief valve, g) a hydraulic pump/motor, h) an oil tank, i) a permanent magnet synchronous motor/generator, j) phase voltage probes, k) phase current probes, l) a frequency converter and a brake resistor R_{brake}, m) a DC voltage probe, n) a DC current probe, o) the connectional panel dSPACE and p) a computer and dSPACE.

Appendix B: Graphic symbols of hydraulic components

Figures courtesy of P.Immonen

Pumps

Fixed displacement hydraulic pump, unidirectional

Fixed displacement hydraulic motor, bidirectional

Variable displacement hydraulic pump, unidirectional

Variable displacement hydraulic pump, bidirectional

Motors

Fixed displacement hydraulic motor, unidirectional

Fixed displacement hydraulic motor, bidirectional

Variable displacement hydraulic motor, unidirectional

Variable displacement hydraulic motor, bidirectional

Pump-motor

Fixed displacement hydraulic motor pump, unidirectional

Cylinders

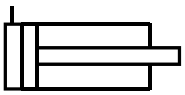

Single-acting cylinder returned by external force

Double-acting cylinder returned by external force

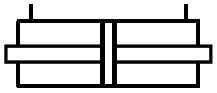

Symmetrical double-acting cylinder (double-ended piston rod)

Valves

Check valve, free flow one direction, blocked flow in other direction

Shut-off valve

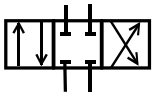

4/3 directional control valve, directional control valve with 4 ports and 3 finite positions

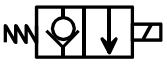

Two-way normally closet poppet valve

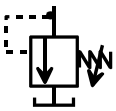

Pressure relief valve normally closed

Basic symbols

Tank

Continuous line-flow line

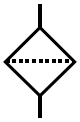

Filter

Spring

Flow restriction

Appendix C: Calculation of pu values

In general, the per unit value is the ratio of the actual value and the base value of the same quantity (equation C.1).

$$\text{per unit value} = \frac{\text{actual value}}{\text{base value}} \tag{C.1}$$

The rated values for power and voltage are used as the bases for the calculations. For instance, the rated stator voltage U_n= 312 V equals to 1 pu. U_n is the base value for the maximum stator voltage U_{max}. By substituting parameters to Equation (1):400/ 312 = 1.28 pu. In the same way, all parameters were converted to per unit values. The measured, rated values and the per unit values for CFM90M PMSM are given in Table C.1.

Table C.1: PMSM machine CFM90M parameters (Sew-Eurodrive, 2007; Minav, 2011b).

CFM90M Machine Parameters		Measured or rated values	Per unit values
maximum stator voltage	U_{max}	400 V	1.28 pu
rated stator voltage	U_n	312 V	1 pu
rated stator current	I_n	10.1 A	1 pu
maximum allowed stator current	I_{max}	40 A	3.96 pu
rated apparent power	S_n	5.46 kVA	1 pu
rated output power	P_n	4.55 kW	0.83 pu
rated speed	n_n	3000	1/min
number of pole pairs	p	3	-
rated frequency	f_n	150 Hz	1 pu
rated angular electrical speed	ω_n	300π rad/s	1 pu
rated stator flux linkage	Ψ_n	0.27 Vs	1 pu
synchronous inductance, direct axis value	L_d	5.72 mH	0.30 pu
synchronous inductance, quadrature axis value	L_q	5.72 mH	0.3 pu
stator resistance at room temperature	R_s (at 20 °C)	0.53 Ω,	0.03 pu
permanent-magnet-produced flux linkage	Ψ_{PM}	0.22 Vs	0.814 pu

Appendix D: Matlab/Simulink system model

Figure D.1 shows the Matlab/Simulink system model. The model of the PMSM with Id=0 and Fuzzy PID control shown in Figure D.2. Figure D.3 shows the Fuzzy PID controller.

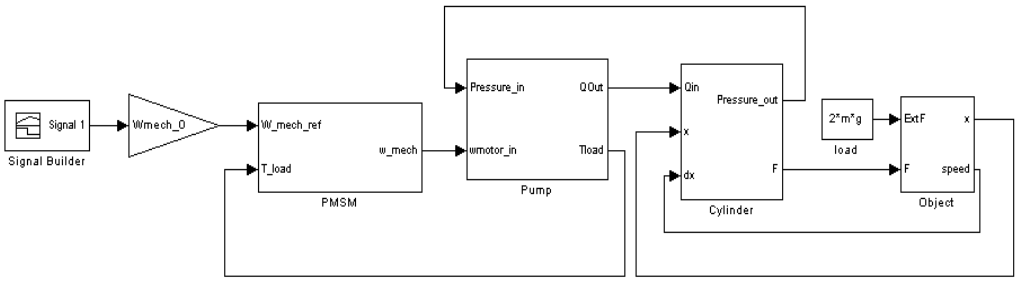

Figure D.1: Matlab/Simulink system model.

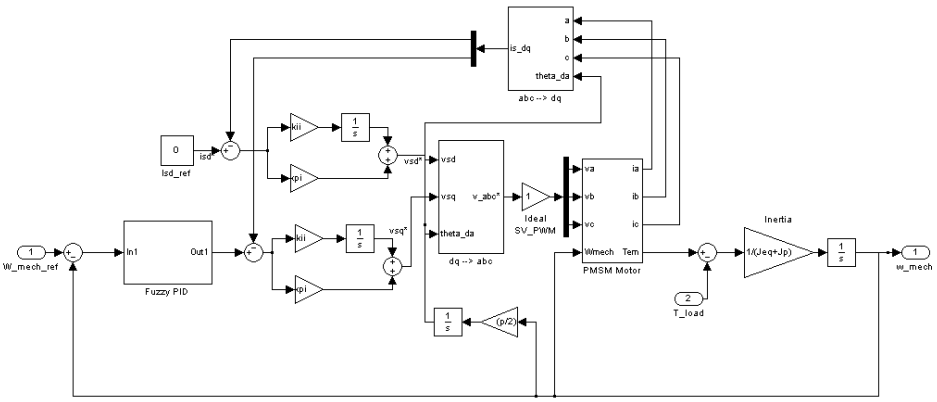

Figure D.2: Matlab/Simulink model of the PMSM with Id=0 and the Fuzzy PID control.

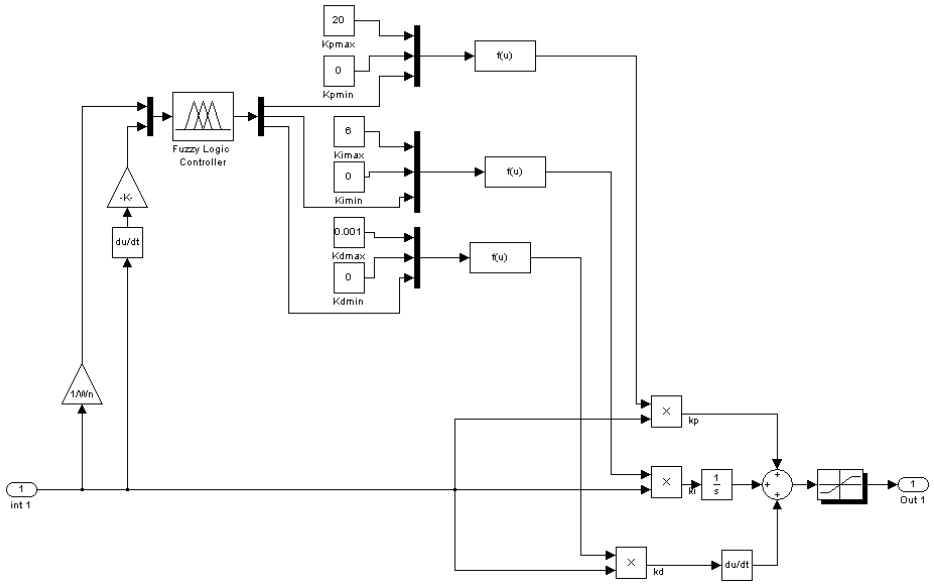

Figure D.3: Matlab/Simulink model of the Fuzzy PID controller.

Appendix E: Programme code

Appendix presented a programme code used in control programme for ripple compensation.

```
x1[0]=sin(angle);                          // ideal flow produced by the first piston

x2[0]=sin(angle+(((2*3.14159)/5)));        // ideal flow produced by the second piston

x3[0]=sin(angle+(((2*3.14159)/5))*2);      // ideal flow produced by the third piston

x4[0]=sin(angle+(((2*3.14159)/5))*3);      // ideal flow produced by the forth piston

x5[0]=sin(angle+(((2*3.14159)/5))*4);      // ideal flow produced by the fifth piston

if(x1[0] < 0){x1[0]=0;}                    // separation delivery (positive)  flow

if(x2[0] < 0){x2[0]=0;}                    //  from suction (negative ) flow

if(x3[0] < 0){x3[0]=0;}

if(x4[0] < 0){x4[0]=0;}

if(x5[0] < 0){x5[0]=0;}

sum[0]=x1[0]+x2[0]+x3[0]+x4[0]+x5[0]; // producing the summary flow of each piston

signal[0]=sum[0]*(-1)*(rpm[0]/1.539)+(rpm[0]*2*1.0250);

// creating signal for compensation ripple, where rpm is the user's speed in rpm.
```

Appendix F: Cycle efficiency Sankey diagrams

Cycle efficiency Sankey diagrams are shown for lifting (Figure F.1) and lowering (Figure F.2). This example is for the combination containing a 10 kW PMSM and an axial piston pump for a speed of 2000 rpm and a payload of 920 kg.

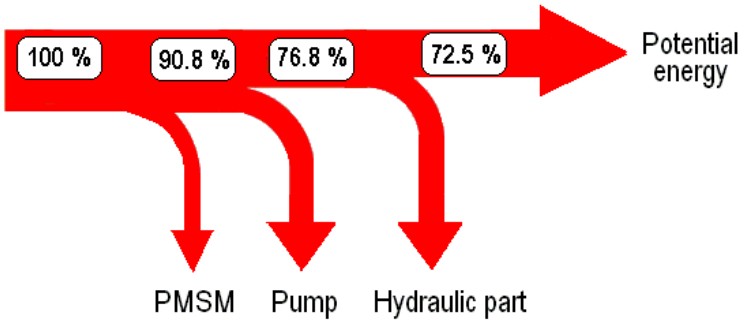

Figure F.1: Cycle efficiency Sankey diagram for lifting with a 10 kW PMSM and axial piston pump for a speed of 2000 rpm and a 920 kg payload.

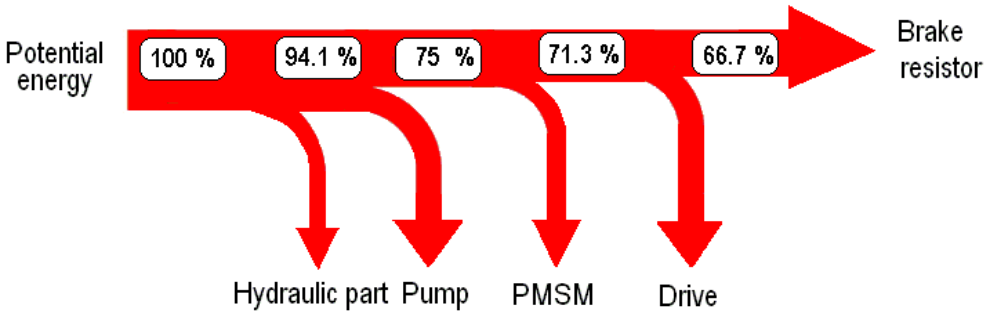

Figure F.2: Cycle efficiency Sankey diagram for lowering with a 10 kW PMSM and axial piston pump for a speed of 2000 rpm and a 920 kg payload.

ACTA UNIVERSITATIS LAPPEENRANTAENSIS

393. KÄHKÖNEN, ANNI-KAISA. The role of power relations in strategic supply management – A value net approach. 2010. Diss.

394. VIROLAINEN, ILKKA. Johdon coaching: Rajanvetoja, taustateorioita ja prosesseja. 2010. Diss.

395. HONG, JIANZHONG. Cultural aspects of university-industry knowledge interaction. 2010. Diss.

396. AARNIOVUORI, LASSI. Induction motor drive energy efficiency – Simulation and analysis. 2010. Diss.

397. SALMINEN, KRISTIAN. The effects of some furnish and paper structure related factors on wet web tensile and relaxation characteristics. 2010. Diss.

398. WANDERA, CATHERINE. Performance of high power fiber laser cutting of thick-section steel and medium-section aluminium. 2010. Diss.

399. ALATALO, HANNU. Supersaturation-controlled crystallization. 2010. Diss.

400. RUNGI, MAIT. Management of interdependency in project portfolio management. 2010. Diss.

401. PITKÄNEN, HEIKKI. First principles modeling of metallic alloys and alloy surfaces. 2010. Diss.

402. VAHTERISTO, KARI. Kinetic modeling of mechanisms of industrially important organic reactions in gas and liquid phase. 2010. Diss.

403. LAAKKONEN, TOMMI. Distributed control architecture of power electronics building-block-based frequency converters. 2010. Diss.

404. PELTONIEMI, PASI. Phase voltage control and filtering in a converter-fed single-phase customer-end system of the LVDC distribution network. 2010. Diss.

405. TANSKANEN, ANNA. Analysis of electricity distribution network operation business models and capitalization of control room functions with DMS. 2010. Diss.

406. PIIRAINEN, KALLE A. IDEAS for strategic technology management: Design of an electronically mediated scenario process. 2010. Diss.

407. JOKINEN, MARKKU. Centralized motion control of a linear tooth belt drive: Analysis of the performance and limitations. 2010. Diss.

408. KÄMÄRI, VESA. Kumppanuusohjelman strateginen johtaminen – Monitapaustutkimus puolustushallinnossa. 2010. Diss.

409. KARJALAINEN, AHTI. Online ultrasound measurements of membrane compaction. 2010. Diss.

410. LOHTANDER, MIKA. On the development of object functions and restrictions for shapes made with a turret punch press. 2010. Diss.

411. SIHVO, VILLE. Insulated system in an integrated motor compressor. 2010. Diss.

412. SADOVNIKOV, ALBERT. Computational evaluation of print unevenness according to human vision. 2010. Diss.

413. SJÖGREN, HELENA. Osingonjakopäätökset pienissä osakeyhtiöissä. Empiirinen tutkimus osakeyhtiölain varojenjakosäännösten toteutumisesta. 2010. Diss.

414. KAUPPI, TOMI. Eye fundus image analysis for automatic detection of diabetic retinopathy. 2010. Diss.

415. ZAKHVALINSKII, VASILII. Magnetic and transport properties of $LaMnO_{3+\delta}$, $La_{1-x}Ca_xMnO_3$, $La_{1-x}Ca_xMn_{1-y}Fe_yO_3$ and $La_{1-x}Sr_xMn_{1-y}Fe_yO_3$. 2010. Diss.

416. HATAKKA, HENRY. Effect of hydrodynamics on modelling, monitoring and control of crystallization. 2010. Diss.

417. SAMPO, JOUNI. On convergence of transforms based on parabolic scaling. 2010. Diss.

418. TURKU. IRINA. Adsorptive removal of harmful organic compounds from aqueous solutions. 2010. Diss.

419. TOURUNEN, ANTTI. A study of combustion phenomena in circulating fluidized beds by developing and applying experimental and modeling methods for laboratory-scale reactors. 2010. Diss.

420. CHIPOFYA, VICTOR. Training system for conceptual design and evaluation for wastewater treatment. 2010. Diss.

421. KORTELAINEN, SAMULI. Analysis of the sources of sustained competitive advantage: System dynamic approach. 2011. Diss.

422. KALJUNEN, LEENA. Johtamisopit kuntaorganisaatiossa – diskursiivinen tutkimus sosiaali- ja terveystoimesta 1980-luvulta 2000-luvulle. 2011. Diss.

423. PEKKARINEN, SATU. Innovations of ageing and societal transition. Dynamics of change of the socio-technical regime of ageing. 2011. Diss.

424. JUNTTILA, VIRPI. Automated, adapted methods for forest inventory. 2011. Diss.

425. VIRTA, MAARIT. Knowledge sharing between generations in an organization – Retention of the old or building the new 2011. Diss.

426. KUITTINEN, HANNA. Analysis on firm innovation boundaries. 2011. Diss.

427. AHONEN, TERO. Monitoring of centrifugal pump operation by a frequency converter. 2011. Diss.

428. MARKELOV, DENIS. Dynamical and structural properties of dendrimer macromolecules. 2011. Diss.

429. HÄMÄLÄINEN, SANNA. The effect of institutional settings on accounting conservatism – empirical evidence from the Nordic countries and the transitional economies of Europe. 2011. Diss.

430. ALAOUTINEN, SATU. Enabling constructive alignment in programming instruction. 2011. Diss.

431. ÅMAN, RAFAEL. Methods and models for accelerating dynamic simulation of fluid power circuits. 2011. Diss.

432. IMMONEN, MIKA. Public-private partnerships: managing organizational change for acquiring value creative capabilities. 2011. Diss.

433. EDELMANN, JAN. Experiences in using a structured method in finding and defining new innovations: the strategic options approach. 2011. Diss.

434. KAH, PAUL. Usability of laser - arc hybrid welding processes in industrial applications. 2011. Diss.

435. OLANDER, HEIDI. Formal and informal mechanisms for knowledge protection and sharing. 2011. Diss.